



**Seismic Attributes Analysis to Enhance 3-D
Seismic Data Interpretation of Upper Cretaceous
Succession in Bualwan, Dor Mansour Fields,
Western Sirt Basin, Libya**

By

Mohammed Najeeb Faraj El-Farsi

Supervisor

Dr. Saad Musbah EL-Shari

This Thesis was submitted in Partial Fulfillment of the
Requirements for Master's Degree of Science in Earth Science.

University of Benghazi Faculty of Science

February 2018

Copyright © 2017. All rights reserved, no part of this thesis may be reproduced in any form, electronic or mechanical, including photocopy , recording scanning , or any information , without the permission in writing from the author or the directorate of graduate studies and training of Benghazi university .

حقوق الطبع 2018 محفوظة. لا يسمح أخذ أي معلومة من أي جزء من هذه الرسالة علي هيئة نسخة إلكترونية أو ميكانيكية بطريقة التصوير أو التسجيل أو المسح من دون الحصول علي إذن كتابي من المؤلف أو إدارة الدراسات العليا والتدريب جامعة بنغازي



UNIVERSITY OF BENGHAZI
FACULTY OF SCIENCE
DEPARTMENT OF EARTH SCIENCE



SEISMIC ATTRIBUTES ANALYSIS TO ENHANCE 3-D SEISMIC
DATA INTERPRETATION OF UPPER CRETACEOUS SUCCESSION
IN BUALWAN, DOR MANSOUR FIELDS, WESTERN SIRT BASIN,
LIBYA

BY:

Mohammed Najeeb Faraj Rajab El-Farsi

Approved:

Supervised:

Dr. Saad Musbah EL-Shari

Examination Committee:

Internal examiner:

Dr. Mohamed B. Abdelmalik

External examiner:

Dr. Belgasem M. El-Saiti

Countersigned by:

Dr. Mohammed El-faitouri
(Head, Earth Science Department)

Dr. Hussein M. El-Barassi
(Dean, Faculty of Science)

ABSTRACT

The generation of seismic attributes has enabled to better interpret certain geologic features. Analysis was on attributes computed from 3D seismic data of Bualwan, Dor Mansour oil fields, with support from well logs. The ultimate goal in this multiattribute analysis is to produce a more accurate interpretation. The integration of the attributes has increased confidence in the seismic mapping horizons of Upper Cretaceous succession with their fault polygon, modeled, automatic fault techniques, fault patches, 3D structural grids and the other numerous subtle lineaments, which were difficult to identify in the input data. Seismic attributes like Variance seem to be very suitable for defining structural elements. Chaos attribute highlights areas where the seismic shows large variation in the locally estimated dip and azimuth. Structural smoothing is to reduce the noise and enhance quality. Ant tracking is applied on the Chaos and structural smoothing volume attribute to search of high energy surfaces (fault planes). 3DEE (3D edge enhancement) helped to increase number of faults manually detected and enhance their resolution.

In details, the faults which make up in the study area displayed a complex en echelon pattern, which is interpreted in terms of riedel shear mechanics. Anticlockwise orientation of the shears to the zonal trend NW-SE, indicate that they formed by sinistral slip. In a situation where the maximum compressive stress of the initial stress field was oriented toward NE-SW. There is, in addition, marked variation in fault pattern and style. In the west, NW-SE trending fault interpreted as a complex series of en echelon fault with associated riedel shears formed small scale of horst and graben structures. In the east, NE-SW trending fault may reflect Hercynian structures orogeny, which are limited in length and not continuous. Discontinuity Attributes were supported by Geoseismic profile through five cross section. Fault system is exhibit a periodic strike-slip, negative to positive flower structures suggested a significant component of a pull-apart transtational movement. Large scale listric faults with minor sets which were mainly associated with the margins of the horst structures were mostly interpreted, which cannot be fully delineated using seismic amplitude data. The fault modeling and pillar gridding process was closely monitored to ensure that the geologic based interpretation is preserved in the modeling

frame. The automatic fault extraction process were used as quality control to maintain interpretation, provide additional overview of fault segments and compare the value of manual interpretation.

Lithological characterization interpreted by four isochron map, well log cross section, with several physical attribute include; GLCM (Grey-Level Co-occurrence Matrices) texture attribute. Sweetness to delineate peaked energy. Cosine of Phase and frequency filters enhances the continuity of reflectors in areas of uncertainty, and highlights the main strata relationships. The advantages of AVO polarization in the convectional studied. Hydrocarbon implication has been discussed the proper location in the plam tree structure or beside the middle depocenter, referring the dry wells were out of structure.

Acknowledgements

I would like to give all thanks to Allah who gave me the strength and made it possible for me.

I express my special thanks with respect to my supervisor Doctor Saad El-Shari, for his efforts in guiding my work and instructing me especially in my report writing. Thanks extend to all Faculty members who helped me during my studies at the university.

I would like to thank AGOCO for providing the dataset, workstation, technical materials. In addition, thanks to all staff members of Exploration Department in AGOCO for their support, and useful discussion.

I wish to express my love and gratitude to my parents, my wife, my son, my brothers, my sisters, and all my friends, for their prayers and endless love.

Mohammed N. El-Farsi

Contents

Title	Page No.
Copyright © 2018	ii
Examination Committee.....	iii
Abstract	iv
Acknowledgements	vi
Contents.....	vii
List of Figures.....	xii
List of Tables.....	xvi
1. Introduction	1
1.1. Overview.....	1
1.2. Location of the Study Area	2
1.3. History of Concession.....	2
1.4. Previous Work.....	4
1.5. Software and Data Used.....	5
1.5.1. Software Used.....	5
1.5.2. Database.....	5
1.6. Statement of Problem.....	6
1.7. Objectives of This Study.....	6
2. Geological Setting	7
2.1. Introduction.....	7
2.2. Tectonic Setting	8
2.2.1. Major Structural Elements Impact In the Bualwan, Dor Mansour Fields.....	9

Title	Page No.
2.3. Depositional Setting and Stratigraphy	11
2.3.1 Lidam Formation.....	11
2.3.2 Etel Formation.....	12
2.3.3 Tagrift Formation.....	12
2.3.4 Sirt Shale Formation.....	13
2.4 Petroleum System in the Study Area.....	15
3. Software Methodology and Visualization Techniques.....	16
3.1 Seismic Data Inputs/ Co-Ordinate Systems.....	16
3.2 Well Log Data.....	16
3.2.1 Lithology Calibration.....	16
3.2.2 Formation Analysis.....	16
3.3 Seismic To Well Tie	18
3.3.1. Log Editor (Despike Sonic Log).....	18
3.3.2. Import Check Shots.....	18
3.3.3. An Estimated Density Log.....	19
3.3.4. Wavelet Extraction.....	19
3.3.5. Synthetic Seismogram	19
3.4 Volume Visualization/Volume wall display.....	21
3.4.1 Color and Opacity Filters	21
3.4.2 Cropping	21
3.4.3 Volume Realization	23
3.4.4 Volume Rendering	23

Title	Page No.
4. Seismic Attributes and Their Significant.....	25
4.1 Introduction.....	25
4.2 Science of Seismic Attributes.....	25
4.3 Classification of Seismic Attribute.....	27
4.3.1 AVO attributes.....	29
4.3.2 Time Slices Attribute.....	31
5. Seismic Data Interpretation and Modelling.....	32
5.1 Regional Structural Overview.....	32
5.2 Discontinuity Attributes for Structural Interpretation and Modelling.....	33
5.2.1 Structural Smoothing.....	33
5.2.2 Chaos Attribute.....	33
5.2.3 3D Edge Enhancement (3DEE).....	35
5.2.4 Automatic Fault Extraction Technique/Ant Tracking.....	35
5.3 Manual Fault Interpretation.....	38
5.4 Structural Architecture.....	40
5.4.1 Profile A-A'.....	40
5.4.2. Profile B-B'.....	42
5.4.3. Profile C-C'.....	42
5.4.4 Profile D-D'.....	45
5.4.5 Profile E-E'.....	45
5.5 Time Structure Map.....	48
5.6 Impact of Regional Stress in the Study Area.....	51

Title	Page No.
5.6.1 Variance Attribute.....	51
5.7 Orientation Analysis of the Structural Features.....	53
5.8 Well Log Correlation.....	56
5.9 Horizon Picking, Making and Interpretation.....	57
5.9.1 Isochron Maps.....	57
5.9.2 Plan View Evolution of Upper Cretaceous History.....	60
5.9.3 Surface Attributes.....	60
5.9.4 Horizon Making	65
5.9.5 Fault Modeling.....	66
5.9.6 Pillar Gridding.....	66
5.9.7 3D Structural Grid Surfaces.....	69
5.10 Lithology Interpretation by Using Seismic Attributes.....	70
5.10.1 Instantaneous Frequency.....	70
5.10.2 Sweetness Attribute.....	70
5.10.3 Cosine of Phase Attribute.....	70
5.10.4 Grey Level Co-occurrence Matrix (GLCM).....	70
5.10.5 AVO.....	73
6. Discussion and Prospectivity.....	74
6.1 Discussion.....	74
6.2 Prospectivity of the Bualawn and Dor Mansour Fields.....	76
6.2.1 Prospect 1.....	77
6.2.2 Prospect 2.....	77

Title	Page No.
Conclusion.....	80
References.....	83
Appendices.....	87
Appendix 1.....	87
Appendix 2.....	90
Appendix 3.....	91

List of Figures

Figure No.	Page No.
1.1 Distribution of sedimentary basins in Libya.....	3
1.2 Satellite image shows boundary, topography of concession 47, and location of the study area.....	3
2.1 The tectonic framework of the Sirt rift complex	7
2.2 Tectonic interpretation of Sirt rift complex	10
2.3 Well W-B3 profile shows five different formations, and composite W-C5 well data.....	13
2.4 Summarized the stratigraphy and structural characterization in the study area	14
2.5 Petroleum system in the western Sirt Basin.....	15
3.1 (A) Header parameters, (B) The seismic volume.....	17
3.2 Base map boundary of the study area.....	17
3.3 Log editor setting to correct sonic readings.....	18
3.4 Synthetic seismogram, Rucker wavelet extraction, estimated density log, sonic, gamma ray, interval velocity log, R.I log and formation tops.....	20
3.5 Synthetic seismogram of W-B3 overlaid on a vertical seismic section.....	20
3.6 Transparent with (A) seismic section with embedded normal wall volume. (B) Well path visualized. (C) Fault stick display. (D) Time slices, and (E) Visualiz grid.....	22
3.7 Color display of realized section, and different seismic attribute.....	22
3.8 (A) Cropped volume, (B) Cropped section for ant track process and visualization.....	23
3.9 (A) Realize volume operations, (B) Original and realized time. (C, 1) Original section,	

Figure No.	Page No.
(C, 2) Continuity of reflectors.....	24
3.10 The gains of rendering in the study area sections.....	24
4.1 Calculate instantaneous seismic attributes from the complex seismic trace.....	26
4.2 (A) Schematic diagram of a reflection at a boundary, (B) AVO crossplot, (C) polarization angle and (D) AVO strength.....	29
4.3 Different time slices at Lidam reservoir level used in this study (A) input seismic, (B) AVO, (C) envelope, (D) sweetness, (E) structural smoothing, (F) variance and (G) cosine of phase.....	31
5.1 Bouguer gravity anomaly map over concession 47.....	32
5.2 (A) Original seismic (B). The attribute Structural Smoothing.....	34
5.3. 3D View display inline crossed by time slice, (A) Original seismic (B) Chaos attribute.....	34
5.4. Shows 3D Edge Enhancement attribute.....	35
5.5 The Ant parameter with ant mode, ant track deviation, ant step size, and stereonet sectors of the dip and azimuth with the seismic inline/cross lines.....	37
5.6 Fault patches generated with a cropped seismic section of the whole seismic volume..	37
5.7 Extracted fault patches with the chaos attribute cropped seismic section.....	37
5.8 Fault sticks shows main fault segments.....	38
5.9 A-A` Seismic reflection profiles with structural interpretations.	41
5.10 B-B` Seismic reflection profiles with structural interpretations.....	43
5.11 C-C` Seismic reflection profiles with structural interpretations.....	44
5.12 D-D` Seismic reflection profiles with structural interpretations.....	46

Figure No.	Page No.
5.13 E-E` Seismic reflection profiles with structural interpretations.....	47
5.14 Structural time map of Sirt Shale Formation with fault polygon.....	49
5.15 Structural time map of Tagrift Formation with fault polygon.....	49
5.16 Structural time map of Etel Formation with fault polygon.....	50
5.17 Structural time map of Lidam Formation with fault polygon.....	50
5.18, (A) Interpreted fault polygon represented impact stress in the study area. Proposed stress model illustrating the structural pattern (B) sinistral displacement toward NW direction and (C) dextral displacement towards direction.....	52
5.19 Plan view of fault polygons, interpreted from the 3D seismic data for each formation showing the spatial and temporal changes in Upper Cretaceous geometry.....	54
5.20 Displacement point for each fault alone, ensure the accuracy with variance attribute to trends and lengths (A), 3D window displayed fault displacement and distance along fault (B).....	55
5.21 Function window to produce a classic fault throw vs. length plot (typically a log-log plot), quantitative evaluate fault 1 and the rest of faults.....	55
5.22 Well correlation panel for the interpreted horizons, and their lateral changes.....	56
5.23, Isochron contour map Sirt Shale, Tagrift Limestone, Etel and Lidam.....	59
5.24, Loop Kurtosis surface attribute functions as applied to Top Lidam with the dark color (red arrows) indicating less heterogeneity in the Frequency. RMS, Average Energy and Window Length.....	62
5.25 Statistical Attributes includes Sum Amplitudes, Sum Magnitude, Threshold Value, Positive to Negative ratio, and Standard Deviation of Amplitude.....	63

Figure No.	Page No.
5.26, Display amplitude surface attribute includes most of, Average Magnitudes, Median and Harmonic Mean at 974 ms Lidam Formation.	64
5.27 3D Structural grid surfaces of the Upper Cretaceous succession.....	65
5.28 Fault model techniques.....	67
5.29 Pillar geometry type and the grid skeleton.....	68
5.30 Interpreted 3D structural grid skeleton for the Upper Cretaceous surfaces.....	69
5.31 Instantaneous frequency attribute.....	71
5.32 Sweetness attribute	71
5.33 Cosine of phase attribute.....	72
5.34 The GLCM attribute.....	72
6.1 (A) Variance time slice at Lidam time, (B) Cosine of phase at at Lidam time and (C) Conceptual 3D model stratigraphic succession with structural framework.....	75
6.2 Lidam time structure maps prospect well location.....	76
6.3 Lidam structure map and variance shows clearly closure bounded fault, AVO fluid strength, AVO, and GLCM at corssline 1340 support from lithology point of view..	78
6.4 Composite seismic crossed wells, geoseismic model and 3D structural grid surfaces prove that the prospect within the horst crested areas shows clearly closure bounded fault.....	79

List of Tables

Table No.	Page No.
1.1 Data List of the Wells in Block-A1A2 (2005, 2000) Used in This Study.....	5
1.2 Formation Tops in Selected Wells.....	6
4.1 Different attributes with specific physical and geometrical class.....	27
4.2 Types of surface attribute used to interpret Lidam time structure map.....	28
4.3 Categories of texture, statistical, and AVO and their objectives.....	30
5.1 Interpreted faults with corresponding seismic coverage.....	39
5.2 Horizons with their corresponding event on seismic.....	57
5.3 Seismic facies analysis and their interpretation supported by AVO attribute.....	58
5.4 Interpretation of isochron map of the Upper Cretaceous succession.....	58
5.5 Comparison between the conventional AVO attributes with the polarization attributes.....	73

CHAPTER ONE

INTRODUCTION

1.1 Overview

The study is concentrated on using integrating of 3D seismic reflection data, seismic attributes analysis, time structure map, isochron map and well log data, with numerous techniques have developed such as visualization, evaluation and modeling, in Upper Cretaceous succession in Bualawn Dor Mansour Fields, western Sirt Basin, Libya.

Upper Cretaceous succession is responsible for the processes controlling the hydrocarbon traps in the basin. The period was significantly controlled by fault kinematics and their patterns. Seismically defined, constrained stratigraphy, internal structure and its tectonic evolution within the framework have been discussed by utilizing specific structural and stratigraphic volumetric attributes. The research is documented stratigraphy of the lithological units by observed changes in their thickness, their syn-kinematic depositional features and the subsurface fault geometry, then discuss the spatial variations in fault controlled deformation patterns. It provides evidence for exist a transtensional and transpresional. Understanding the variation between the two structure styles and their related stress is important.

The implications for hydrocarbon exploration have discussed. The source rock is Sirt Shale as dominated in the western Sirt Basin. The Dolomite supratidal flat in the upper part of Lidam Formation represents the primary reservoir. The secondary reservoir rocks are calcarenite in the lower part of Tagrift Limestone. The main trap style in the study area is the tilted fault blocks related to en echelon faults.

1.2 Location of the Study Area

Sirt Basin is considered to be a holotype of a continental rift area, bounded by Gulf of Sirt to the north, to the south by the Tibisti Massif, to the west by Al Qarqaf Uplift, Ghdamis and Murzuq Basins, and to the northeast by Cyrenaica Platform (Figure 1.1).

The area under investigation is the Bualawn Dor Mansour Fields located on the western part of concession 47, which is situated in the central part of west of Sirt Basin. Its cover an area about 450 Km², which is located between (latitude; 28° 30` and 28° 35` north, and longitude; 18° 35` and 18° 45` east). Topography of the Concession has highs and lows, which is subdivided into three parts in the north Haram Ridge, in the east Kotla Graben, and in the west Bualawn, Dor Mansour merged fields in which the study area have been carrying out, illustrated in Figure (1.2).

1.3 History of Concession

On December 1953 was granted to California Astistic Oil Company and Texaco Overseas Petroleum. American Overseas Petroleum Limited worked as an operator and started drilling from 1958 to 1973 about fifty-three wells , seven of those wells are oil producers; (Beda B1-47, Labiba K12-47, Kotla C2-47, Haram S1-47, Sarab T1-47, Bualawn GG1-47, and Warid HH1-47) and the others are dry wells. In 1974, the American company was nationalized and all its concessions and oil fields were turned to the National Oil Corporation (N.O.C) of Libya. Between 1975 and 1979, Umm-al-Jawa by Oil Company started exploration and drilling in the concession. On December 4, 1979, the two national companies Umm-Al-Jawaby and Arabian Gulf Exploration Company (AGECO) formed the Arabian Gulf Oil Company (AGOCO). Now, the concession belongs to AGOCO.

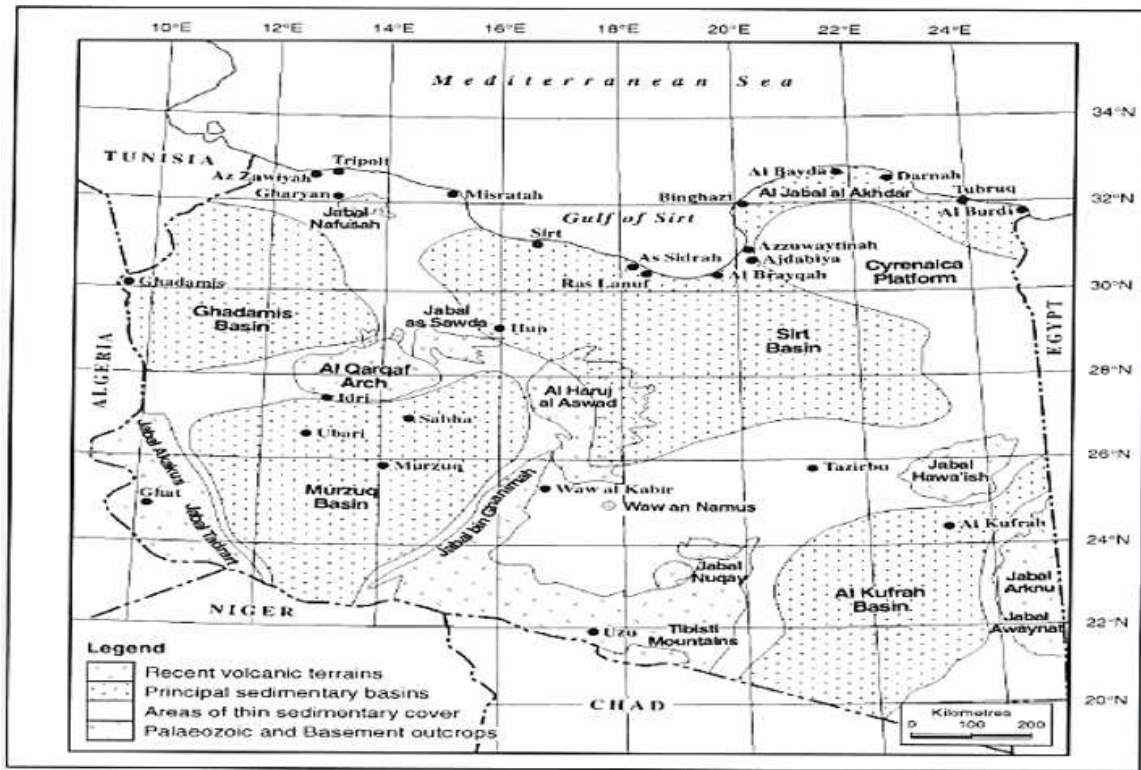


Figure 1.1, Distribution of sedimentary basins in Libya, which include Sirt, Kuffra, Murzuk, and Ghadames basins (Fuzyun and Jawzi, 1996).

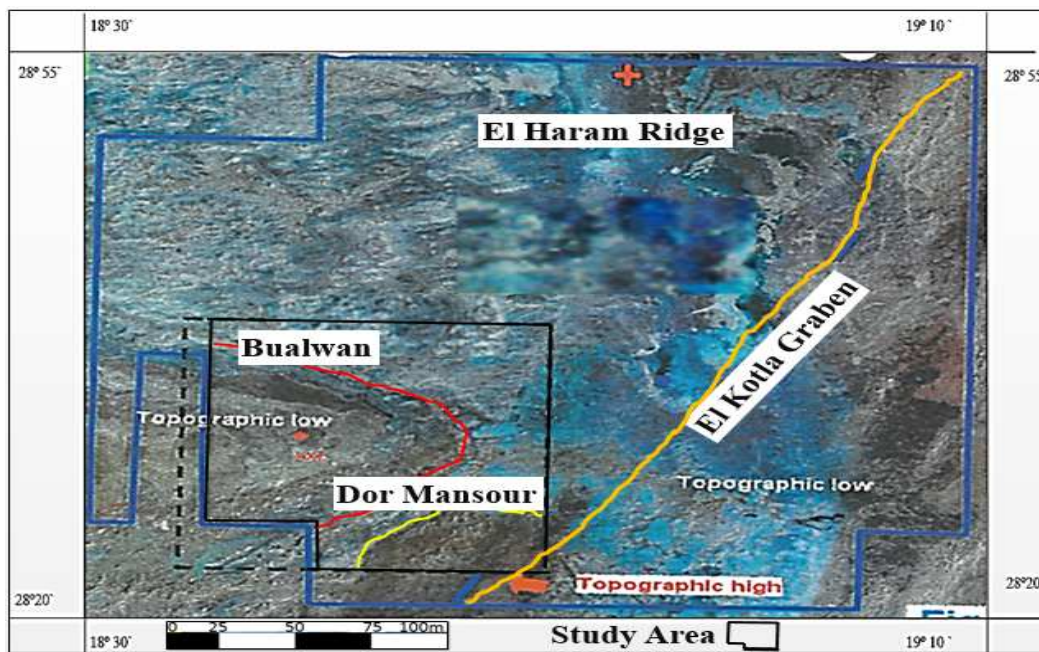


Figure 1.2, Satellite image shows boundary and topography of concession 47, and location of the study area.

1.4 Previous Work

A number of studies discussed regional evaluations of the structural and stratigraphic of the Sirt Basin. Regionally, the tectonic phases was developed corresponding to plate reorganization related to the evolution of the Atlantic and the Tethys (Finetti, 1982); Futyan and Jawzi, (1996); Guiraud and Bosworth, (1997). Abadi (2002) subdivided these tectonic into four main stages, summarized; the first during the Late Jurassic to the Early Cretaceous (144.2-112.2 Ma), which represents the subsidence in the southeast of the basin along an E-W structural trend. The second is related to the Late Cretaceous (93.9-65 Ma) with five time interval including Cenomanian (98.9-93.5 Ma), Turonoain (93.5-89 Ma), Coniacian and Santonian (89-83.5 Ma), Campanian (83.5-71.3 Ma) and Maastrichtian (71.3-65 Ma). Phase (3) is related to the Palaeocene until early Eocene (65-49 Ma). Phase (4) is related to the Middle Eocene until the present day (49-0 Ma).) .He suggested that phases 1, 2 and 3 were caused due to fault activities which are related to renew rifting during these pahses, while the phase 4 was caused by sediments load and thermal relaxation within the basin. Anktell, (1996) has introduced a tectonic model in the basin, include first intercontinental rifting (Late Carboniferous-Early Cretaceous). Second sinistral wrenching fault (Middle Jurassic-Early Cretaceous). Third dextral wrenching fault (Late Cretaceous-Middle Eocene) and Fourth dextral lateral wrenching and N-S compression extending from Late Eocene to the present. He also explained structural history of the Sirt Basin and its relationships to the Sabratah Basin and Cyrenaican Platform, which suggested the first faults occurred in the southern part of the basin is the Sabratah-Cyrenaica Fault Zone, which identified as E-W and WNW-ESE trends, causing the pull apart in the basin. Kroner, (1993) discussed structural weakness as a series of N-S to NW-SE of uplift and subsidence commencing with the Pan African orogeny, then Hercynian orogeny in NE-SW trends. Abadi, (2002) studied the stratigraphic units, their distribution and thickness variation, to find out that controlled by basement structures related rift complex configuration, which is divided the whole Sirt Basin into discrete structural features. Harding, (1984) discussed Graben hydrocarbon occurrence that aided to feed high area by vertical migration. Roohi, (1996) introduced agreement to hydrocarbon migration pattern. Sinha and Mriheel, (1996) suggests the Upper Cretaceous period appears to have been relatively more eventful from the view point of tectonic evolution and the attendant sedimentation history. El Shari (2008) confirm that result by subsidence analysis at the eastren margin of Sirt Basin. He concludes that a large subsidence combined with a sedimentation rate occurred during the Upper Cretaceous times.

1.5 Software and Data Used

1.5.1 Software Used

As the main targets of this study are to integrate attributes analysis and their benefit, construct time maps and subsurface correlations, and modeling; the following software were used:

- **Petrel Software-2015:** this software used to visualize and interpret subsurface seismic data by using attribute analysis, extracting different subsurface maps; as well as constructing cross sections to improve structural and stratigraphic interpretations.
- **Corel Draw:** used for create geoseismic to illustrate a complicity of subsurface geology in easy view.

1.5.2 Database

The main dataset used in this study are:

- **Seismic data**

3D Seismic reflection data of Block (2005-2000), has inline (880 - 1420) and crossline (868 - 1458), which is covered 450 Km².

- **Well Database**

The data included well logs for 7 wells scattered through the study area ranging in TD about 6900 ft. In the table (1.1) list of the wells used for calibrate them with seismic through synthetic seismogram. Table (1.2) shows the formation tops of the Upper Cretaceous succession.

Table-1.1: Data list of the wells in Block-A1A2 (2005, 2000) used in this study.

Well Number	VSP	DT	GR	Ω	Status
W-A7	yes	yes	yes	-	Oil well
W-B3	yes	yes	yes	-	Oil well
W-B4	yes	yes	yes	-	Water well
W-A2	yes	yes	yes	-	Oil well
W-B2	yes	yes	yes	yes	Oil well
W-C4	yes	yes	yes	-	Oil well
W-C1	yes	yes	yes	-	Oil well

Table 1.2 Formation tops in selected wells

Formation Tops (ft.)	W-A7	W-B3	W-B4
Sirt shale	5187	4964	5064
Tagrifet	5434	5258	5337
Etel	5584	5497	5512
Lidam	5957	5768	5854

1.6 Statement of Problem

- Deteriorates notably at Lidam Dolomite reservoir within fault zones.
- The complicated tectonic style and small size of some closures.

1.7 Objectives

The main objective of this study is focused on extended 3D seismic interpretation by using attributes to gain better understanding of geologic features and reveal the ability of attribute to play important role in further exploration to avoid risks.

The Specific objective of this study can be summarized in the following points.

- Identify the structural style and recognize the regional implication.
- Using multi visualization techniques to enhance structural and stratigraphic features.
- Optimize synthetic seismograms to calibrate the well depth with seismic times.
- Improve results and accuracy of structural and stratigraphic identification and delineation.
- Using stratigraphic attribute in interpreting horizons, seismic facies and zonation.
- Using discontinuity attributes to enhance interpretation of fault modeling, pillar gridding and 3D structural grids by manual and automatic fault extraction.
- Using texture attribute to understand the lithology characterization.
- Study the achievement of polarization AVO (Amplitude with Versus Offset).
- Using well log correlation to define the structural and thickness variation of formations.
- Using statistical attributes to measure brightness, delineate closures and fluid location.
- Qualitative and quantitative of fault displacement.
- Recommend potential hydrocarbon prospect for future hydrocarbon exploration.

CHAPTER TWO

GEOLOGICAL SETTING

2.1 Introduction

Sirt Basin represents a major part of North Central African rift systems, it covers an area of approximately 600,000 km² and is mainly composed of discrete of horsts and grabens. The origin of the rift is believed to be related to the opening of Atlantic resulted in an apparent eastward movement of Africa relative to Europe (Anktell, 1996). Geology and structure of the basin was developed as a result of extensional regime with different orientation subjected to strike slip movement (Abadi, 2002). The tectonic features are represented from east to west by Ajdabiya Trough, Hameimat Trough, Sarir Trough, Marada Trough, Kotla Graben, Zella Trough, Dor El Abida Trough and finally Hun Graben. They are separated by Amal Platform, Rakb High, Zelten Platform, Beda Platform, Dahra Platform, Waddan Uplift (Figure 2.1).

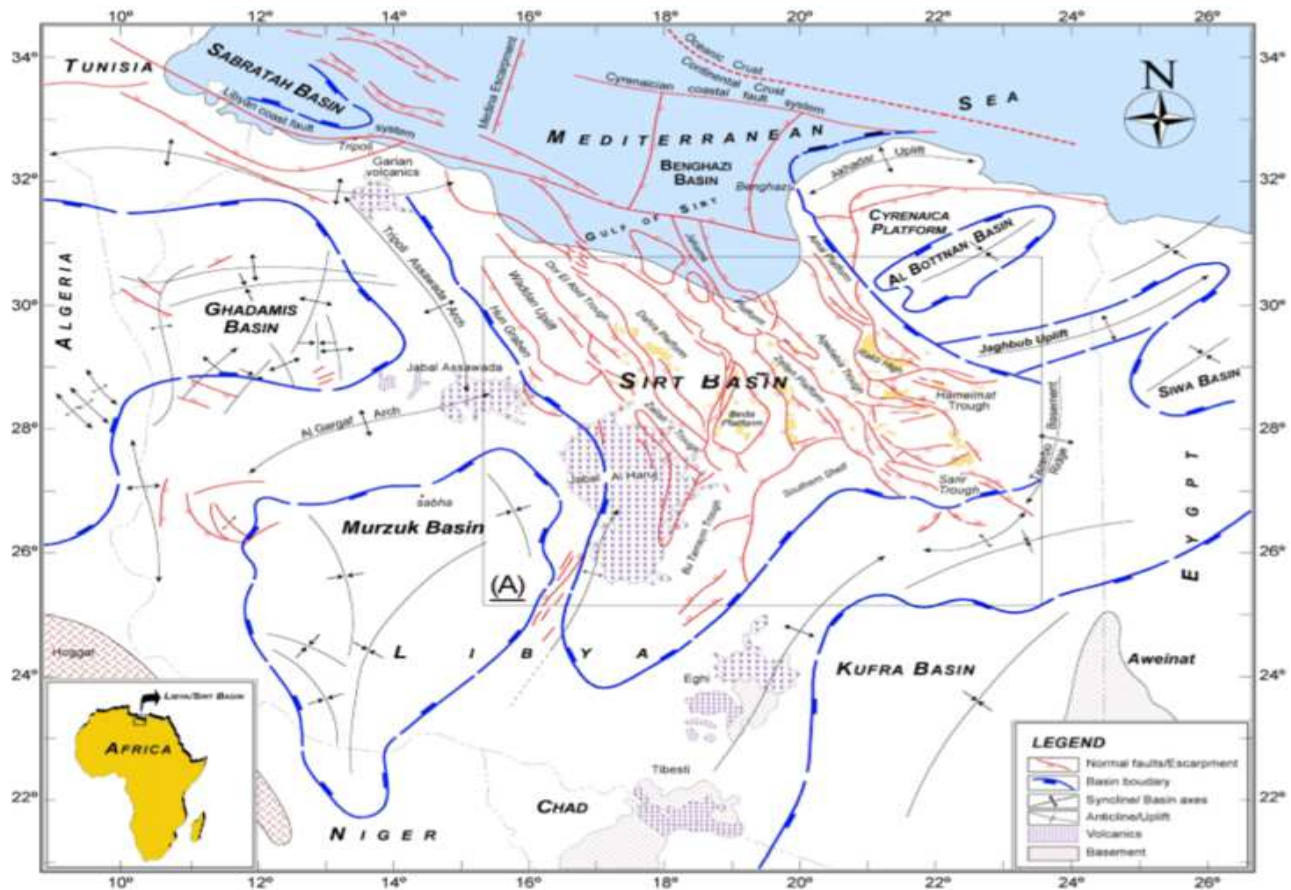


Figure 2.1, Structure map showing the tectonic framework of the Sirt rift complex (Abadi, 2002).

2.2 Tectonic Setting

The Sirt Basin is a part of the Tethyan rift system development include plate tectonics of relative motion between Africa and Europe (Futyán and Jawzi, 1996; Guiraud and Bosworth, 1997). The structural weakness of the area is exemplified by a series of N-S to NW-SE of uplift and subsidence originating in Late Precambrian time, commencing with the Pan African orogeny that consolidated a number of proto-continental fragments into an early Gondwanaland (Kroner, 1993), which controlled sedimentation in the early Palaeozoic (Bellini and Massa, 1980; Anketell, 1996), followed by Carboniferous deltaic deposition. Hercynian orogeny during Permian to Jurassic resulted uplift remove Paleozoic sediment and the deformation in NE-SW trends (Hallet, 2002).

Sirt Basin experienced multi-phase subsidence from Cretaceous to recent periods in response to the changes of regional crustal stress, which is contains may mechanisms are combined to form the basin and affect in its deposition. It was initially believed that main phases could be distinguished as following;

- The first phase of subsidence was fairly active and widespread, characterized by early stage of rifting and Late stage of thermal contract sagging (Hallet, 2002). The combination of strike slip movement of sinistral shear zone related to Sabratah-Cyrenaica Fault Zone (SCFZ) toward E-W and WNW-ESE structure domain, and normal extension mechanisms that strongly controlled clastic deposition in several rift troughs (Anktell, 1996). In Aptian age, concurrent transtension subsidence set of NE- SW faults (extension direction) initiated in syn-rift stage related to a paleostress field associated with the interaction between Europe and Africa (Anktell, 1996; Gras, 1996; Guiraud and Bosworth, 1997; Ambrose, 2000; Hallett, 2002).
- The next phase is compressional event at the Santonian age was dominated by the northern motion of Africa (closing the Tethys) and movement of the Arabo-Nubian block toward the west. Theses has been effect the attributed of collision the African with Europe plate. During this phase the basin uplifted (structural inversion) by dextral transform movement and was exposed to erosion. As a result of this compression event, negative and positive flower and numerous hydrocarbon traps have been developed (Anktell, 1996).

- In Campanian, the second stage of subsidence is characterized by NE-SW developed the reactivation of extension. The extension was resulting from sharp change of the direction motion of Africa from east to northeast. As a result of the NW-SE crustal compression started during Santonian period by produced sinistral shearing, movements along the main faults (Hallett, 2002).
- The third phase of subsidence occurred between middle Eocene to Paleocene periods. The extension movements create a sag phase related to African plate motion toward west then north east (Gumati and Kanes, 1985).
- In Latest Eocene ages, a major compressional event occurred along Tethyan African–Arabian margin, reactivated the NWSE faulting a strike-slip feature associated with the relative motion of two plates (Gumati and Kanes, 1985). In Oligocene-Early Miocene, the change in the relative movement between Africa and Europe seemed similar to those recorded during the Paleocene, bringing a dextral strike-slip reactivation, a structural reversal (Gumati and Kanes, 1985). In Miocene to Present, a large tectonic movements are responsible for another reactivation of NW-SE faults in response to the dextral strike-slip motions of the Sabratalh-Cyrenaica Fault Zone (SCFZ). The African Plate moved distinctly towards the north (Gumati and Kanes, 1985).

2.2.1 Major structural elements impact in the Bualwan, Dor Mansour fields

The study area is located in the south western part of Dahra Platform, where it occupies a 40,000 km² area (Figures 2.1). Located in the western part of the Sirt Basin between the Dur El Abida and Zallah Troughs to the west and the Maradah Trough to the east and is bounded on the south by the NNE-SSW trending Kotlath Graben which separates it from Al Bayda Platform. Major fault zones as following;

- Gedari fault is one of major fault zone in the western Sirt basin, which lies close to the assumed junction between the basement west and east African plates. Gedari fault was active during the Cretaceous and reactivated as sinistral wrench faults in Paleocene and early Eocene time (Anketel, 1996; Jerzykiewicz, et al.2002). The next phase of extensional faulting combined with strike-slip movements along the Gedari fault is recorded in late

Eocene and post-Eocene times, which is defined by NNE-SSW trending, which provide a sense of relative down throw across the fault zone.

- On the southwest margin, the Gattar Ridge is formed by down faulting to the WSW (Anketel, 1996).

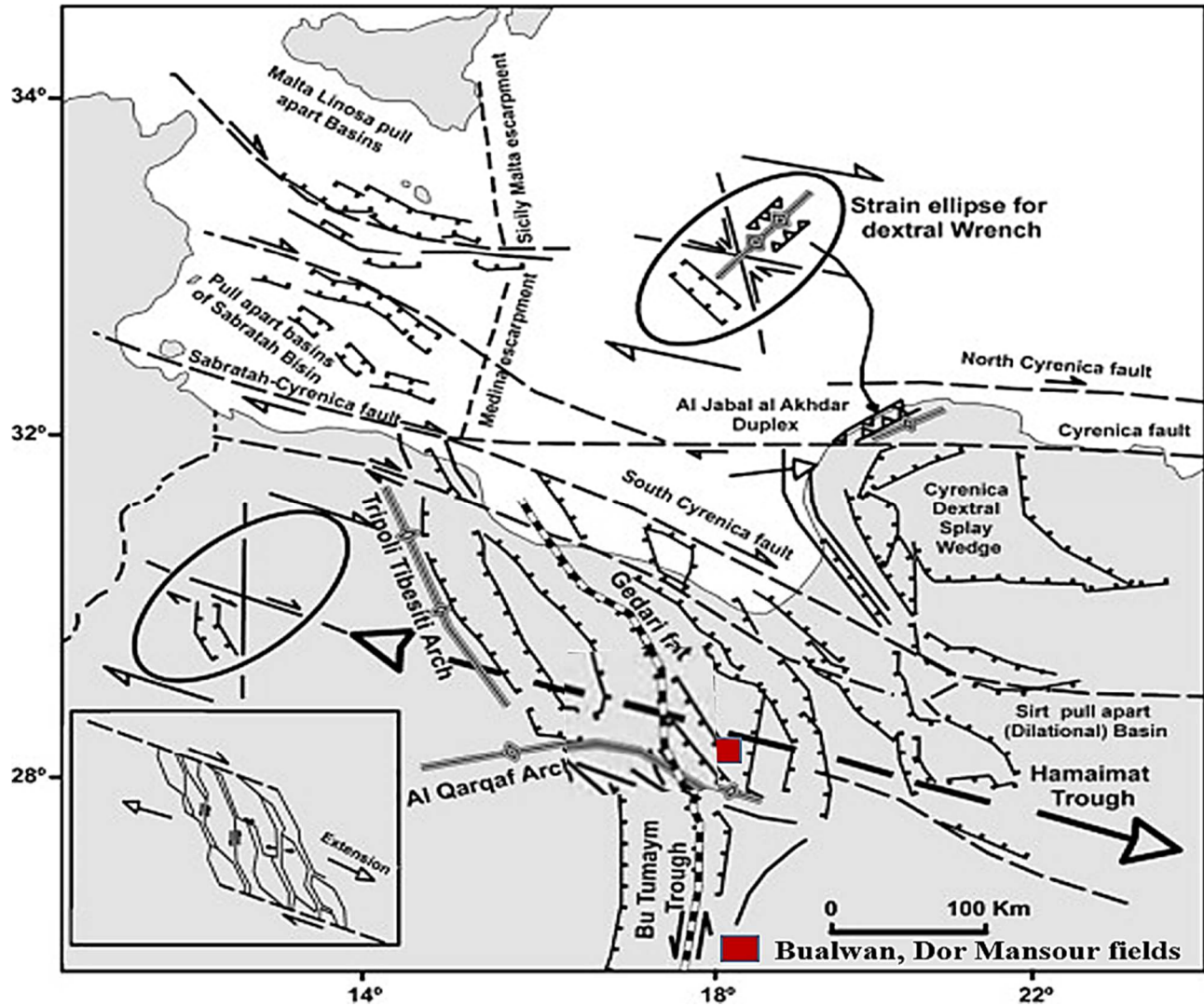


Figure 2.2, Tectonic interpretation of Sirt rift complex (Anketell, 1996).

2.3 Depositional Setting and Stratigraphy

In the Bualwan, Dor Mansour fields, three rift cycles base on W-B3 composite well log data are recognized and dates (Figure 2.5). Each tectonic cycles seems to consist of a rift initiation phase, active rifting phase and thermal sag phase, as following;

The first cycle is Pre-rift sediments (Paleozoic-Triassic).

The second cycle is Syn-rift basin, subivied into three stages are;

- Syn-rift (1) began with continental-marine siliclastic rocks.
- Syn-rift (2) deposition characterized by marine siliclastics and carbonate rocks.
- Syn-rift (3) finally characterized by continental siliclastic strata.

The third cycle is Post-rift basin fill, deposition characterized by carbonate and evaporate strata.

In this progress work, the study is limited in Upper Cretaceous marine sediments. Many authors suggested this period have more eventful to tectonic evolution and the attendant sedimentation history, which was probably controlled by a combination of tectonic, structural movement and sea-level changes (Sinha and Mriheel, 1996).

Upper Cretaceous Syn-rift basin fill (2), consists of four formations are Sirt shale, Tagrift limestone, Etel and Lidam. The total thickness over 1300` feet. Deposited above the unconformity includes the Gergaf Group represents stable shield sedimentations unconformably on the Pre Cambrian basement., which is filling grabens and lows areas as a result of transgressive and regressive depositional cycles (Gumati and Kanesh, 1985).

2.3.1 Lidam Formation (Cenomanian)

The first distinctive marine formation overlying the Gergaf (Early Cretaceous deposits) and overlain by Etel open marine deposits, as an excellent cap for the oil entrapment. The thickness based on well W-B3 about 380 ft. The environment of deposition is lagoonal to intertidal based on W-C5 composite well (Figure 2.4). As the first unit of the Cenomanian marine transgression, acts as good indicators for paleogeography of the Sirt Basin (Hallet, 2002).

The diagenetic history of the Lidam Formation in the northwest Sirt Basin was studied by El-Bakai (1992). He concluded that the Formation has been greatly affected by diagenesis which began shortly after deposition with the burrowing activities of algae and fungi, and ended with extensive dolomitization which occurred after lithification and compaction. He interpreted limestone and dolomite as accumulating units of Lidam in tidal flat settings of supratidal, intertidal and subtidal environments. The upper part of Lidam (reservoir section) is shallowing up-ward sequences dominated by intertidal-upper subtidal environment, which is considered as a significant oil reservoir in several areas (Hallet, 2002). Lidam is the primary reservoir in the study area.

2.3.2 Etel Formation (Turonian)

Lidam overlain by thin bedded open marine carbonate, which is gives a distinctive contrast during the interpretation. The Etel thickness variance from 150-365 ft, which is conformably overlain by the Tagrift Limestone Formation. The environment of deposition is sabkha /logoonal (Hallet, 2002).

2.3.3 Tagrift Formation (Late Santonian-Early Campinain)

Tagrift Limestone is the secondary reservoir is in the area, which is deposits in very shallow water deposits. The lower part consist mainly of well indurated, porous calcarenite, and the upper part is usually a more argillaceous calciluttite, less porous with occasional shale interbeds with limestone/ anhydrite beds. The distinct limestone horizon, which is conformably overlain by the Sirt Shale and overlies the Etel formation. . However, limestone stringers occasionally develop in the basal Sirt Shale giving the contact a gradational appearance as shown in Figure (2.4).

On the well cross section, the log interpretation of Tagrift Limestone was indicating that three intervals in W-B3 well, consists of argillaceous limestone are common and glauconitic and pyritic in parts in the lower part. The GR log response is usually high against the limestone, according to the high radioactive contents in the limestone of Tagrift beds.

2.3.4 Sirt Shale Formation (Campinain-Maastrichtan)

Sirt Shale at the top of the Upper Cretaceous succession, is conformably overlain by the Gheriat Formation, and the contact can be picked clearly either by lithologic or electric-log characteristics, and it disconformably overlies Tagrift Limestone Formation. The formation was initially deposited in a shallow restricted marine environment, rapidly subjected to deepening (Duronio and Colombi, 1983). According to Barr and Weeger (1972) Sirt Shale consists of a shale sequence with thin limestone interbeds and consider as sealing limestone for Tagrift Limestone reservoir. On the well cross section (Figure 2.3), Sirt Shale has reflect very high reidoactive value, the upper limestone-rich part consists of argillaceous limestone in parts and changes to pure shale upward.

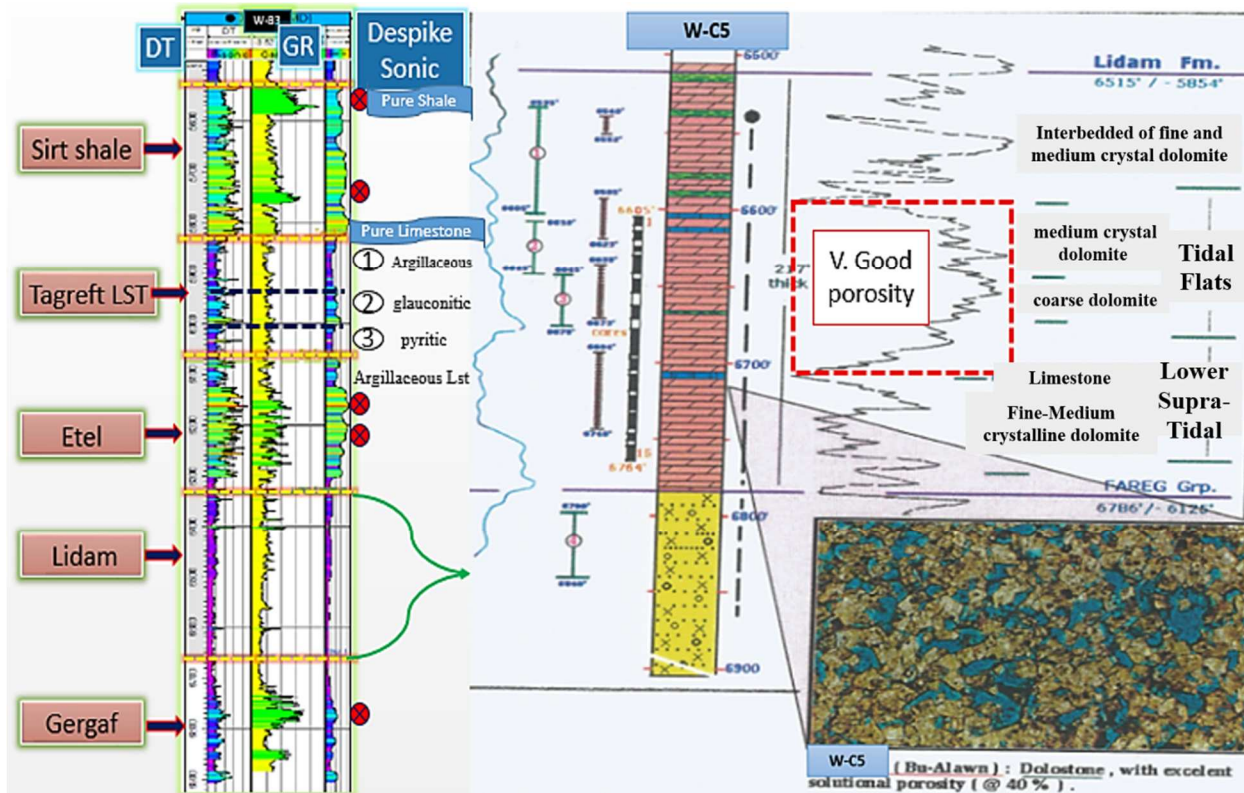


Figure 2.3, Well W-B3 profile shows five different formations where interpreted based on the wireline- log lithology changes and composite well data of well W-C5 within Lidam Formation (AGOCO, 2009).

2.4 Petroleum System in the Study Area

The significant source rock and different type of seals such as anhydrite, and salt/evaporates related to El-Kotla Graben has a production potential from carbonate reservoirs rocks up to 5000 BOPD per well (Hallett, 2002). Roohi, (1993) suggested the charged by vertically migrated pathway from El-Kotla graben along the fault zones adjacent to horsts and grabens. However, impermeable rocks are the most importance to petroleum accumulation because of forming essential seals for the hydrocarbon migrating out of the Upper Cretaceous to fill Lidam and Tagrift reservoirs (Barr and Weeger, 1972). Hallett, (2002) (Figure 2.5) simulated the petroleum system as the vertical migration of oil in the western Sirt Basin from major troughs to the horst. In the study area the charged oil vertically pathway from El-Kotla Graben.

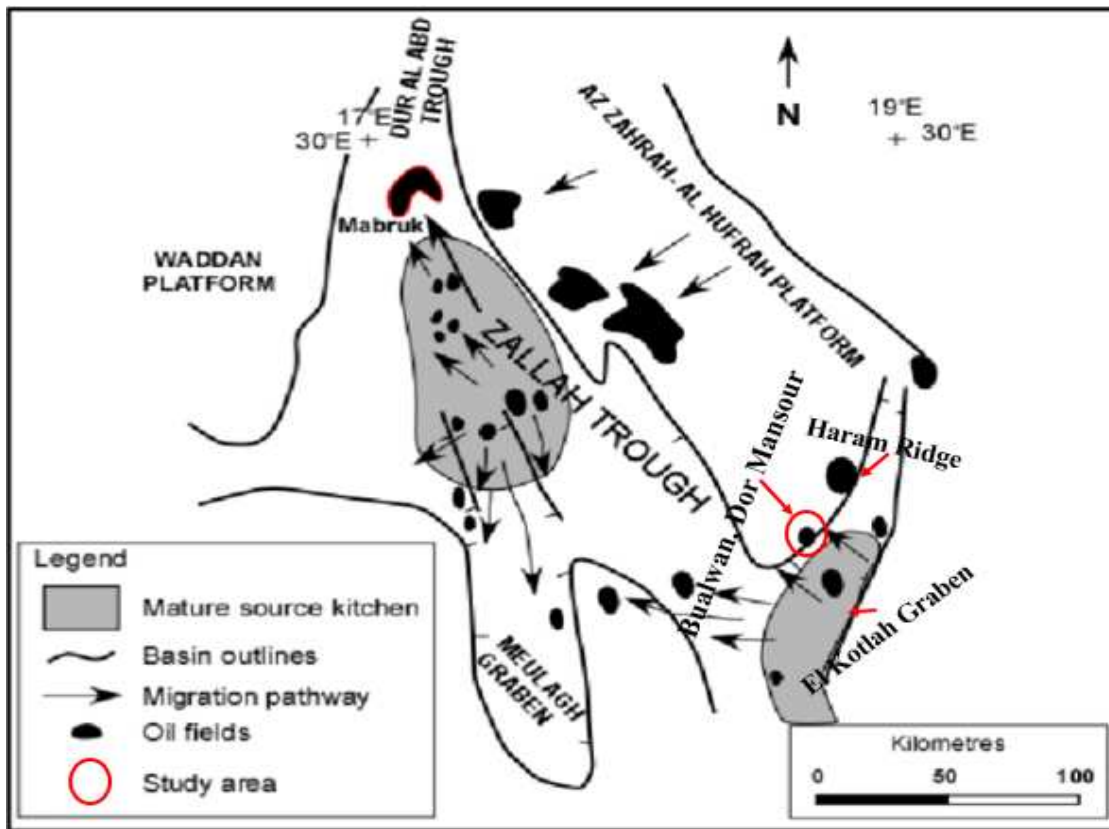


Figure 2.5, Petroleum system in the western Sirt Basin (Hallett, 2002).

CHAPTER THREE

SOFTWARE METHODOLOGY AND VISUALIZATION TECHNIQUES

3.1 Seismic data inputs/ Co-ordinate systems

The 3D seismic data volume Seg Y files imported into Petrel 2015 work station and the location of the seismic volume referenced to the geographical coordinate system, The Universal Transverse Mercator (UTM) coordinate system was applied by AGOCO Processing Department using grid method to specify locations on the surface of the Earth and a practical application of a 2D Cartesian coordinate system (as shown in Figure 3.1 A). Interpreted seismic data have been used by seismic volume and attribute analysis includes the inline, cross line, arbitrary line and time slice (Figure 3.1 B). The 3D seismic data volume contains 500 inline numbered from 859 to 1459 and 600 crosslines numbered from 880 to 1380 (Figure 3.2). The interpretation concentrates on Upper Cretaceous succession ranges from 600 ms to 1200ms based on formation tops and established synthetic seismogram.

3.2 Well Log Data

The data includes well logs for twenty one wells scattered through the investigation area (Figure 3.2). A set of logs for each well include: sonic, gamma ray logs, well velocity survey (check shot) (Appendix, table 1) and formation tops.

3.2.1 Lithology Calibration

This step was very important in order to interpret Upper Cretaceous lithologies accurately. GR logs were used in the calibration and correlation.

3.2.2 Formation Analysis

Upper Cretaceous succession were identified on the basis of trends of lithologic interpreted from wireline logs. These orders indicate the depositional environmental change in variable scales.

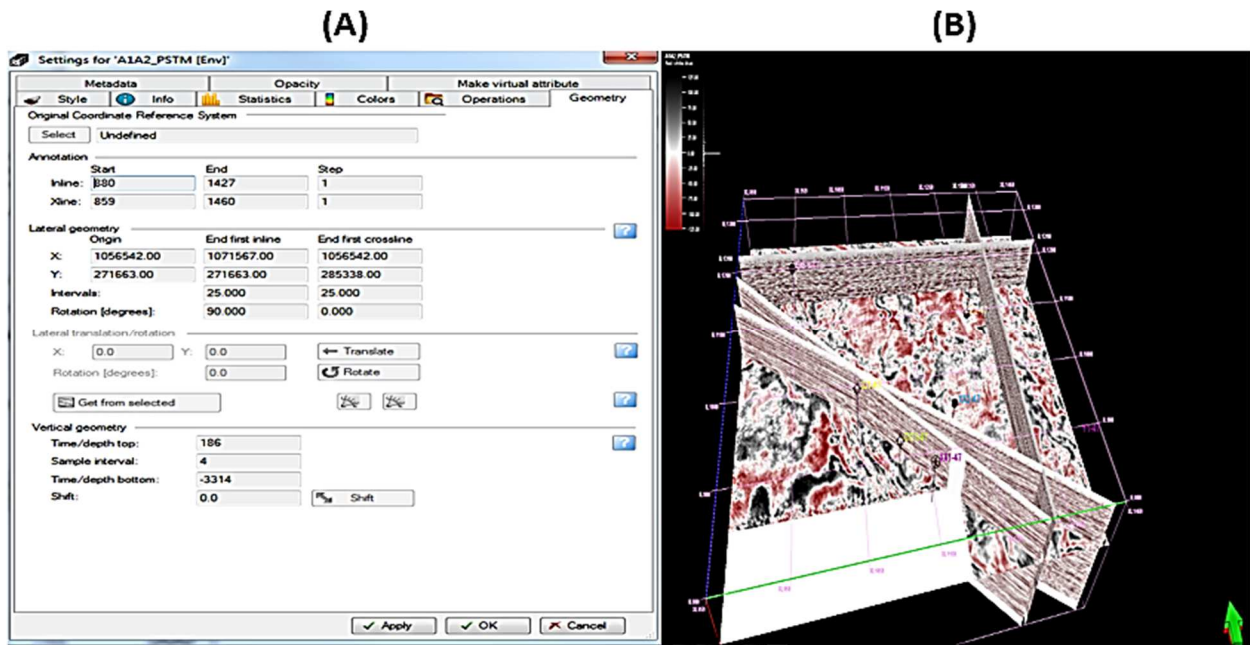


Figure 3.1 (A) header parameters, inline and crossline ranges, co-ordinate systems of lateral geometry, and vertical geometry, (B) the seismic volume, capturing the inline, cross line, arbitrary line, and time slice.

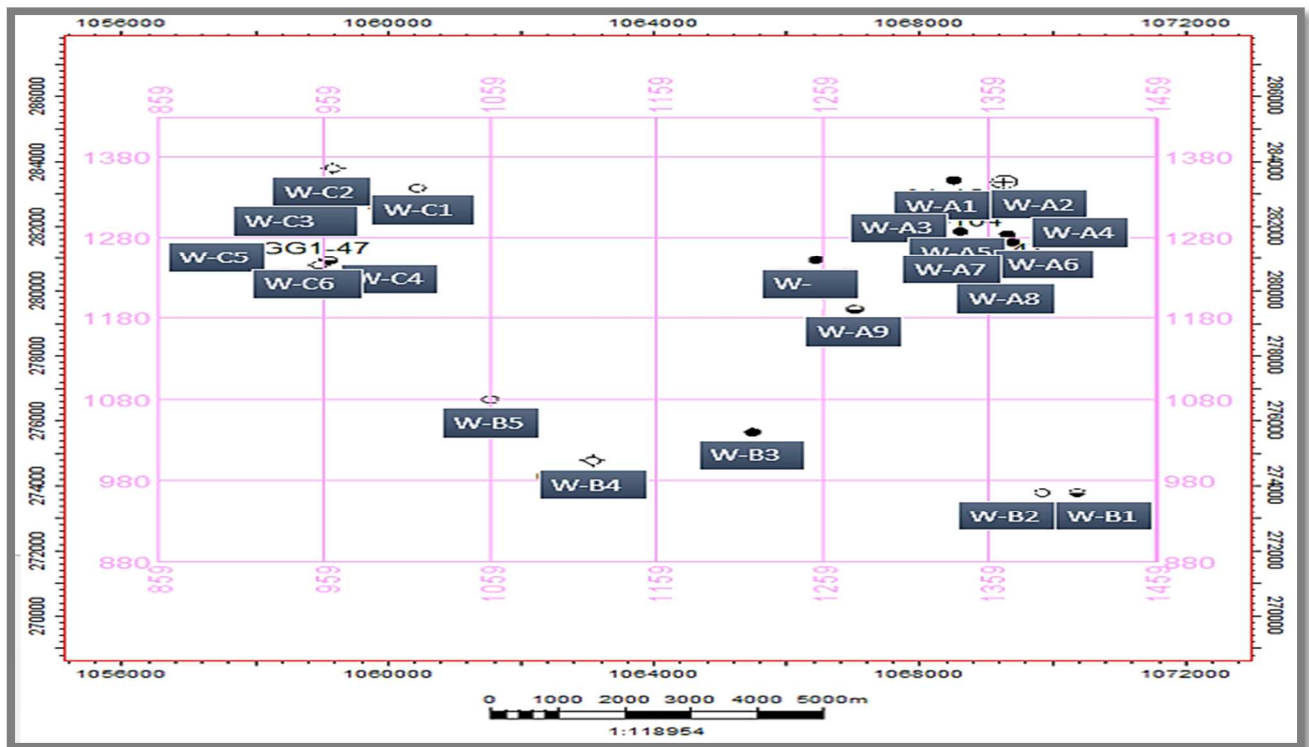


Figure 3.2, Base map shows inline, crossline with location of 20 wells scattered in the study area (AGOCO).

3.3 Seismic to Well Tie

The fundamental inputs are sonic logs, checkshots, density log and extracted wavelet from seismic data, it is a critical step because poor quality log input to synthetic seismogram generation can give inconsistent results.

3.3.1 Log Editor (Despike Sonic Log)

Sonic correction used to remove spike values (Despike), because error readings will accumulate when integrating the sonic value and effect in velocity measurement. On the well W-B3 used 0.4 Std. deviation and 3 length gives satisfied result (as shown in Figure 3.3).

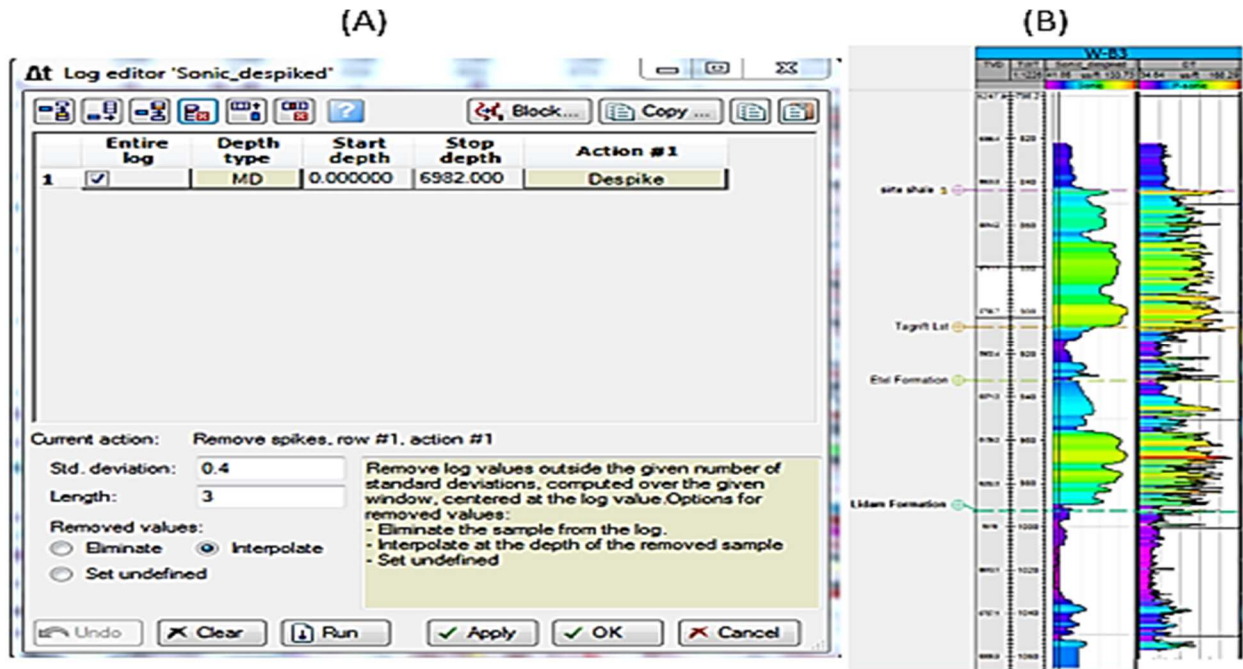


Figure 3.3, Log editor setting to correct sonic readings (A) parameter settings, (B) Despike Well log profile of W-B3 aid to recognize easily Upper Cretaceous sequence by remove spike values.

3.3.2 Import Check Shots

Checkshots (CS) are used to place the sonic log in depth and time correctly, based on total vertical depth (TVDSS) referenced to mean sea level (MSL). The average and interval velocity values are derived from the input time-depth pairs, while sonic time and sonic interval velocity come from the input sonic log, and drift is the difference between the two data sources.

3.3.3 An Estimated Density Log

The density log of well W-B3 was unavailable, so the Gardner approximation equation used to establish an estimated density log (RHOB) from despiked sonic log. (Figure 3.4).

Gardner approximation equation: $Density \left(\frac{g}{c^3} \right) = Constant * Sonic^e \left(\frac{ft}{s} \right)$

Constant (imperial) is 0.229907; Exponent is 0.25.

3.3.4 Wavelet Extraction

Wavelet extraction was created based on 3D seismic cube and well W-B3. However, the calculation of acoustic impedance as the ratio between density and despiked sonic log and reflection coefficient derived from acoustic impedance. This was applied by time shift plus half sample operation in Petrel. So that an impedance log and reflection coefficient are generate from the velocity and density profile, (Figure 3.4).

3.3.5 Synthetic Seismogram

Generation synthetic seismogram was performed to tie seismic reflections data with specific well data. Bulk shift has been used to set a good visual matching of individual peaks and troughs seismic reflection and their patterns of formation boundary near well W-B3, (Figure 3.4) Interval velocity profile and density log with seismic section inline 1040 have been used which gives critical value for delineating lithology accurately. The higher interval velocity at Sirt Shale and Etel more than reservoir interval Tagrift and Lidam. As well as the higher density value at reservoir sections more than Sirt Shale and Etel formations (Figure. 3.5).

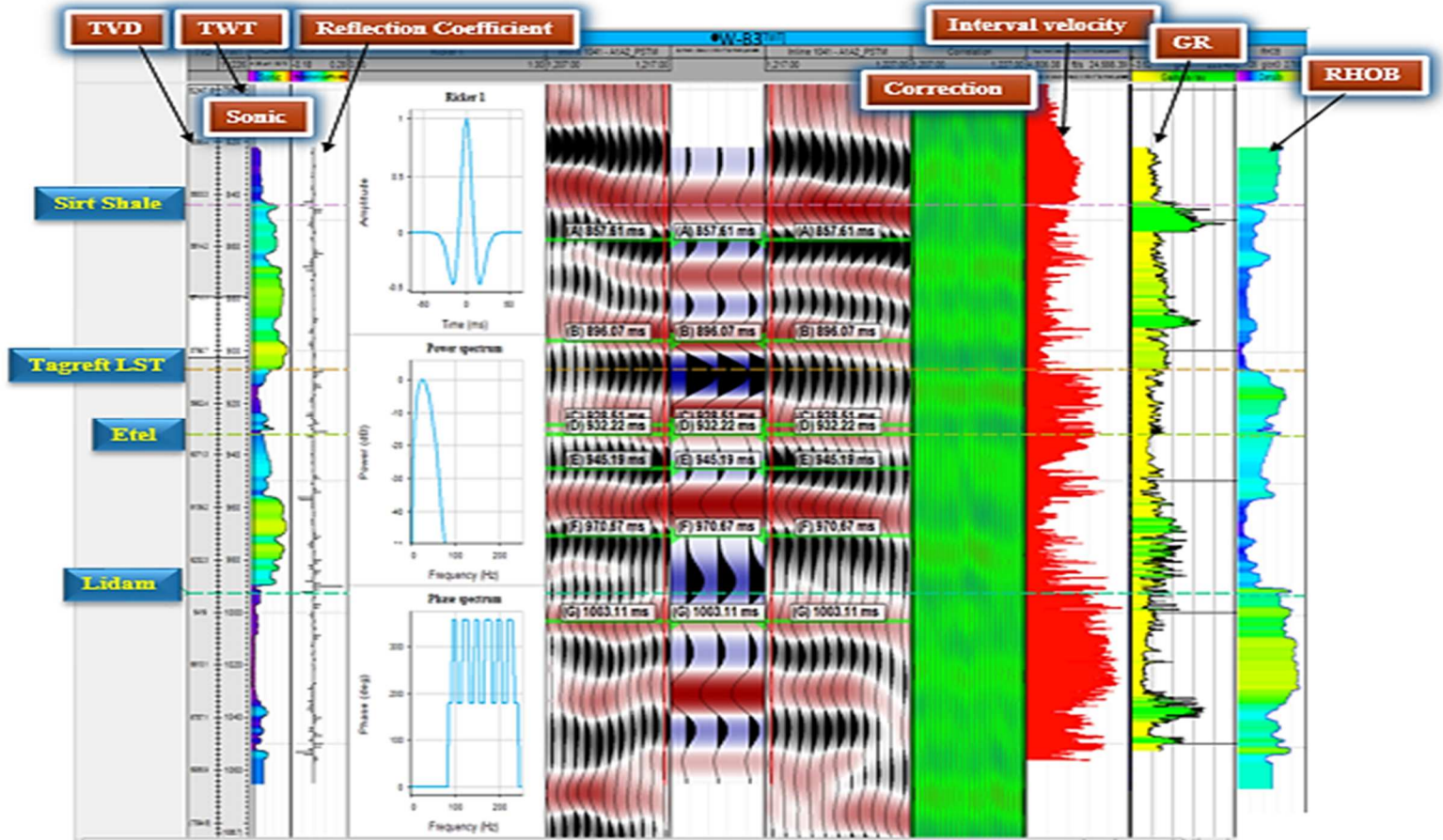


Figure 3.4, A synthetic seismogram constructed for well-B3 Wavelet extraction of Rucker (zero phase), with power spectrum, and phase spectrum. Estimated density log, and GR log.

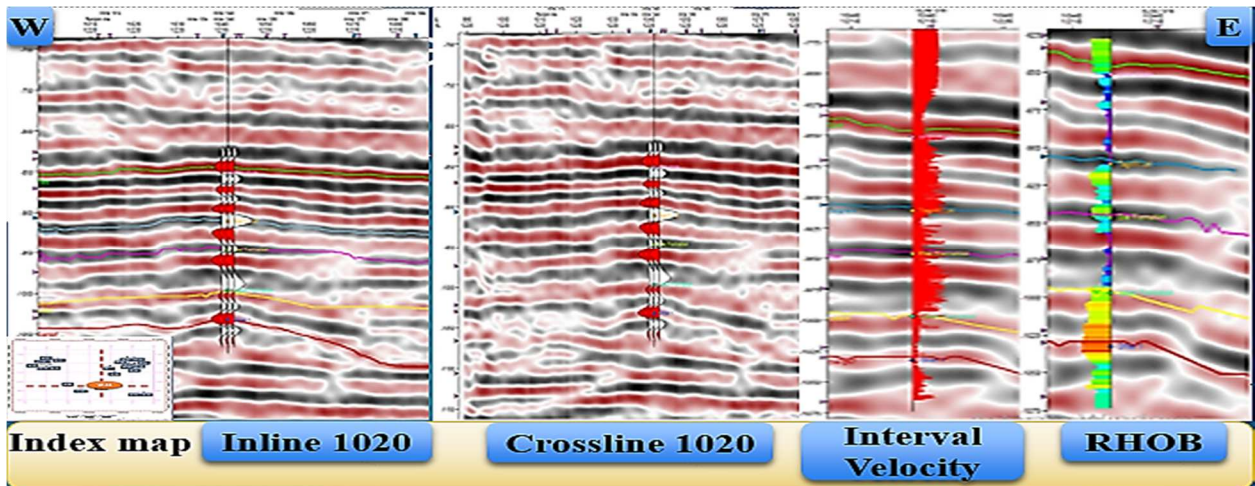


Figure 3.5, A synthetic seismogram of well-B3 overlaid on a vertical seismic section crossline 1220 with inline 1040, and five horizon picked on seismic.

3.4 Volume Visualization/Volume wall display

Visualize 3D volume used to enhance quality of interpretation by viewed relation of geological features with attributes. In this study, three techniques have been used including normal wall displays, transparent and inside display. Normal wall displays viewed solid 3D volume provides outward frame of general trend of interest features such as large fault planes, listric normal fault, horst and graben structures (Figure 3.6 A). Transparency inside wall displayed the internal relationship of features in the seismic to other data, for example, first viewed seismic volumes with the internal well geometries and spatial position, gives information of the well target depths either shallower or deeper when compare to the reservoir depths to determine the suitability of the wells for correlation purposes (as shown in Figure 3.6 B). Second provides better understanding of seismic features with fault sticks interpretation (Figure 3.6 C). 3D view of transparent displayed interested section with grid surface, which is give a reference dimension of segment (Figure 3.6 D).

3.4.1 Color and Opacity Filters

Visualizing seismic property applied by ranging color scales related to amplitude spectrums or frequency distribution, with different attribute. It is continuity of reflectors were easy to define with specific color scales for seismic interpretation (Figure 3.7).

3.4.2 Cropping

Cropped used to isolate specific depths interval include Upper Cretaceous succession ranging from 600 ms to 1200 ms entire seismic volumes (Figure 3.8), to allow extra advantage of speed in carrying out interpretation by minimize size of store to be much easier and quicker, and to validate properties of the sub volume before making general applications. Attribute analysis such as ant track process of fault extraction cropped at specific target zones to pre tested before final parameter application to the whole seismic volume.

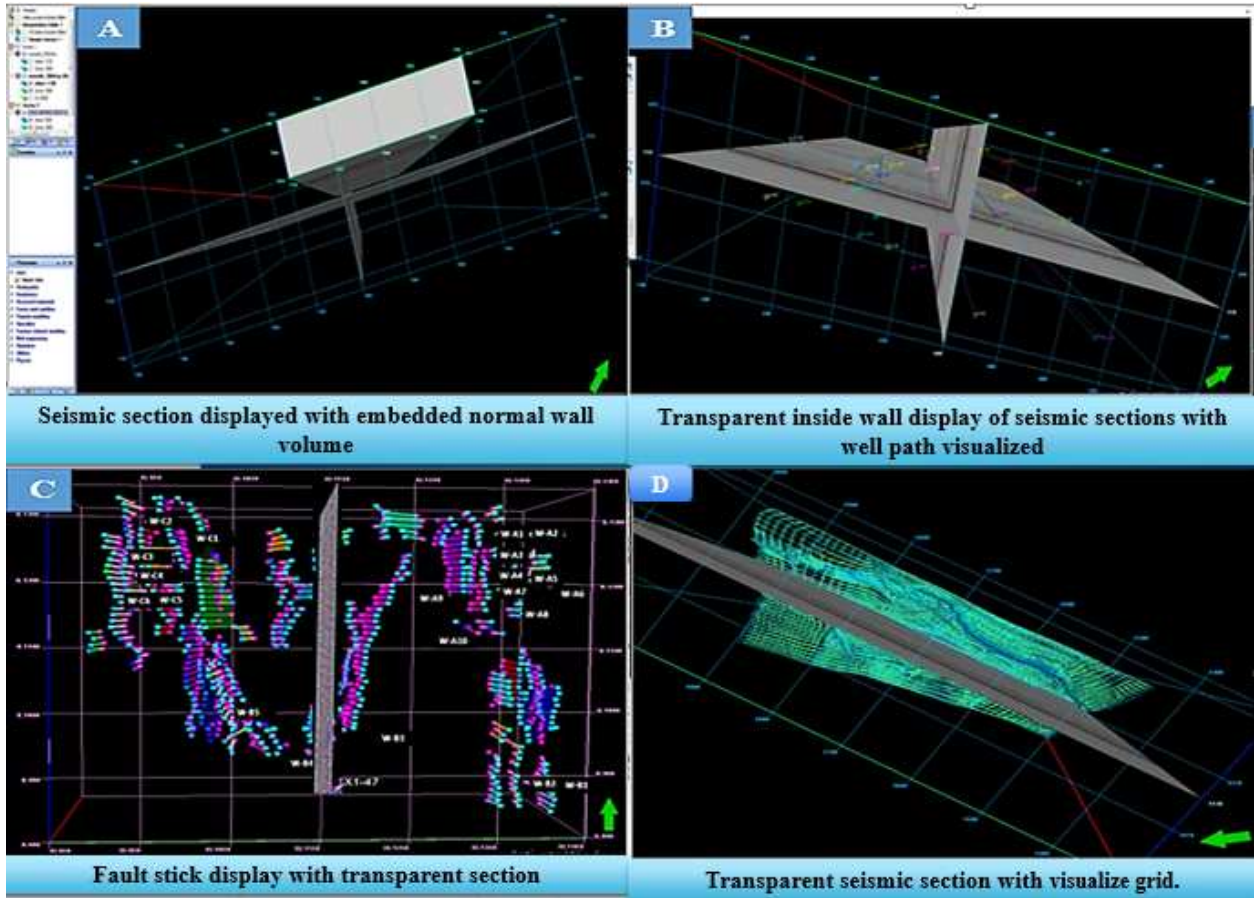


Figure 3.6, (A) seismic section displayed with embedded normal wall volume. (B) Transparent inside wall display of seismic sections with well path visualized. (C) Fault stick display with transparent section. (D) Time slices. (E) Transparent seismic section with visualize grid.

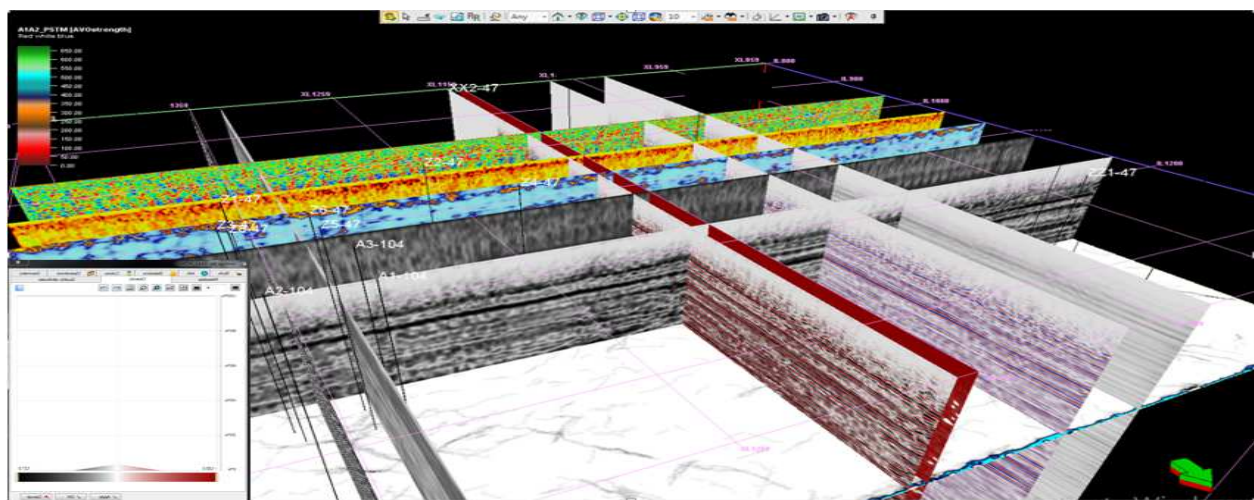


Figure 3.7, Color display of realized section, and different seismic attribute.

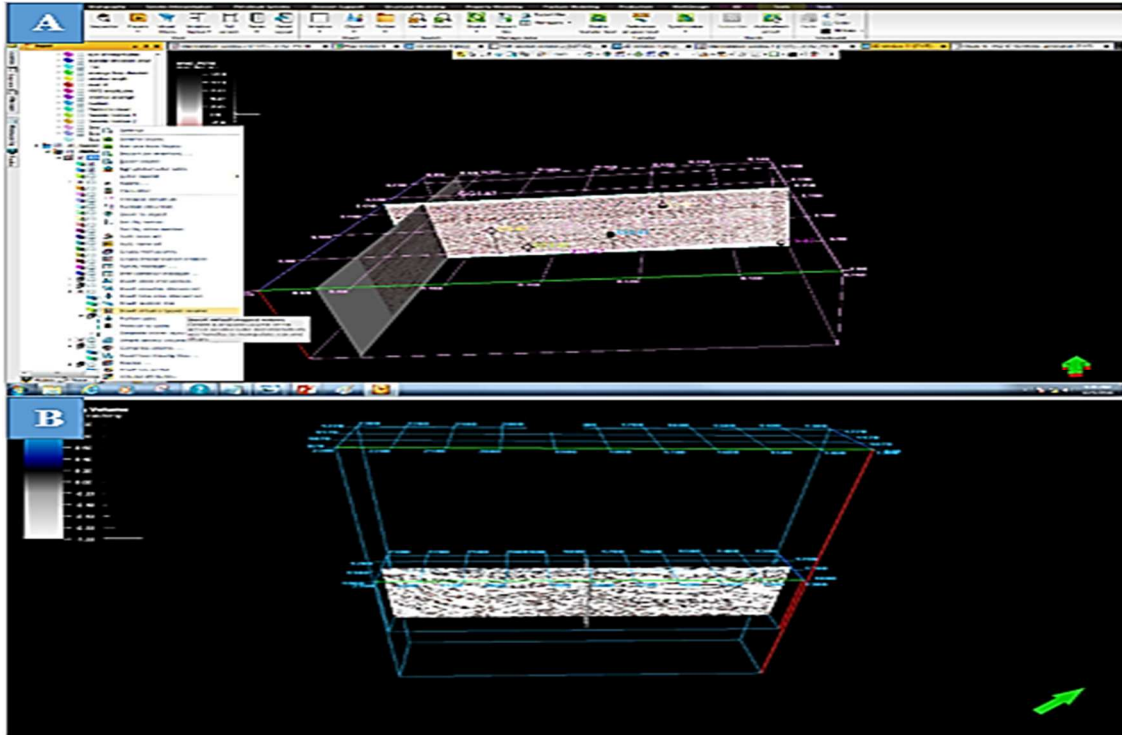


Figure 3.8, (A) Create a cropped volume of the active seismic cube and interactively use handles to manipulate size and shape. (B) Cropped reservoir section realized for ant track process and visualization.

3.4.3 Volume Realization

Realize volume used by create exact physical copies of the original seismic (Figure 3.9, A) to make final comparison between original volume and changes in the value resolution. The realization of time slice used with typical differences in color to observe property changes, such as detecting structures effective, and determine the extent of fault planes, (Figure 3.9, B). Realized seismic section introduce more advantage by interpreted structural and stratigraphic features easier, such as view the continuity of reflectors.

3.4.4 Volume Rendering

Volume rendering used by sum total of all visualization techniques have been discussed, which is applied for corrections, quality assurance of interpretations of faults, and to provide collection of the interesting geologic elements for complete interpretation, such as relation of

interpreted surface seismic horizon to the seismic volume (Figure 3.10, A), automatic fault patches module derived from ant track volume (Figure 3.10, B). fault model derived from manual fault extractions (Figure 3.10, C), and rendering provides a dynamic property change in relative position of features in 3D view, which is not available in display function (Figure 3.10, D).

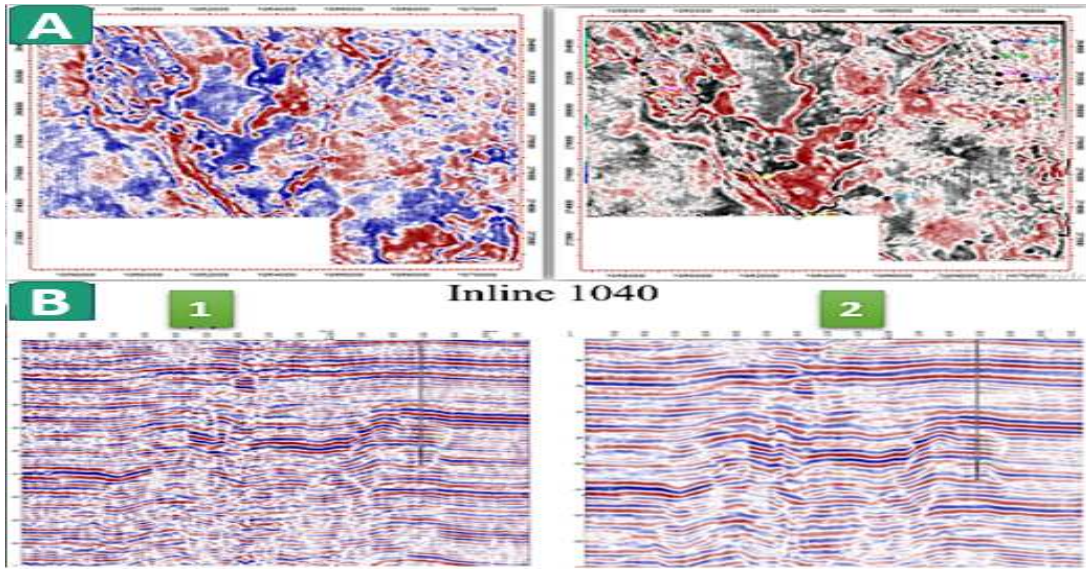


Figure 3.9, (A) Realize volume operations, (B) Original and realized time.

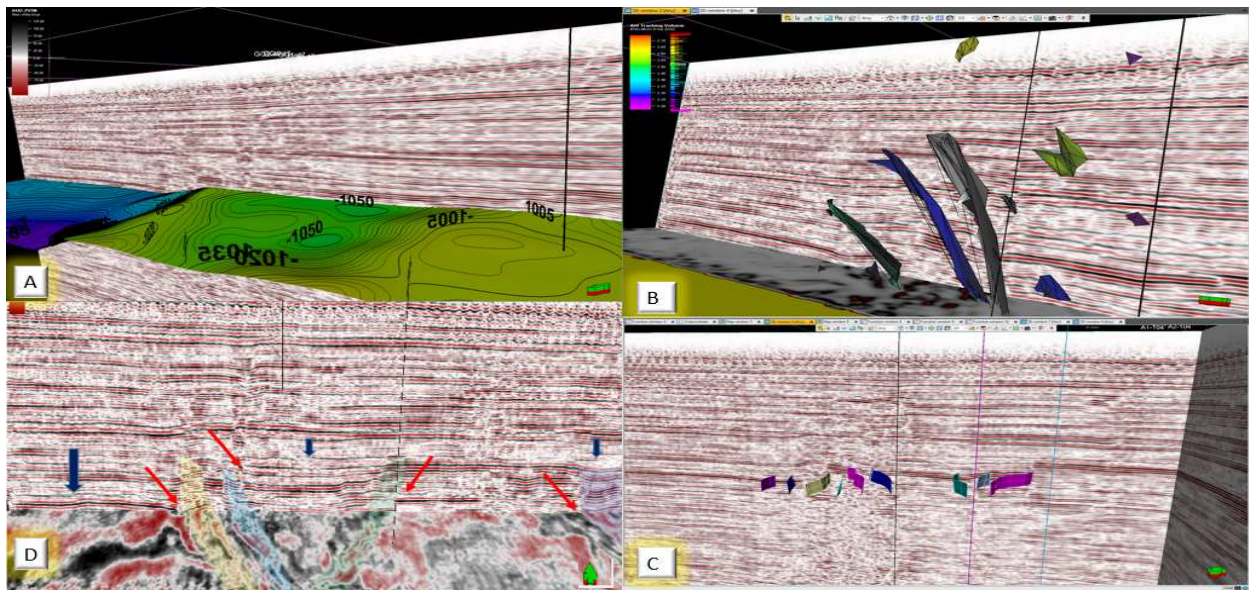


Figure 3.10, Relation of seismic volum with (A) lidam map, (B) fault patches, (C) fault model, and (D) display the gains of rendering process.

CHAPTER FOUR

SEISMIC ATTRIBUTES AND THEIR SIGNIFICANTS

4.1 Introduction

Seismic attributes defined as all the information obtained from seismic data, either by direct measurements or by logical or experience based reasoning (Liner et al, 2004). The concept of attribute is to provide a dynamic, geometric and kinematic characteristic of a seismic volume. Critical parameter for attribute analysis could be structure related petrophysical properties, internal architecture and hydrocarbon properties (Cosentino, 2000).

Seismic attributes were introduced in the early 1970's as a display form and later combined with seismically derived measurements to become an analytical tool for interpreters to study reservoir characteristics (Taner, 2001). In the mid 1970's Anstey introduced there were three attributes are reflection strength, mean frequency attributes and showed color overlays of interval velocity, by compute rate of change of any of these with respect to time or space, Taner et al (1979). Today there are over 300 defined attributes (Taner, 2001).

4.2 Science of Seismic Attributes

The Hilbert transform is used to calculate attributes in seismic interpretation includes amplitude, phase, and frequency instantaneously (Hardage, 2010), where the computed in the manner of radio wave reception like wave propagation and simple harmonic motion.

The recognition of the recorded signal representing as the kinetic portion of the energy flux, Koehler proceeded and development of the frequency and time domain Hilbert transform programs to compute the potential component from its kinetic part, then realizing the potential component for extracting useful instantaneous information, which made possible practical and economical computation of all of the complex trace attributes.

The complex trace $z(t)$ is comprised of the real seismic trace $x(t)$ and an imaginary seismic trace $y(t)$. The imaginary trace $y(t)$ is calculated using the Hilbert Transform to apply a 90 degrees phase shift to every sinusoidal component of a signal. The real trace $x(t)$ and the imaginary trace $y(t)$ calculated using the Hilbert transform are added to generate the helical complex trace $z(t)$ has 3 dimensional space (x , y , and t), t is time, x is the real data plane, and y is the imaginary data plane (Figure, 4.1). At any time on this trace, a vector $a(t)$ can be calculated that extends perpendicularly away from the time axis to intercept $z(t)$ from this point, instantaneous amplitude, instantaneous phase, and instantaneous frequency can be calculated.

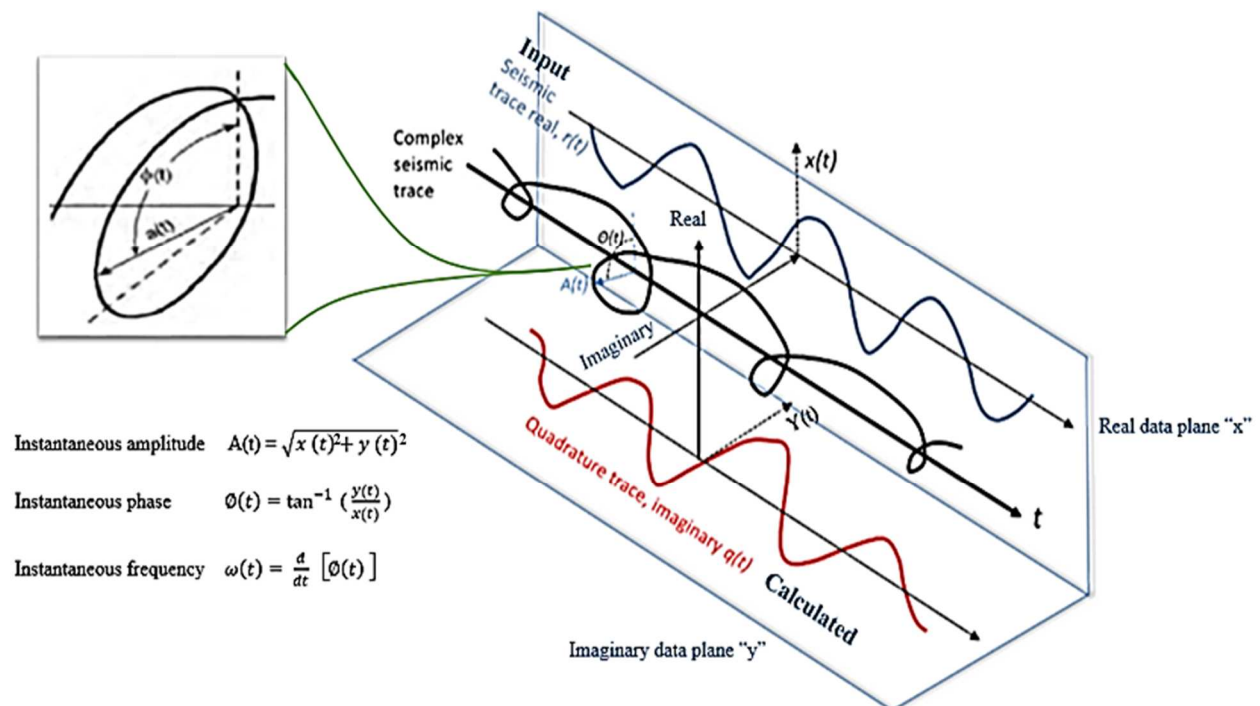


Figure 4.1, Calculate instantaneous seismic attributes from the complex seismic trace (Hardage, 2010, Modify).

Many of attributes have been used in both 3D seismic volume as well as to time structure map for each formation within Upper Cretaceous succession as surface attributes. These attribute measured successfully plenty of geologic criteria that aid for enhancing the interpretation. Twenty-nine attributes were generated to analyze more deeply since they aligned best with structural and stratigraphic variations. The attributes were generated for 3D volume and then applied to top of Lidam surfaces, which subdivided based on Schlumberger's Petrel 2015 Software into several categories contain types of attribute.

4.3 Classification of Seismic Attribute

Seismic attributes were classified based on their characteristics and measurements, which each kind of attributes introduce advantages that enhance and guide the interpretation to bring more details from seismic data. The attribute analysis have been used in this study divided into different categories, such as physical, geometric, amplitude surface attributes, texture attribute, statistical attribute, and AVO attributes. The long list of attributes combining all the categories means that its application has to be managed to produce the desired effect so as not to disabuse their application.

Table 4.1, Different attributes with specific physical and geometrical class, used in the progress work.

Classification of seismic attributes		
Physical Attributes Related to the wave propagation and lithology.		Geometrical Attributes Relate to shape of horizon as lateral continuity to emphasize discontinuous events.
<p>Instantaneous computed sample by sample and indicate instantaneous variations of various parameters.</p>	<p>wavelet attributes computed at the peak of the trace envelope (energy), represents characteristics of wavelet and their amplitude spectrum.</p>	<p>Structural Smoothing</p> <ul style="list-style-type: none"> Applied in local features to improve lateral continuity of seismic horizons especially fault surfaces, by smoothing the input signal. <p>Cosine of Phase Attribute</p> <ul style="list-style-type: none"> In delineating structural events as a guiding in interpretations in areas of poorly defined amplitudes, thin beds indicators. <p>3D Edge Enhancement</p> <ul style="list-style-type: none"> Enhance spatial discontinuities by measuring changes in the signal amplitude. In the local dip estimate of the reflection layers. Changes in the direction of the reflector will produce vectors with larger magnitudes. <p>Variance Attribute (edge method)</p> <ul style="list-style-type: none"> Measures the similarity of waveforms or traces adjacent in lateral and/or vertical windows. Therefore, it is a very effective tool for delineation faults on both horizon slices and vertical seismic profile. <p>Time Gain</p> <ul style="list-style-type: none"> Allow to increase the amplitude gain to better understand in a more complicated area. <p>Chaos Attribute</p> <ul style="list-style-type: none"> used in delineating directly positions of reflector disruption, by signal pattern within seismic data
<p>Phase</p> <ul style="list-style-type: none"> amplitudes independent Measured in degree showing lateral continues /discontinues of event relates to the phase component of wave-propagation detailed visualization of stratigraphic elements, because wave fronts are defined as lines of constant phase <p>Frequency</p> <ul style="list-style-type: none"> time derivative of the instantaneous phase and is measured in hertz Its related to the centroid corresponds to average frequency of the power spectrum of the seismic wavelet . responds to both wave propagation effects and depositional characteristics, as discriminator. 	<p>Signal Envelope</p> <ul style="list-style-type: none"> amplitude independent of phase useful in highlighting discontinuities, changes in lithology, changes in deposition, sequence boundary and gives packages of amplitudes. <p>Sweetness</p> <ul style="list-style-type: none"> is best though of a relative value for ease of understanding physically, calculated by $\frac{\text{signal envelope}}{\sqrt{\text{inst. frequency}}}, \frac{\text{amplitude}}{\sqrt{\text{hertz}}}$ 	

Table 4.2 Types of surface attribute used to interpret Lidam time structure map.

Surface attribute	Lidam Surface interpretation
Loop Kurtosis	Measures the loop surrounds the interpreted horizon of Lidam reservoir Formation; It uses the trapezoidal approximation as the basis to provide the amplitude response on the seismic trace peaks as a statistical distribution.
Root mean squared (RMS) Amplitude	<ul style="list-style-type: none"> • RMS attribute aided to reduce the background noises and amplitude which are irrelevant to the main amplitudes. So that it is introduced a better capabilities to define geologic features and shed light to Direct Hydrocarbon indicator (DHI) from the surfaces. • structural trends interpreted of higher amplitudes within parts of the structures indicated with red colors.
Average energy	used to map direct hydrocarbon indicators as it represents in the hot color, which the most oil wells are drilled
Measurable interval (Window length)	Helpful in indicates Lidam thickness above tuning when using peak and trough, based on interpreted Lidam horizon.

Amplitude Attributes	Lidam Surface interpretation
Most of	Captures the most commonly occurring data value within the analysis window. A histogram is computed from the input window, and the value from the bin with the highest count is output for each trace location.
Median	All arrangement from the lowest to highest value not picking distinguished trend, where 50% of the values in the window are below the median value. The Median is less sensitive to extreme values than the computation of the Mean
Average magnitudes	Because of having large numbers than RMS amplitude, the measures of reflectivity is less sensitive. But this attribute could isolate geologic features that express themselves as anomalous amplitudes relative to background values as shown in the middle and SW direction.
Harmonic mean	The attribute is used with the averaging of rates and delineate the lateral changes in thickness and lithology, as closure dark blue express oil pool.

Statistical Attributes	Lidam Surface interpretation
Sum Amplitudes	Measure of brightness as reflect of Lidam thickness, which is gives the heights value within closure in the NW direction.
Sum Magnitude	Measure reflectivity with amplitude independent. It is clear that low value within oil well drill location.
Threshold Value	High amplitude patches of green color was preserved in areas of structural reliefs, this could be due to fluid properties.
Positive to Negative ratio	Measures number of positive values divided by the number of negative values. The negative values were found in the interval, so can not used as a divisor.
Standard Deviation of Amplitude	Measures the variability of the seismic amplitude values within the extraction window. But this attribute undefined, because the number of samples within the extraction window is less than 2.

4.3.1 AVO attributes

Amplitude variation with offset (AVO) attributes are considered valuable for evaluating anomalous seismic amplitude responses on large 3D datasets, which have been used in discriminating hydrocarbon filled reservoirs (Ostrander, 1984), characterization of fractured reservoirs (Ramos, 1996), and in lithology determination (Nada and Shralow, 1994). In Figure (4.2 A) explanation of the resulting AVO intercept (A) and gradient (B) traces are crossplotted, from the convolution of the reflectivity series with a wavelet.

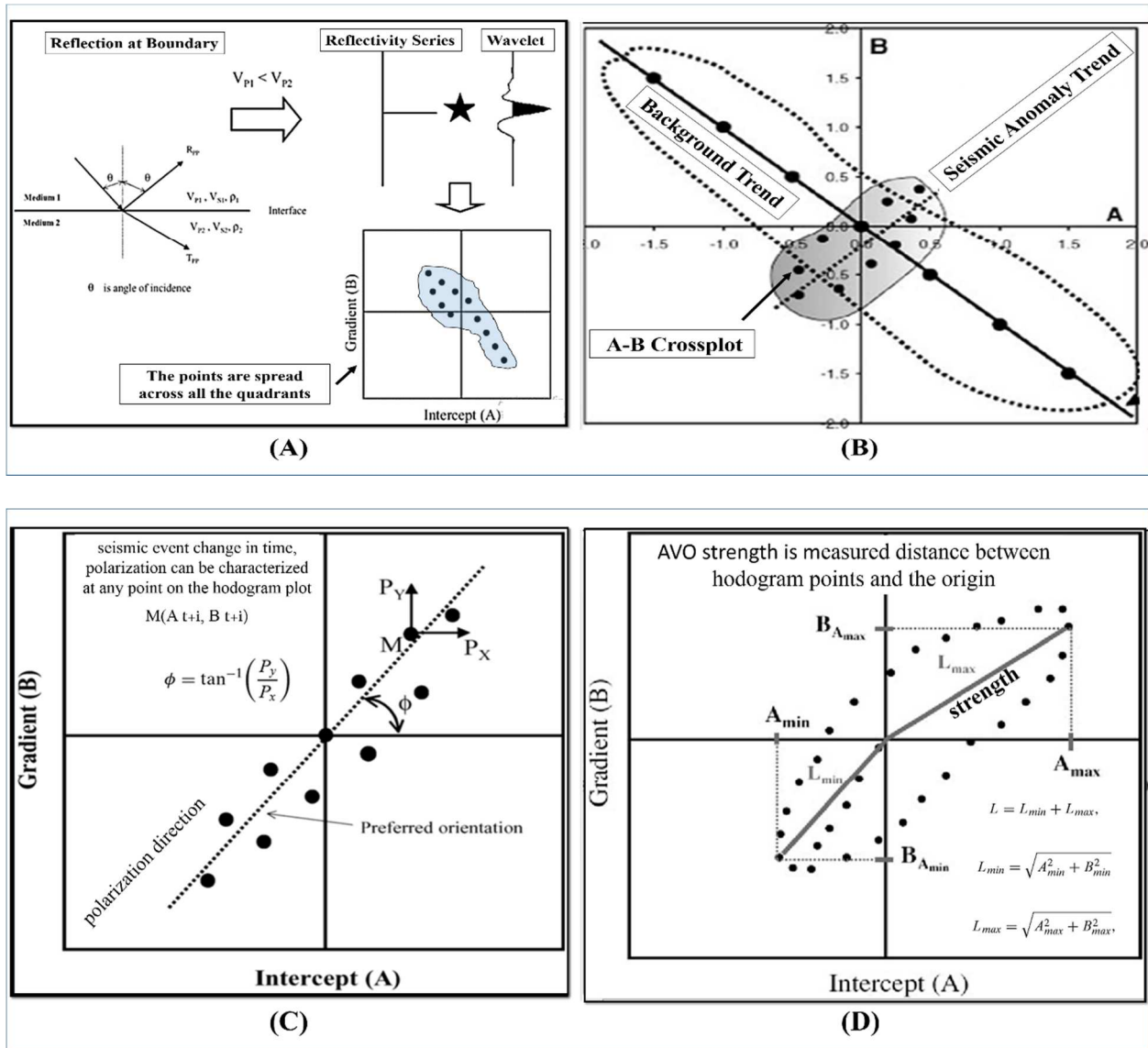


Figure 4.2, (A) Schematic diagram of a reflection at a boundary, (B) AVO crossplot, (C) polarization angle and (D) AVO strength (Patrice, 2001).

Crossplotting AVO attributes helps in establishing trends against or separations from a background trend, which anomalous amplitude behavior can be seen (Ross, 2000) (Figure 4.2 B). Successful use of an AVO crossplot requires a deviation of anomalous events “background” trend.

An alternative approach to identifying AVO anomalies is to consider the AVO polarization in the AVO intercept–AVO gradient (A-B) plane, this approach does not require deviations from a background trend and takes into consideration the wavelet as it is convolved with the reflectivity series. At any given interface, sample points resulting from a reflection have a preferred orientation and can be spread across the four quadrants in the A-B plane (intercept-gradient space). The angle defining any preferred orientation in the intercept gradient space is called the polarization angle (Figure 4.2 C) and in Figure (4.2 D) AVO strength select sample point from plot to enhance the interpretation.

Table 4.3, categories of texture, statistical, and AVO and their objectives, used in the progress work.

Classification of seismic attributes			
Texture attribute	AVO attributes		
	conventional	polarization	
Grey-Level Co-occurrence Matrices (GLCM) <ul style="list-style-type: none"> related to the geologic environment in which their constituents were deposited represent the joint probability of occurrence of grey-levels for pixels with a given spatial relationship in a defined region. to generate statistical measures of properties like contrast and homogeneity of seismic textures, which are useful in the interpretation of oil and gas anomalies. 	Amplitude Versus Offset (AVO) attributes <ul style="list-style-type: none"> The basic physics of the strength of a reflection not depend on the acoustic impedance, but it depends on the angle of incidence. Which is useful for define geological features related to lithology, fluid, and porosity. General concept : collect data from different angles. It's clear that some of the ray paths bounce off the geological strata at relatively small incidence angles, closer to straight down-and-up, when this angle is 0, produce a vertical or zero-offset, ray. Others, arriving at receivers further away from the source, have greater angles of incidence. 	AVO Strength <ul style="list-style-type: none"> measure of the distance of the hodogram points from the origin within the time window of the analysis. The sample points, from the intercept (A) and the gradient (B) traces, on the plot can be considered as a cloud of points of a certain length to enhance interpretation of structure and stratigraphic interest section (Figure 4.2). The stronger the seismic event with large gradient value, the larger L is. While the weaker the event with small value, the small L is. When there is no data, $L = 0$. 	AVO Fluid Strength <ul style="list-style-type: none"> The AVO polarization angle computed along a time window that slides down each trace for the whole volume, and the background trend angle can be determined by fitting a background trend line from a box probe cross plot window, the background trend will then be the arctangent of the change in gradient divided by the change in intercept and the AVO strength volume.

4.3.2 Time Slices Attribute

Time slices are horizontal sections in a 3-D seismic volume, which is provide an internal view on the horizontal geometric pattern of interpreted horizons to aid in seismic interpretation on the 2-D vertical sections. Visualizing time slices within the interested interval proved that structural events like fault surfaces could be fitted into the seismic interpretation workflow from time slice based realizations

In the progress study using time slices plane is useful for study different subtle and sub-seismic structures features, missed by conventional seismic interpretation such as closures and faults, also to lithology distributions patterns without a prior knowledge of velocity and/or density. seven attributes includes Amplitude, Structural smooth, Choas, Cosine of phase, Envelope, Ant truck, Variance, Sweetness and AVO (Figure 4.3) were extracted and displayed as flattened maps at slices for each of the interpreted horizons, at 826 (top of Sirt Shale), 886 (top of Tagreft), 922 (top of Etel), 974 (top of Lidam), and 1066 (top of Gergaf).

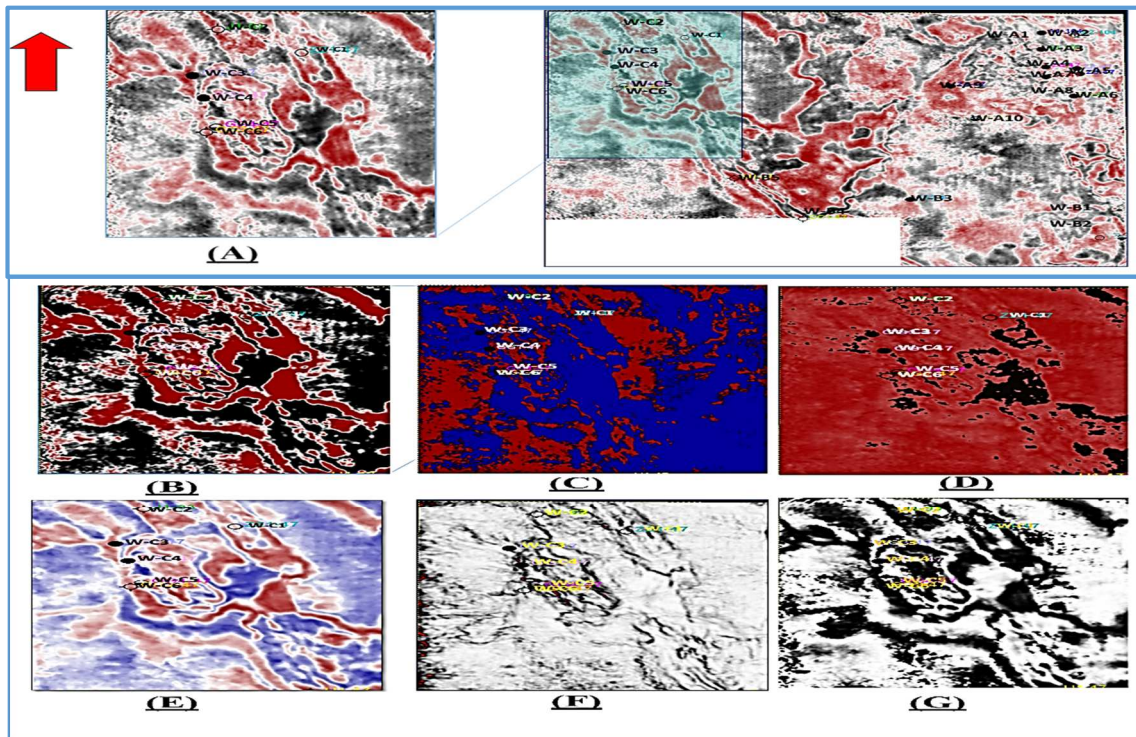


Figure 4.3. Display different time slices at Lidam reservoir level used in this study (A) input seismic, (B) AVO, (C) envelope, (D) sweetness, (E) structural smoothing, (F) variance and (G) cosine of phase.

CHAPTER FIVE

SEISMIC DATA INTERPRETATION AND MODELLING

5.1 Regional Structural Overview

The Bouguer gravity map in the concession-47 (Figure 5.1) delineated the regional structures are different due to the location and orientations in relation to tectonic events. The concession subdivided into three main oil fields are Haram ridge in the north, Bualawn, Dor Mansour fields in the southwest and El-Kotla Graben in the NW-SE trend. The gravity interpretation (Figure 5.1) shows the Haram ridge and Bualawn, Dor Mansour fields are considered to be a positive anomaly reflect high area, whereas the El-Kotla Graben is a negative anomaly. Based on G. de snoo (1961) the seismic reflection data confirmed this result and he suggested that dips of sedimentary formations caused by basement, which seems to be influenced to a large extent by faulting, some faults remained active or reactivated during the deposition of Cretaceous sediments.

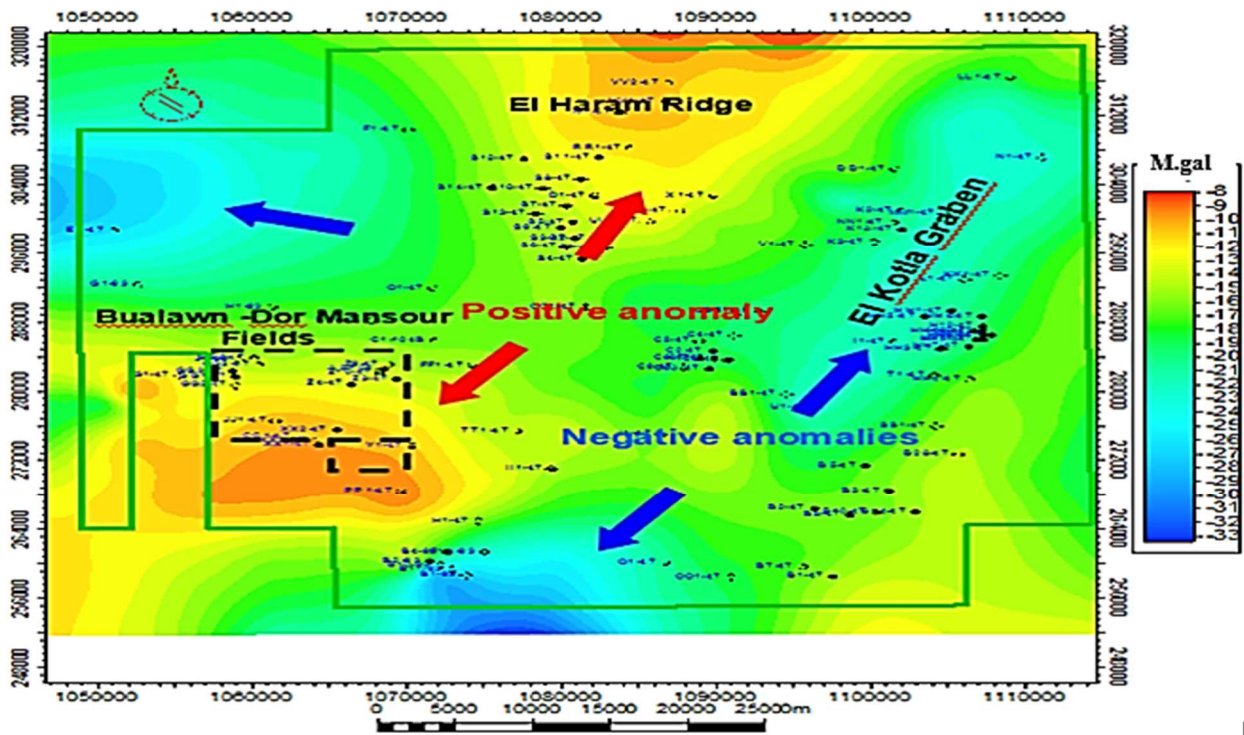


Figure 5.1 Bouguer gravity anomaly map over Concession 47 (CI: 1 mg) (modified from AGOCO, 2009).

Fault patterns can be Determine by residual anomalies (Narrow bands of isogals) to produce maxima along the up-thrown side of a fault anomaly (basement highs) and minima along the down thrown side. The rock density in general about 2.20 g/cm^3 were used in various blocks for elevation correction factor, which it is increase laterally away from the center of the maximum, but the influence of the basement high would be the dominated factor.

5.2 Discontinuity Attributes for Structural Interpretation and Modelling

The research aimed to use different techniques in carrying out manual interpretation of faults and automatic fault extraction methods which are mainly gathered to creating fault patches in the 3D model frame. Structural surfaces and grid skeletons at each phase of the model building, which form the necessary framework for the models. Different attributes functions were applied on 3D seismic reflection data. The process of applying this techniques starts by first creating physical copies or realizing the seismic reference line; this provides the opportunity to compare and contrast the impact of the attribute application to the seismic line. Creating a virtual copy of the seismic line from the realized copy to run several types of attributes on the virtual copy and erase their impact if does not provide the relevant results.

5.2.1 Structural Smoothing

Smoothing attribute played an important role to understand structure revolution and their effects in Cretaceous deposits by delineating features in terms of horizons and faults, extending of faults in the deeper depth with different intensities and styles, reflect activity tectonic deformation. The advantage displayed in Figure (5, 2).

5.2.2 Chaos Attribute

The study used chaos attribute to distinguish lithology variation based on different sediment facies, Upper Cretaceous marine deposits includes dolomite, limestone and shale, can be either in continuity or discontinuity bed. As shown in Figure (5.3) uncolored values indicate minimum chaoticness correspond to continuity, and zones of maximum chaoticness indicate discontinuity of reflector character, which forms a basis to detect faults for automatic extraction.

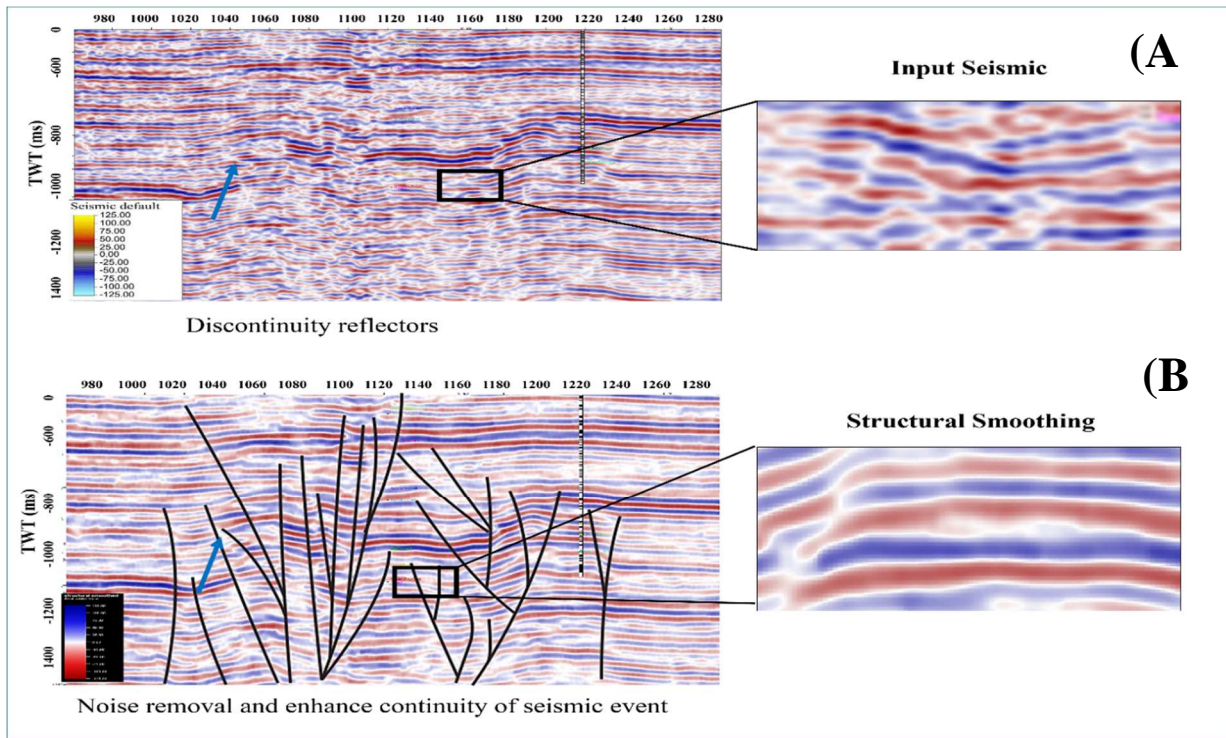


Figure 5.2 (A) original seismic associated with poor amplitude (B). The attribute Structural Smoothing produces an aggressive noise cancellation and improves the continuity of the seismic events.

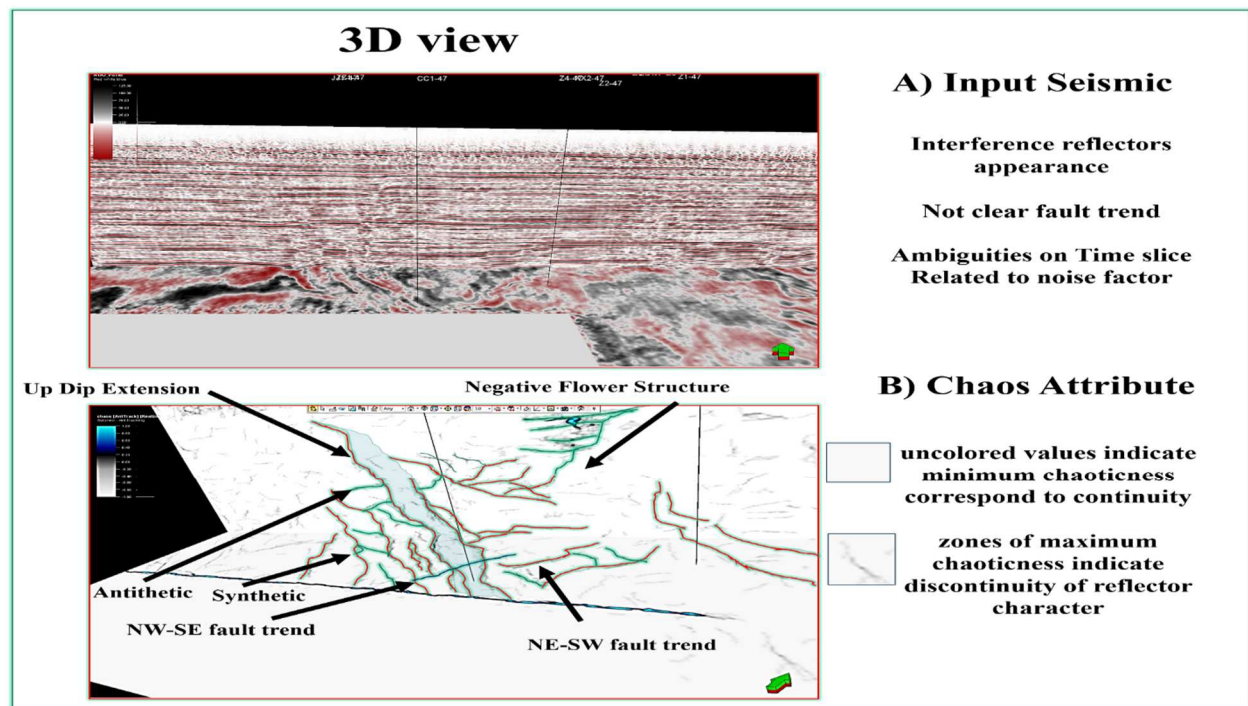


Figure 5.3. 3D view display inline crossed by time slice, (A) original seismic (B) chaos attribute.

5.2.3 3D Edge Enhancement (3DEE)

Applied 3DEE attribute helped to increase the number of faults and fractures have been identified and further enhance their resolution. This makes workload easier to get effective fault interpretation. 3DEE in Inline 1040 detected the tilted fault blocks related to extension normal fault with strike slip, produce negative flower structure below TWT 600 ms because of Cretaceous rift, which ends in Paleocene. The overburden loading of Paleocene accumulation caused to increase tectonic reactivation of fault intensity (Figure 5.4).

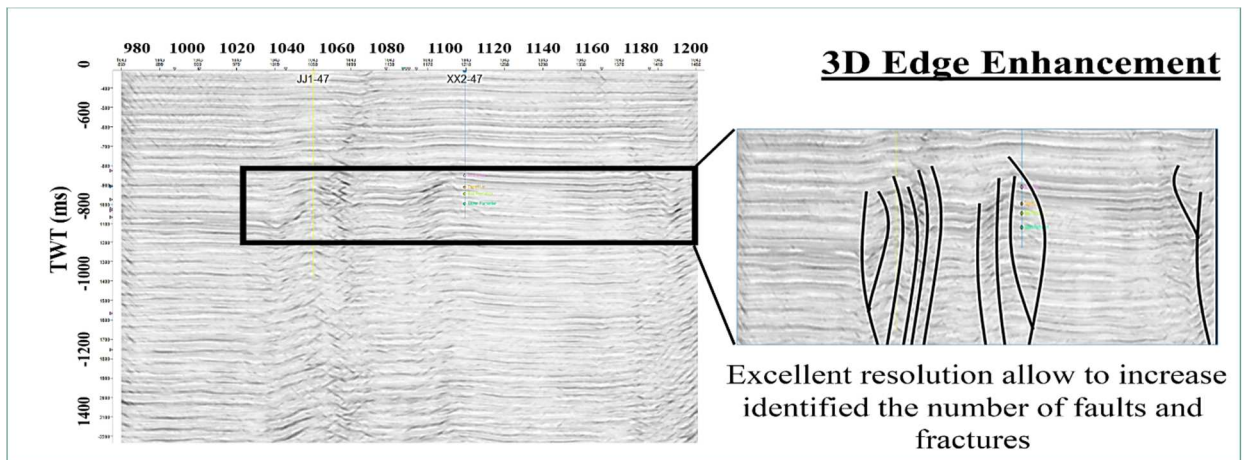


Figure 5.4. Shows 3D Edge Enhancement attribute.

5.2.4 Automatic fault extraction technique/ant tracking

In this study, ant tracking used as seeds to interpret areas with discontinuity, to deliver automatic fault extraction process for the models.

Generating ant track volume starts by preconditioning the seismic volume, as following steps:

- Used visualization techniques includes realized or create physical copies.
- Applied structural smoothing attribute to achieve the continuity of the reflectors to enable the ants to isolate easily discontinuous zones. The next step
- Created chaos or variance volumes attribute, to determine the amount of disorganization in dip and azimuths as a basis to determine local chaotic textures and displacements for fault interpretation, as structural realized attribute volumes.

- Select aggressive mode which is applied to detect discontinuities, and to see how much it could illuminate uncovered major regional fault and subtle faults.
- Used Stereonet tab to provide an orientation filters for the ant agents which places restriction to the azimuths and dips that the agents would allow for searching the seismic inlines and crosslines. Areas that are marked with gray shades are ignored by the ants. (Figure 5.5).
- Create fault patches which is gives information to the fault details as to their trends /nature and provides a much faster of structural overview for interpretation, modeling, and provide a quicker step to generate the fault into the 3D structural grids.

The ant agent parameters listed and described based on determining spacing, direction, and distance of the ant agent would pass through in its search for discontinuities (Appendix, Table 2).

Observations of Ant truck fault interpretation

- In the study area, the lack of adequate dip and azimuth made a difficult prospect to achieve in Stereonet, to solve this challenge, crop volumes were tested within Upper Cretaceous zones with different parameters as a basis to train the ants to optimize the actual parameter that would preferred in the whole volume. For example, selected 15 increment of azimuth and dip, as localized within the interest sectional fault zones were automatically generated a distinctive fault patches.
- The fault patches accuracy was a challenge due to lack of data in defining the stereonet and the accurate ant parameters. This means from visual observation that some manually interpreted faults with clear fault displacements were not picked by the ants, in this case editing the fault patches can be used, in order to use extracted patches forms as direct inputs into the pillar grid process (Figure 5.6).
- The fault planes that were interpreted included the main horst associated faults and other minor faults which were captured by the ants, where it helped to localize the interest zone with more fault patches, It also gives information to the fault details as to their trends /nature and provides a structural overview of the fault systems (Figure 5.7). Again it proves to provide a much faster interpretation and modeling which provides a quicker step to generate the fault into the 3D structural grids.

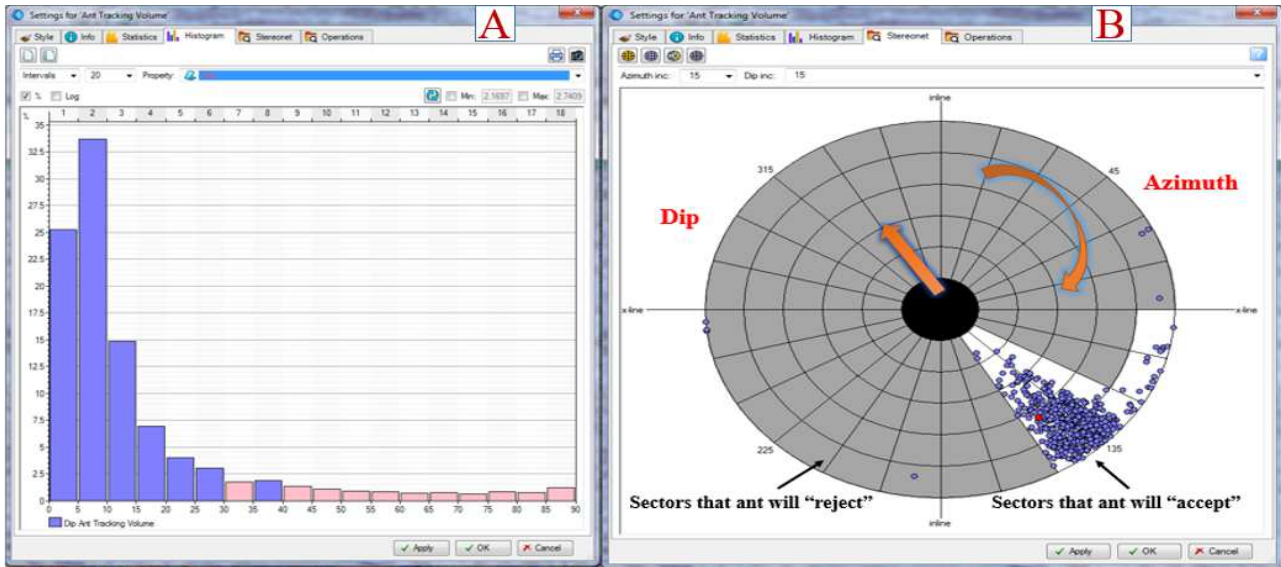


Figure 5.5, 5, Frame (a) shows the ant parameter with ant mode, ant track deviation, ant step size. Frame (b) shows the stereonet sectors of the dip and azimuth with the seismic inline/cross lines.

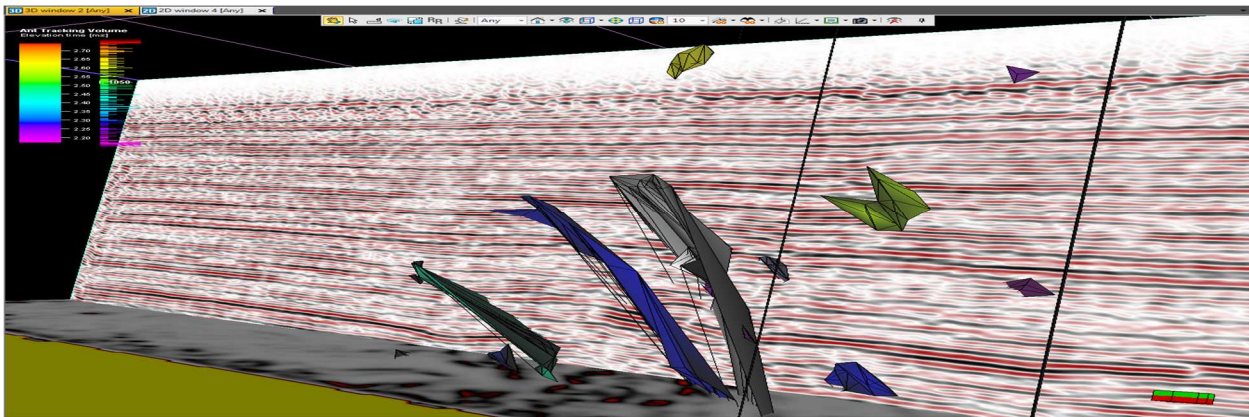


Figure 5.6, Fault patches generated with a cropped seismic section of the whole seismic volume.

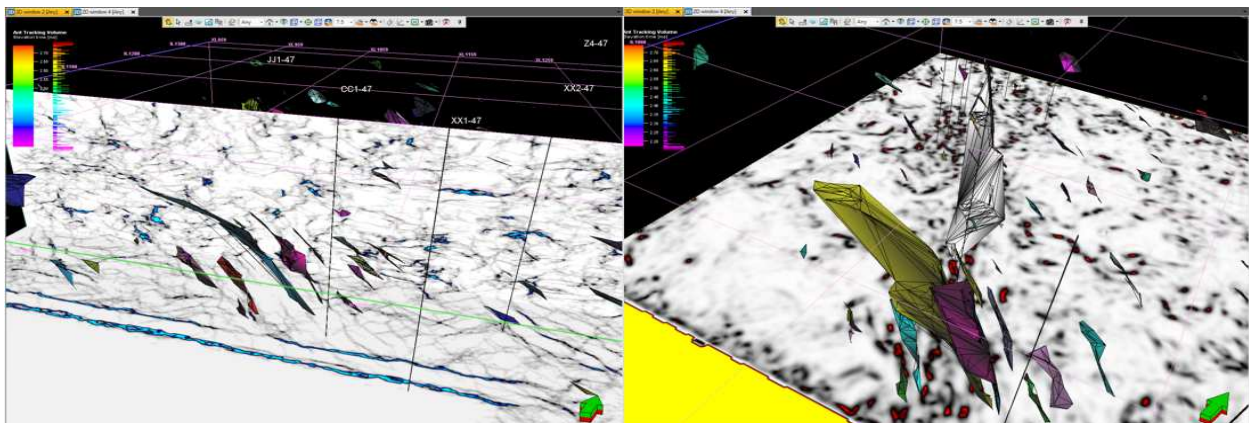


Figure 5.7, Extracted fault patches with the chaos attribute within cropped seismic section.

5.3 Manual Fault Interpretation

The fault picked manually starts by assigned fault segments picking on inline sections of seismic with the trace appearing on the corresponding cross lines, within the Upper Cretaceous succession into basement from 600 ms to 1400 ms. A total of thirty faults were identified and interpreted as fault sticks then converted to fault polygon. These represent line data of the interpreted faults and their geometry, some extending through the extent of the field known as major regional growth faults, few flank faults appearing on few of the lines (Figure 5.8).

A large regional faults are observed in conjugate direction, an uplifted fault-bounded structure with triangle shaped feature, the faults have trends either in NE-SW or NW-SE direction. The F2 is the regional fault trending NW-SE parallel more or less to Gedari Fault (Anketell, and Kumati, 1996). According to its movement it can be divided into three major segments (F3, F4, and F5) (Figure 5.8) are transtensional (oblique) faults. These fault was initiated during the rift cycle in the Early Cretaceous and reactivated again during the deposition of all other formations. The NE-SW faults trend (F1, F7, F8, and F9) are most likely related to the tectonic movement below and reactivated processes. Both two trends cuts through the horizons but the degree of intensity is absolutely different. The segmentation of several faults show relatively diversity as shown in Table (5, 1) are always occurring with steep and straight fault surface, those faults are trending mainly east or west. Other faults are small and minor faults, but are very important because they control and form the structural hydrocarbon traps.

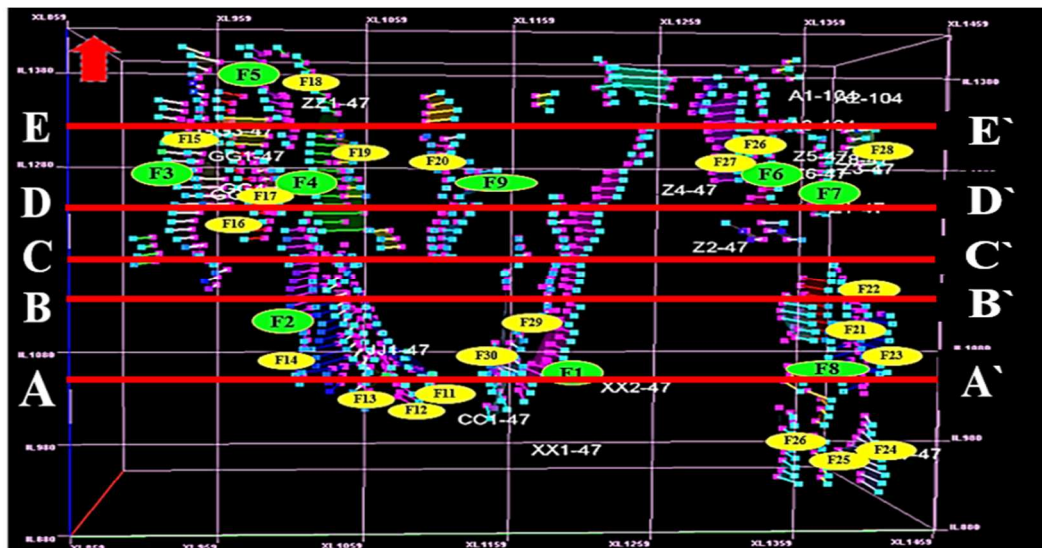


Figure 5.8, fault sticks shows main fault segments of the Bualawn and Dor Mansour merged fields.

Table (5.1) Showing interpreted faults with corresponding seismic coverage.

FAULTS	DIP DIRECTION	INLINE COVERED	FAULT TYPE
F1	West–Northwest	1000-1300	Major Regional Growth Fault
F29	East	1040-1250	Flank Fault (Antithetic)
F30	East	1040-1090	Flank Fault (Antithetic)
F2	East	1060-1270	Major Regional Growth Fault
F11	West	1040-1280	Flank Fault (Antithetic)
F12	West	1040-1280	Flank Fault (Antithetic)
F13	West	1040-1280	Flank Fault (Antithetic)
F14	East	1030-1270	Flank Fault (synthetic)
F3	East	1150-1350	Major Regional Growth Fault
F15	South	1250-1300	Flank Fault (Antithetic)
F16	South	1230-1320	Flank Fault (Antithetic)
F17	South	1240-1340	Flank Fault (Antithetic)
F4	East	1200-1390	Major Regional Growth Fault
F19	West	1250-1310	Flank Fault (Antithetic)
F5	East	1300-1390	Major Regional Growth Fault
F18	south	1300-1390	Flank Fault (Antithetic)
F6	West	1250-1380	Major Regional Growth Fault
F26	South	1260-1350	Flank Fault (Antithetic)
F27	South	1250-1360	Flank Fault (Antithetic)
F7	East	1500-1310	Major Regional Growth Fault
F28	west	1270-1310	Flank Fault (Antithetic)
F8	East	900-1180	Major Regional Growth Fault
F21	west	1100-1160	Flank Fault (Antithetic)
F22	west	1000-1140	Flank Fault (Antithetic)
F23	west	1140-1180	Flank Fault (Antithetic)
F24	west	980-1000	Flank Fault (Antithetic)
F25	west	920-990	Flank Fault (Antithetic)
F9	West	1180-1280	Major Regional Growth Fault
F20	west	1200-1350	Flank Fault (Antithetic)

5.4 Structural architecture

The internal structure of the investigation area have been studied along six seismic profiles (A-A' through F-F'). The study delineate along-dip and across-strike variations in the distributions and thicknesses of the stratigraphic units, using the well-recognized seismic interfaces, and map the fault geometries and patterns affecting the stratigraphy at depth.

5.4.1 Profile A-A'

Inline 1040 seismic profile in the southern part of study (Figure 5.9) area represents major faults have divergent style showing a negative flower structure of strike-slip fault , however produce a pull apart opening in E-W blocks with opposite upthrown horst structure trending to NW-SE, steeply dipping in south western part as distinctive depression, and to NE-SW dipping in the northwest as a subsidence in the north central part between to master fault (F1 and F2), which was related to the extension, accumulate sediment load, and reactivation in Paleocene period. These two faults intersect in the basement at nearly 1200 ms, with high angle faults that bound horsts and grabens, which is represent extension related fragmentation (Figure 5.9). The second is low-angle detachments faults with associated basement. Both types of faults are related to the development of two superimposed stress fields, one related to tectonic and the other to gravitational collapse. The NW-SE faults that are parallel to the major structural trend of the basin controlled the rate of rifting and subsidence. Whereas the NE-SW structure modifies the pattern formed by previous system to form the block structures.

Geoseismic model speculative possible propagation of secondary faults above major faulting resulting in horst and grabens and half grabens, these secondary faults have parallel and subvertical geometry influenced on sedimentary arrangement. Changes of stress on both side of fault gravitational sliding in transtensional stress to the east, and contracted vertical and lateral duplexing in the transpressional stress to the west, this reflect changing in the tectonic event, because of strike-slip fault system corresponds to ancient deep fault related to basement.

5.4.2. Profile B-B'

Inline 1080 profile is divided into two structural domains by the oblique-slip fault. The NW (F1) and NE (F2) Master Faults with moderately to steeply dipping planes begin to increase amount of depression toward the central north. The structural domain to the east side is characterized by a series of high-angle normal faults that are antithetic to synthetic to the NE Master Fault. The sedimentary strata in the hanging wall of this boundary fault show a major rollover anticline that is more clearly defined in the younger formations, and thicken toward the fault plane as a result of syn-depositional growth faulting (Figure 5.10).

The structural domain to the west side overall displays a well-developed negative flower structure, associated with steeply-dipping oblique-slip fault branches that conjugate at the depth (Figure 5.10). The seismic reflectors in this domain show local anticline-syncline features as part of the negative flower structure. The deposition of Sirt shale Formation during the Upper Cretaceous exhibit significant thickening, indicating that a major episode of tectonic subsidence occurred within the basin. The western domain defines the South west Sag, whereas the eastern domain to its east characterizes the Central Uplift within the middle segment (Figure 5.10).

5.4.3. Profile C-C'

Inline 1100 seismic profile C-C' farther north within the middle segment of the study area. The seismic reflectors below the Sirt Shale Formation in the eastern domain of the basin are either tilted toward the NE or NW Master Fault direction, and show eastward thickening towards it, typical of growth faulting (Figure 5.11). Negative flower structures related to the sinistral Fault are more pronounced in the western domain in comparison to those observed along Profile D-D' and E-E'. However, significant thickening of the sedimentary sequences from east to west, toward the Faults, is well developed in the western domain. This feature interpreted as a result of tectonically induced subsidence and rotational deformation associated with a transtensional stress regime along the NW-SE fault. Thus, the interpretation infer that transtensional deformation played a major role in increasing the accommodation space within this part of the study area in the Upper Cretaceous periods.

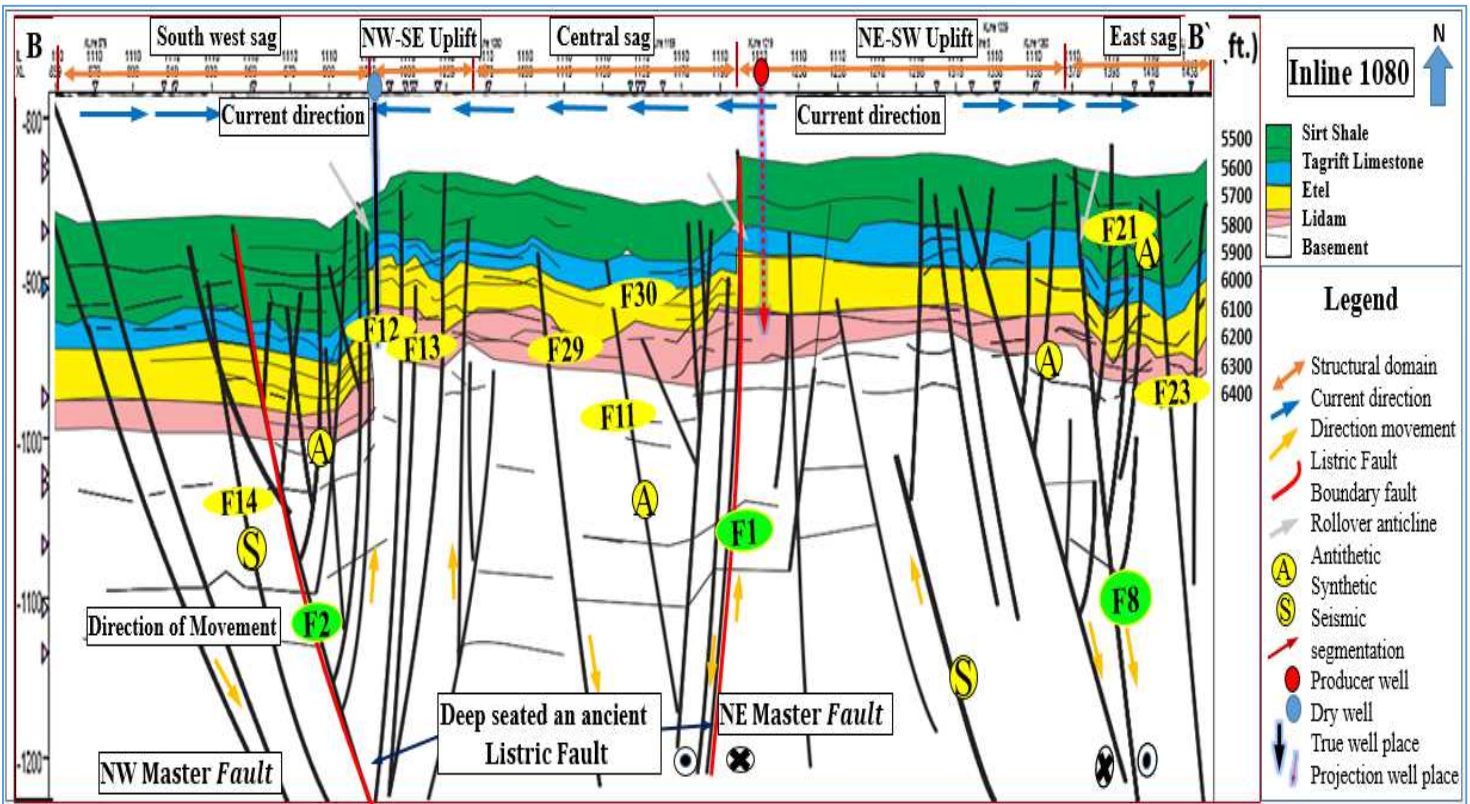
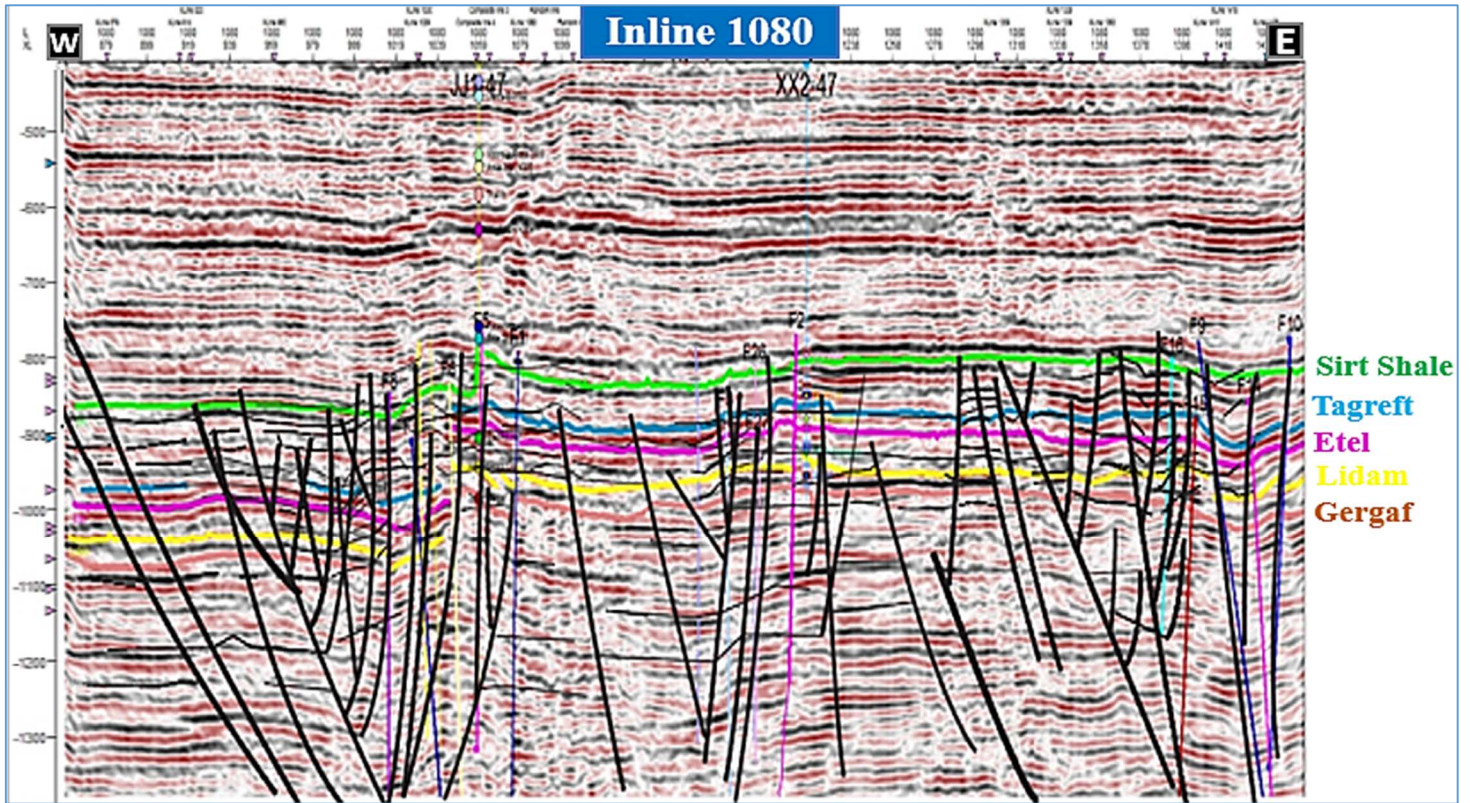


Figure 5.10 B-B' Seismic reflection profiles with structural interpretations. The major seismic reflectors recognized.

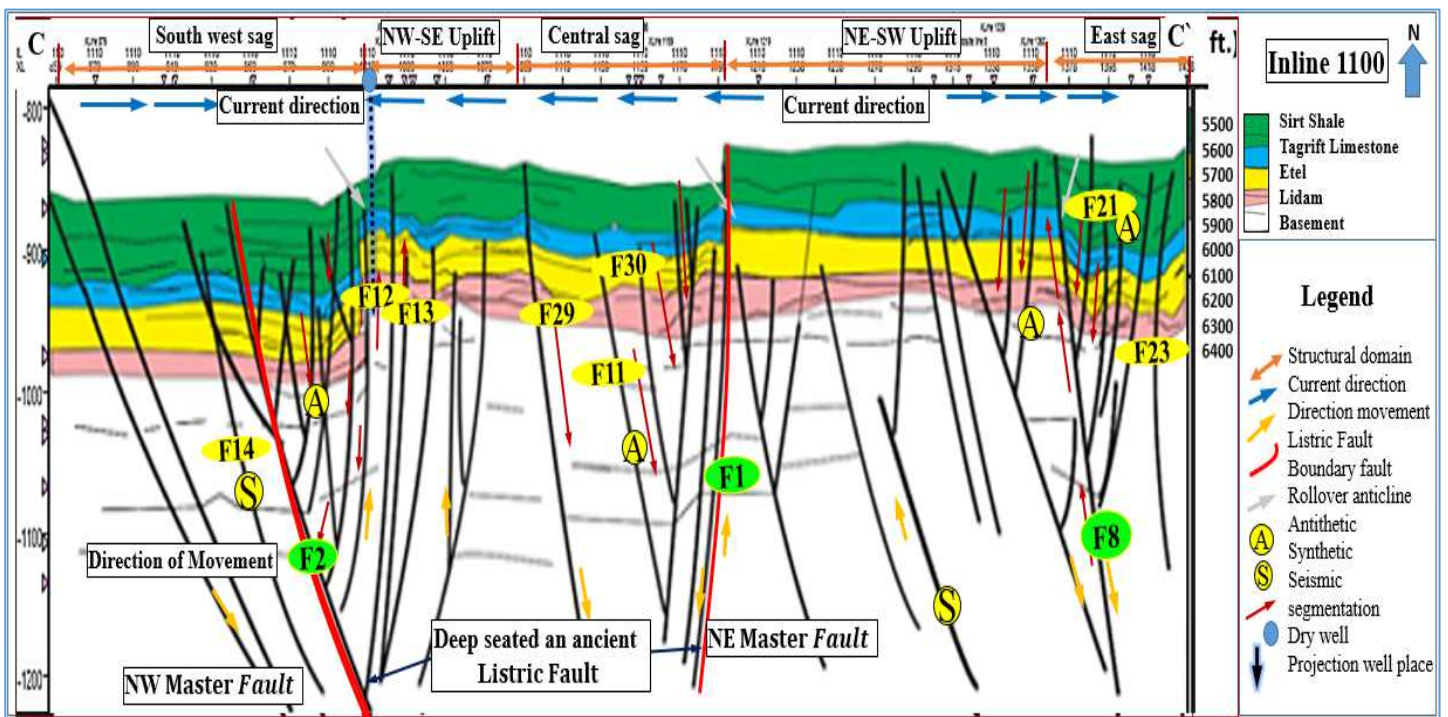
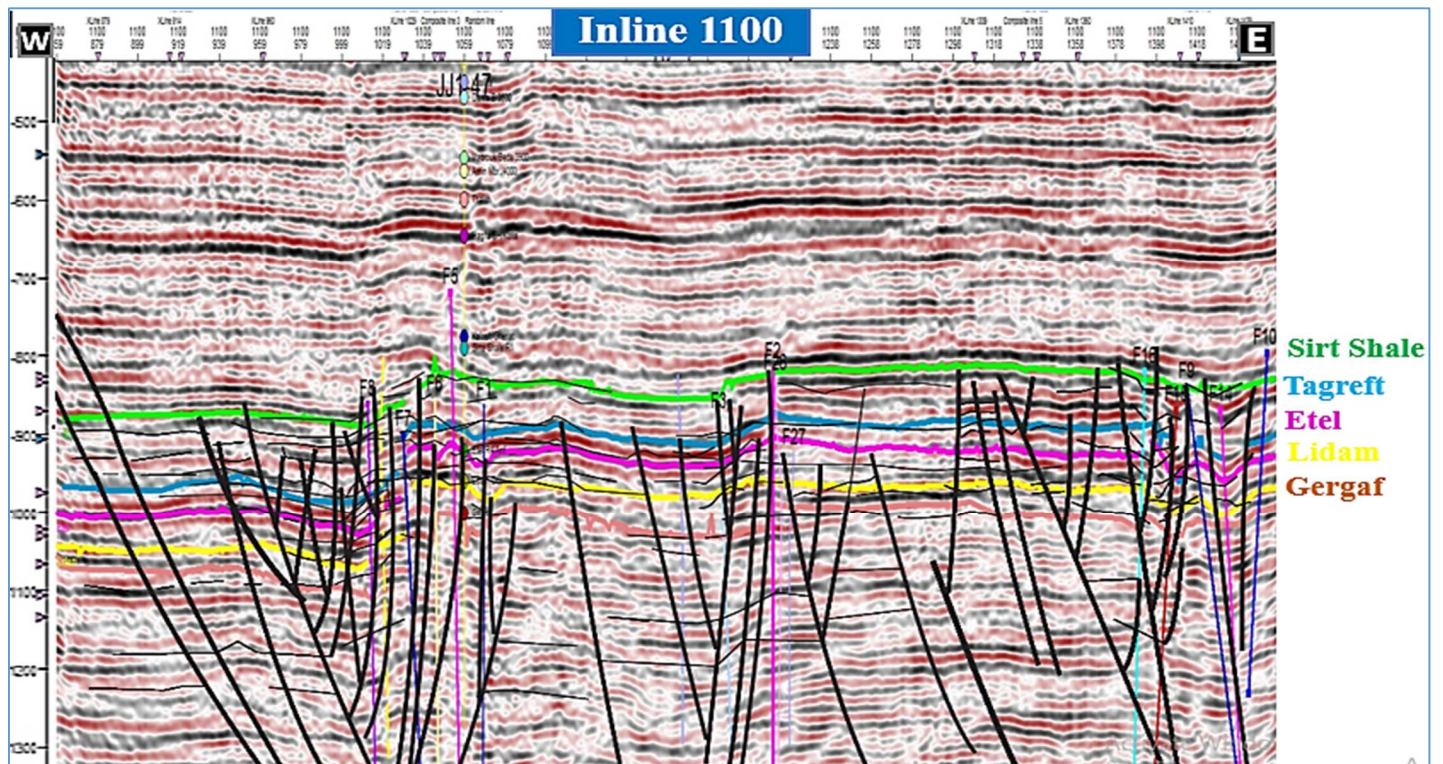


Figure 5.11 C-C' Seismic reflection profiles with structural interpretations. The major seismic reflectors recognized.

5.4.4. Profile D-D'

Inline 1260 seismic profile goes through several structural domains. In the west of the profile a mild structural high in the pre-Cambrian basement have been observed, above which the seismic reflectors are displaced by positive flower structure. In the mid-section of the profile, all formation and member boundaries display downward sagging, and the formation thicknesses increase, particularly that of Upper Cretaceous Formations. These observations suggest that a major episode of subsidence might have occurred in this part of the basin during the Upper Cretaceous. In the eastern end of the profile, there are a major uplift of the pre-Cambrian basement beneath the sedimentary strata (Figure 5.12). A series of high-angle, west reverse faults and fault-propagation folds occur in the pre-Cambrian basement and in the Cretaceous strata, forming the Uplift. The research interpret these reverse faults and the associated west, asymmetrical folds as transpressional structures, which helped create the Uplift within the field. Diminishing effects of reverse faulting and folding stratigraphically upwards in the Upper Cretaceous (the Sirt Shale Formation) sedimentary units indicate that the main episode of transpressional deformation was completed by the end of the Upper Cretaceous succession.

5.4.5. Profile E-E'

Inline 1370 profile E-E' goes across the very northern end of the field (Figure 5.13). In the western part of profile (northwest of study area), the reverse fault splays appear to form a positive flower structure (F5, F16, F17) which is responsible for the development closure (located at producer well W-C1) toward the NW uplift trend, separated by constrain graben at dry well W-C1, because of drilled out of structure. In the central part, the stratigraphic features interpreted as a manifestation of fault-controlled rapid subsidence and increased accommodation space development in the early to middle Cretaceous. In the eastern part, The structural high within the pre-Cambrian basement, it observed high-angle splays of reverse faults forming a positive flower structure (F26, F27 and F28), The steeply east dipping dextral master Fault (F1) shows a significant normal component that was responsible for the development of a half graben structure where the steeply western dipping Fault dissects the structural high of the NE Uplift,

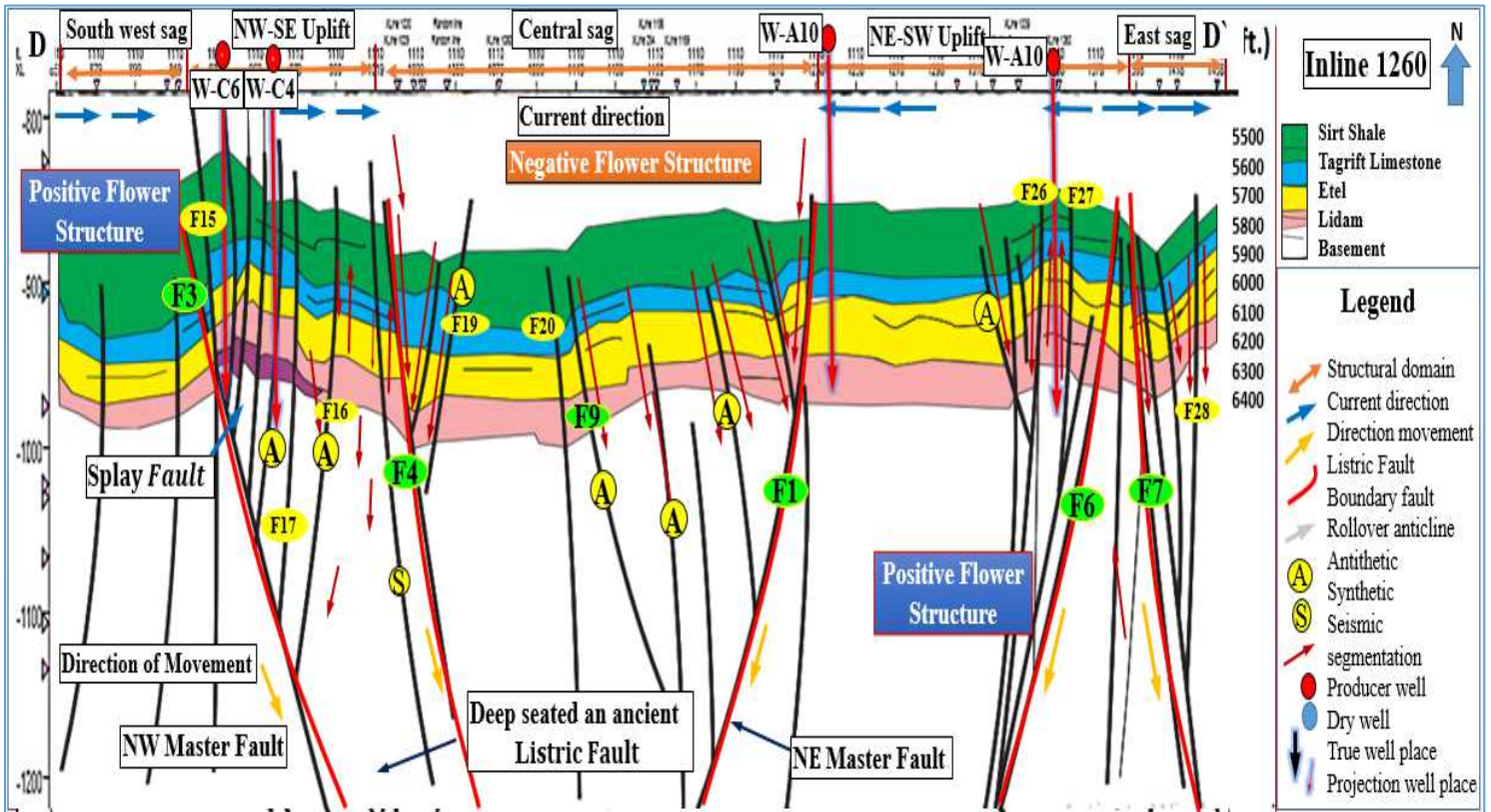
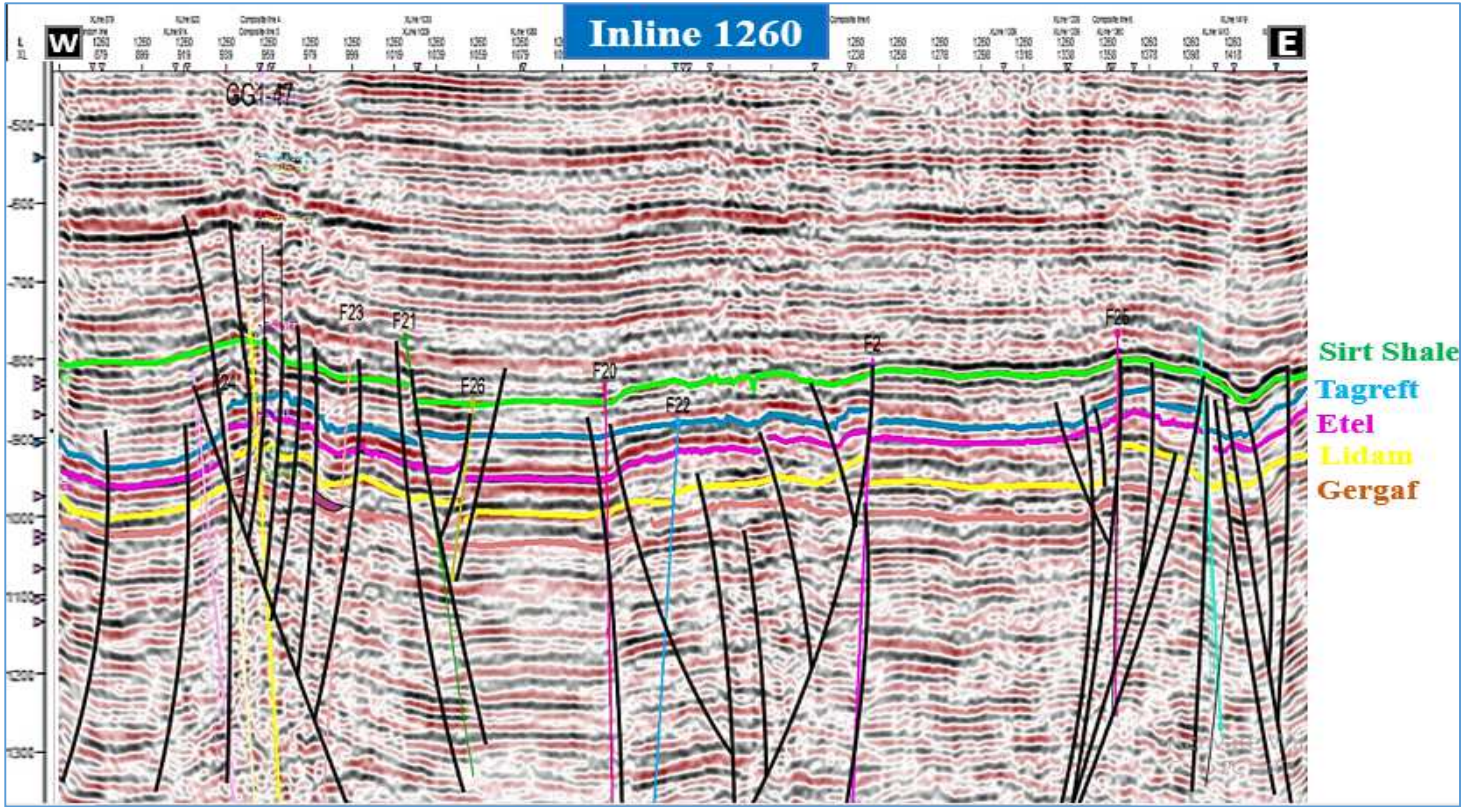


Figure 5.12 D-D' Seismic reflection profiles with structural interpretations. The major seismic reflectors recognized.

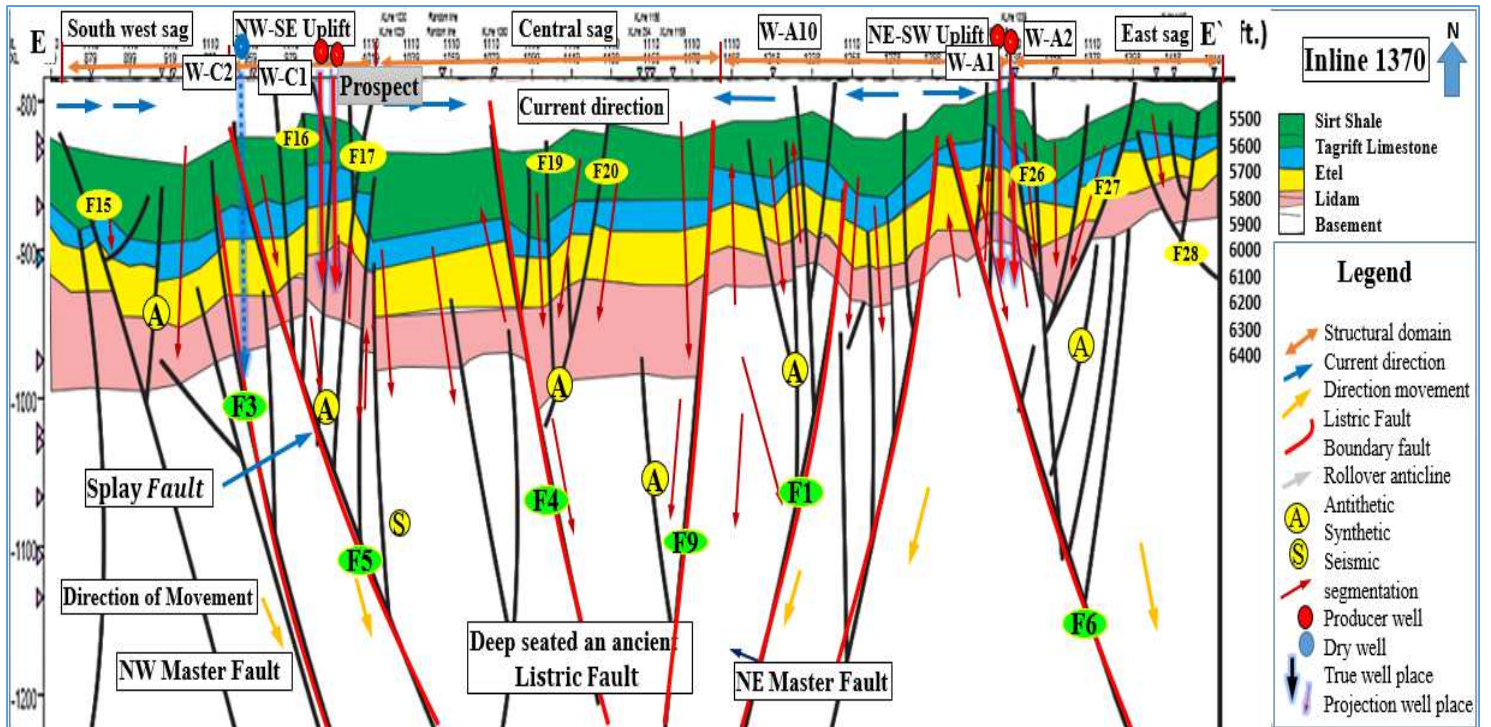
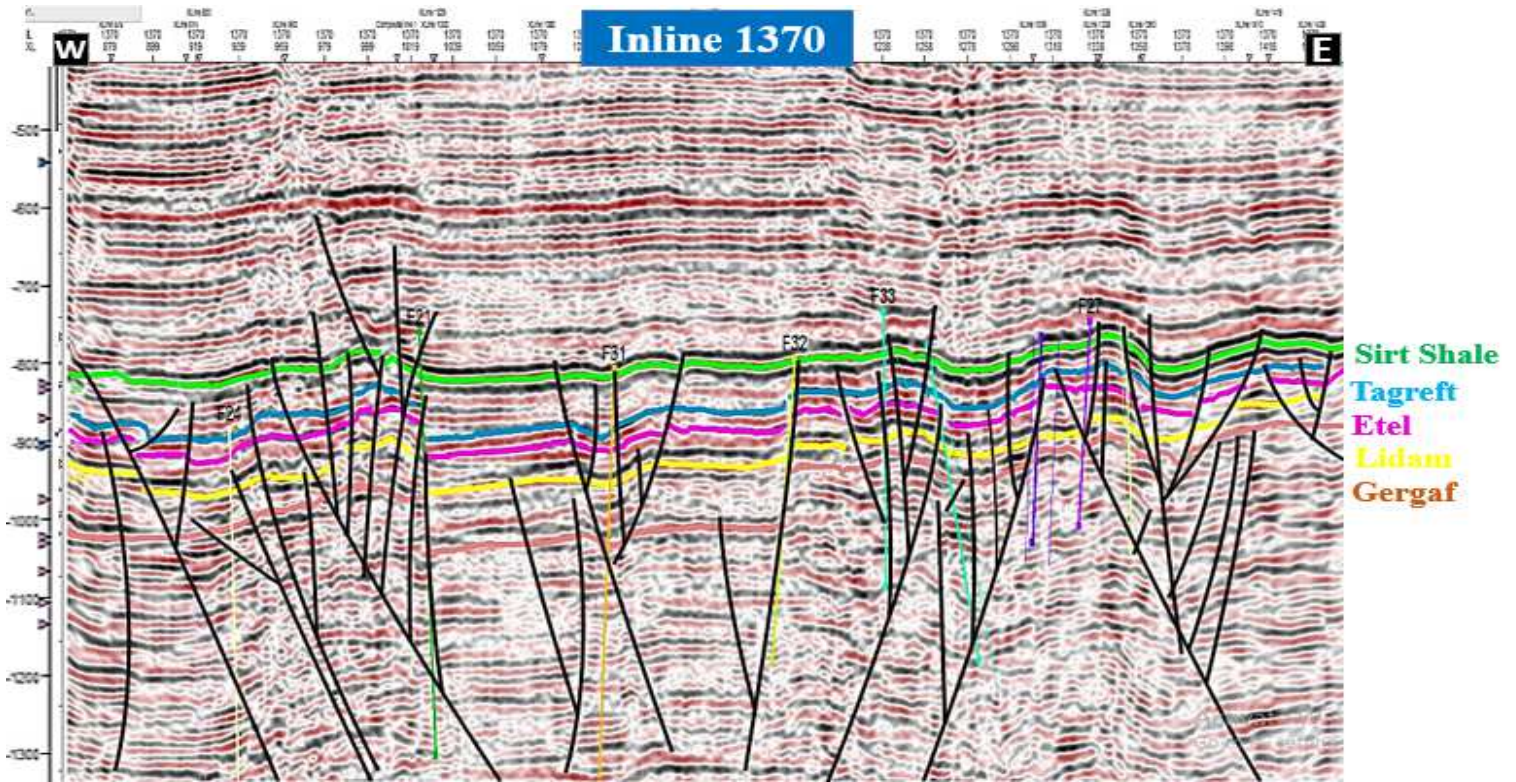


Figure 5.13 E-E' Seismic reflection profiles with structural interpretations. The major seismic reflectors recognized.

5.5 Time Structure Map

Understand subsurface geology by delineating the structural features is depend on generating structural maps for each individual horizon within Cretaceous succession, with respect of interpreted fault polygons. Furthermore these surfaces are typical inputs in the make horizon process in the modeling work flow and for surface attributes.

The operation workflow summarized by interpreted seismic horizons accurately and detecting fault crossed with driven horizon to produce fault polygons. These polygons operated by eliminate inside function, which make delineate the dimensions of the faults easier. Finally, applying the smooth function to eliminate false positive relief closures and contouring problems. In order to deliver a geologic reasonable surface and also to deliver prospective drillable locations.

The structural architecture of the Bualwan, Dor Mansour fields are controlled by two major fault systems NW-SE related to Cretaceous syn-sedimentary faults corresponds to the direction of the Sirt rift system, branches into uplift closures as shown in Sirt Shale time structure map (Figure 5.14), but the intensity of faults obviously increase through Tagrift Limestone, Etel, and Lidam structure time structure maps (Figure 5.15, 16, 17). The NE-SW Faults being considered as a reactivation of pre-rift faults basement plaeozoic related to Tethys rifting. The reactivation interpreted due to master zonal fault NW-SE (sinsitral displacement), which cause to reactivate conjugate faults (NE-SW) bend around the horst blocks, its considere to be restraining bends along dextral strike slip fault, their effect diminished slightly toward Sirt Shale (Figure 5.15). The development extension in the E-W direction, which consists major depressions (sags) in the north center of study area (clearly define in all time structure map levels). The two structural uplifted trend in a triangle shape toward NW-SE and NE-SW (Figure 5.15-16-17-18) whose occurrence and distribution are strongly affected by these fault systems, due to deposited after the rift. Normal faults and fracture zones occur on the side opposite to the bounding fault indicating extension, especially at north central part during Santonian age at Sirt Shale (Figure 5.14). Finally, major collapse in the south western part very distinctive in all time structur maps (in profile AA`, Figure 5.9) the study is interpreted such a depression in both side of NW-SE uplift trend related to the maximum stress in the NE-SW direction (5.18A).

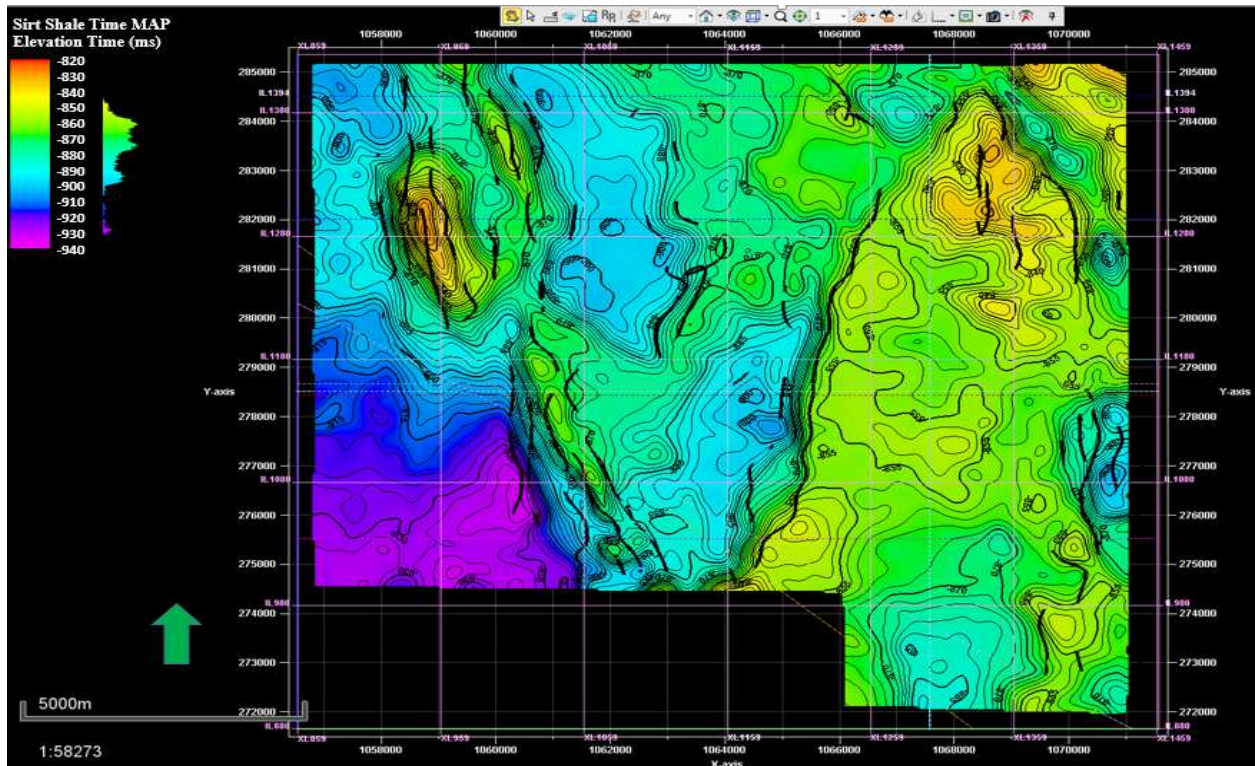


Figure 5.14, structural time map of Sirt Shale Formation with fault polygon.

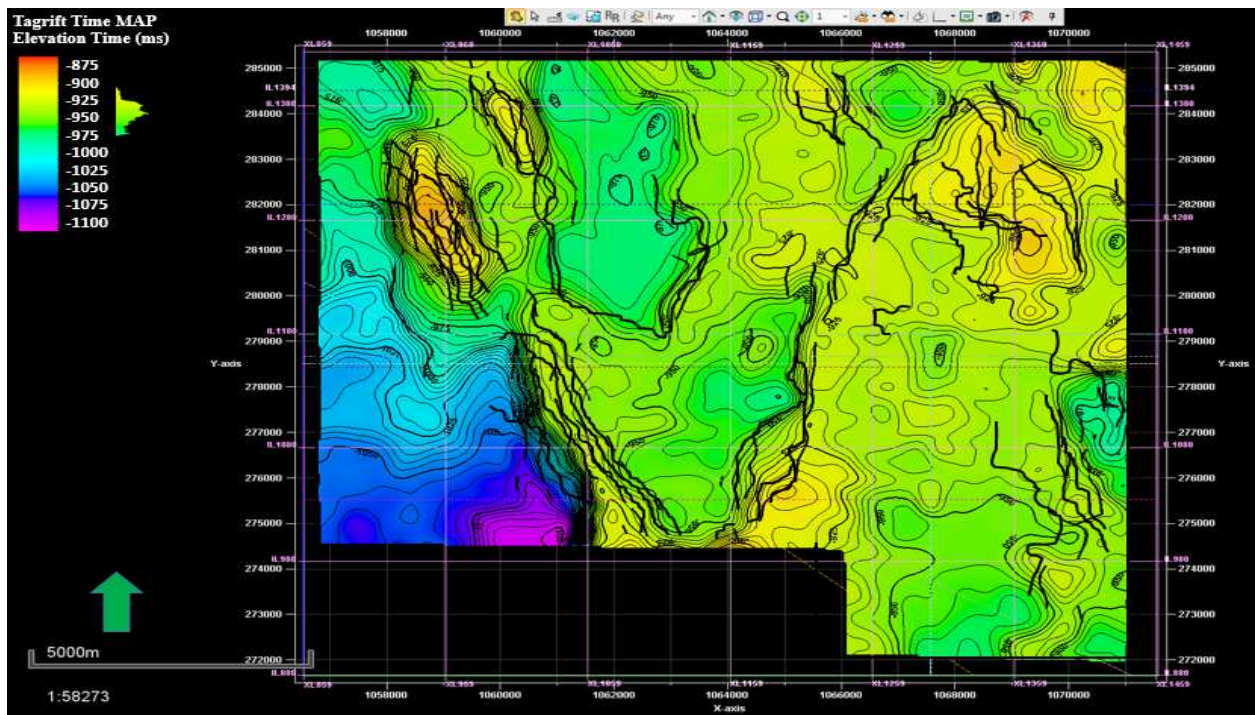


Figure 5.15, structural time map of Tagrft Formation with fault polygon.

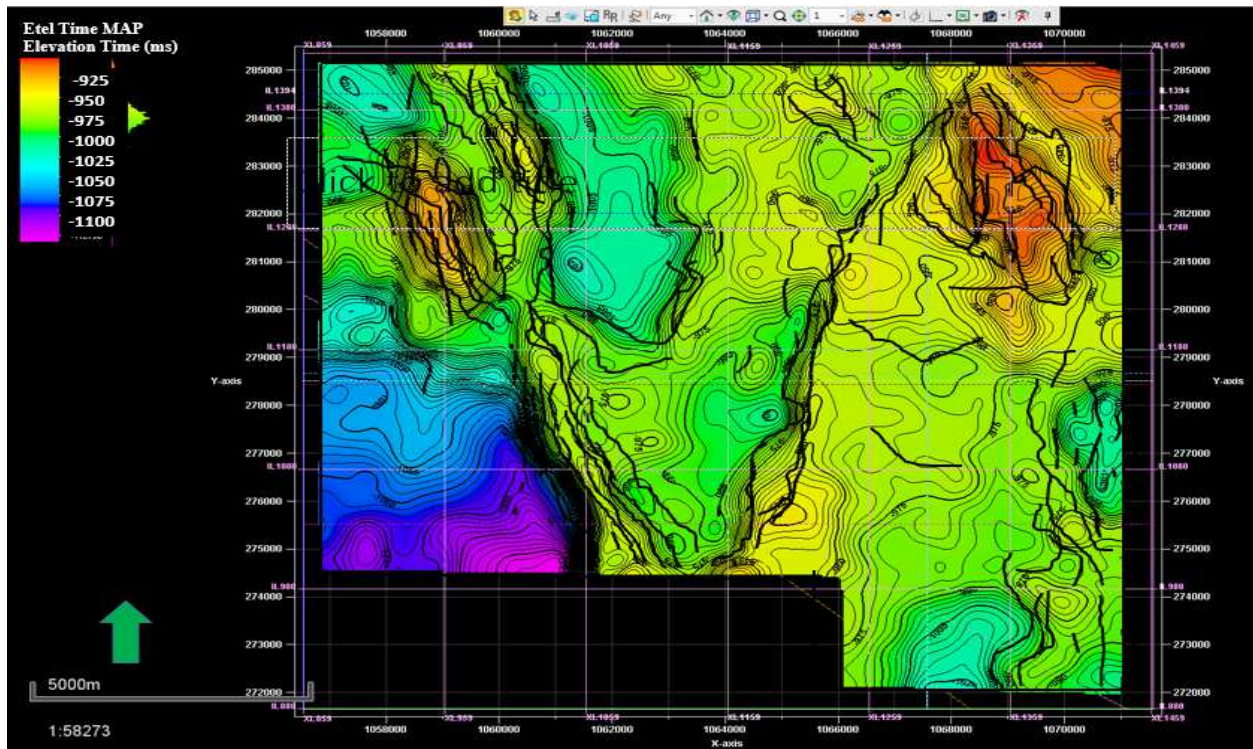


Figure 5.16, structural time map of Etel Formation with fault polygon.

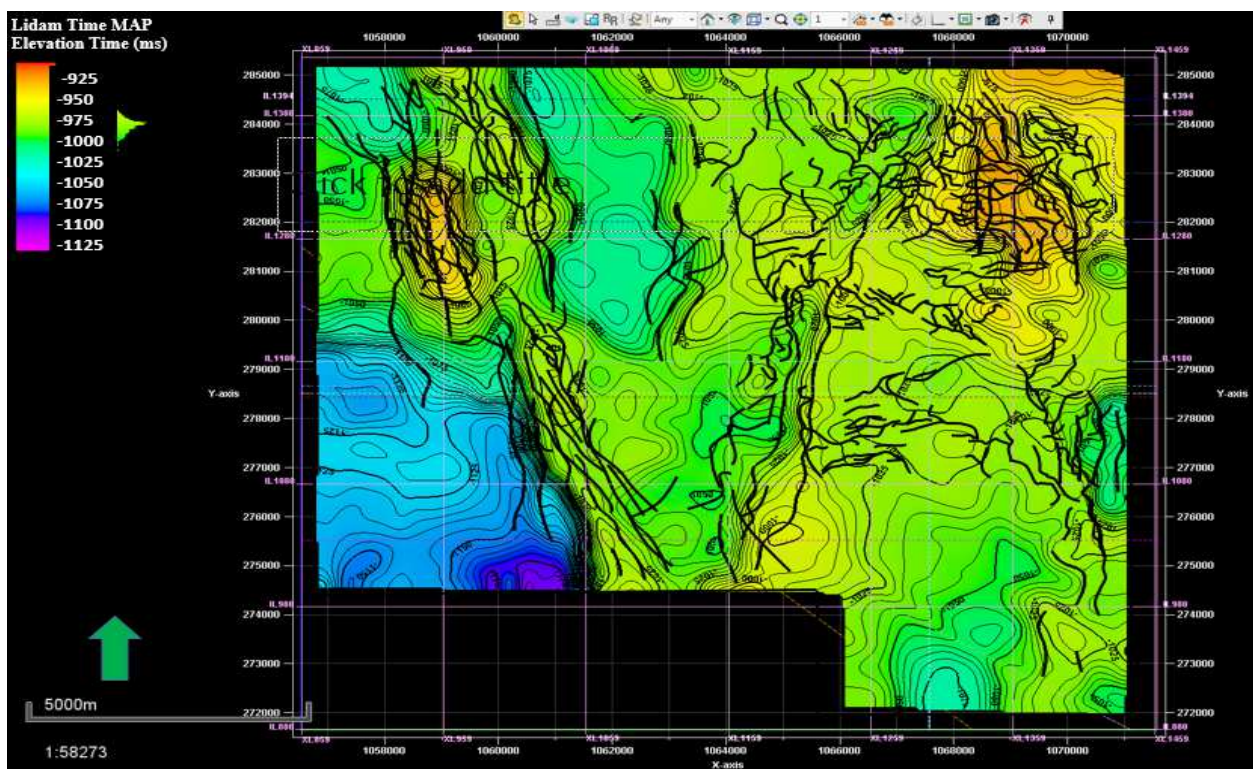


Figure 5.17, structural time map of Lidam Formation with fault polygon.

5.6 Impact of regional stress in the study area

Fault zones display Riedel shears with orientation, which are consistent with sinistral displacement on basement faults. Sinistral strike/ oblique-slip on preexisting NW-SE directed maximum compressive stress field (5.18A). The sinistral movement in the study area influenced locally by Gedari fault zone, as well as can be interpreted in terms of two African sub plate in which the E-African sub plate moved north at greater velocity than the sahara sub plate (Anktell, 1996; Hallet, 2002).

The study of faults allows to find that each major fault consists of subsystem of several fractures with minor en echelon arrangement of their own. En echelon exist associated with fault and shear zones, which is development and occurrence along major zones of weakness. Sense of movement along fault zones can be determine by existence of antithetic (R'), synthetic (R) and synthetic opposite riedel shear (P) in place of tension gashes (T). Major en echelon structure like ridge ranges seem to consist of linear groups of minor individual ridges with a sinistral en echelon arrangement along NW-SE , because shear movements are antithetic with respect to the main fault (Figure 5.18 B) and dextral en echelon arrangement along NE-SW zones (Figure 5.18 C).

In general the NW-SE trends form a series of an elongate fault segments arranged as overlapping normal faults dipping to the SW, changing to NW dip where the faults are arranged in a closely spaced en echelon pattern with NW-SE trend. NE-SW can be interpreted as major P shear, viewed as a part of a regional Riedel shear system. The final E-W orientation of the faults would imply a local counterclockwise rotation show evidence of left lateral shear, formed by Miocene deformation and reactivation of older Hercynian structures especially around the Al Qargaf Arch (Anketell, 1996). The strike-slip transtensional model explain that the subsidence could be related to migration of movement within the releasing overstep between the main faults.

5.6.1 Variance Attribute

In order to test the accuracy of manually interpreted faults represented by fault sticks. Variance has advantage to reveal the discontinuities, so in this study variance used as structural guide by make the comparison. An over lay of variance detection with the manual fault interpretation sticks and polygons showed excellent agreement between variance attribute showing

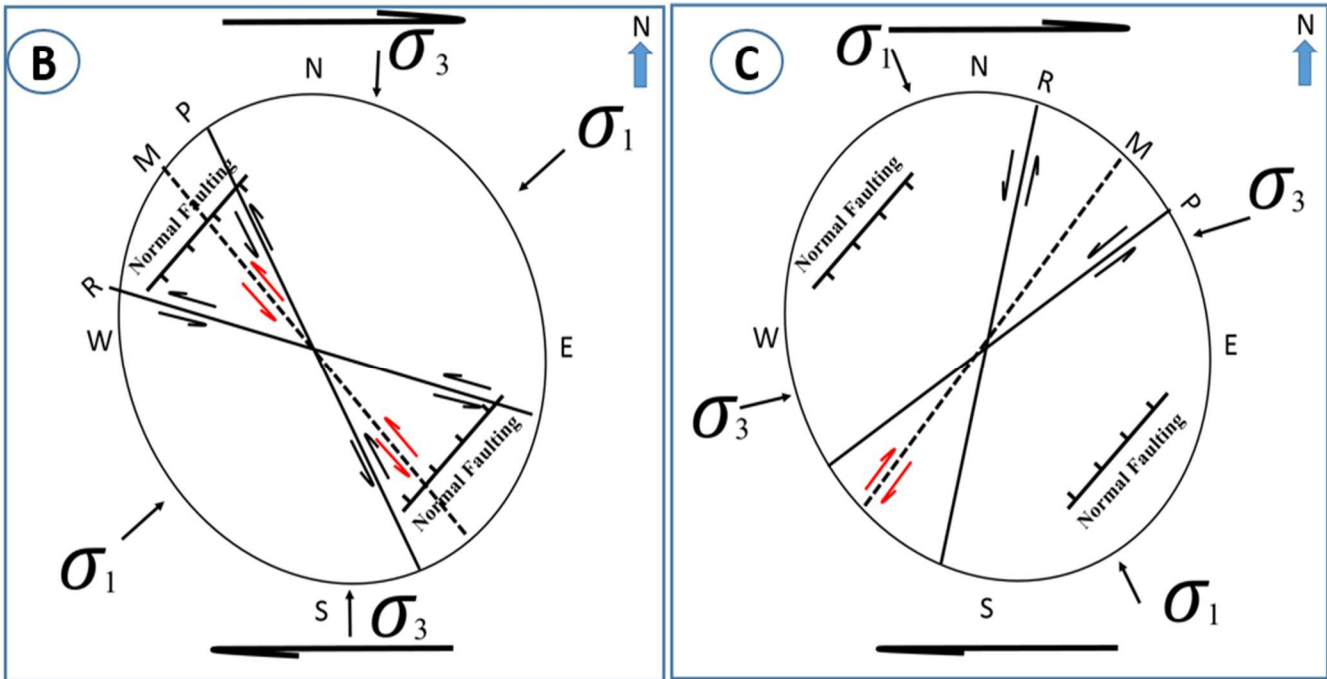
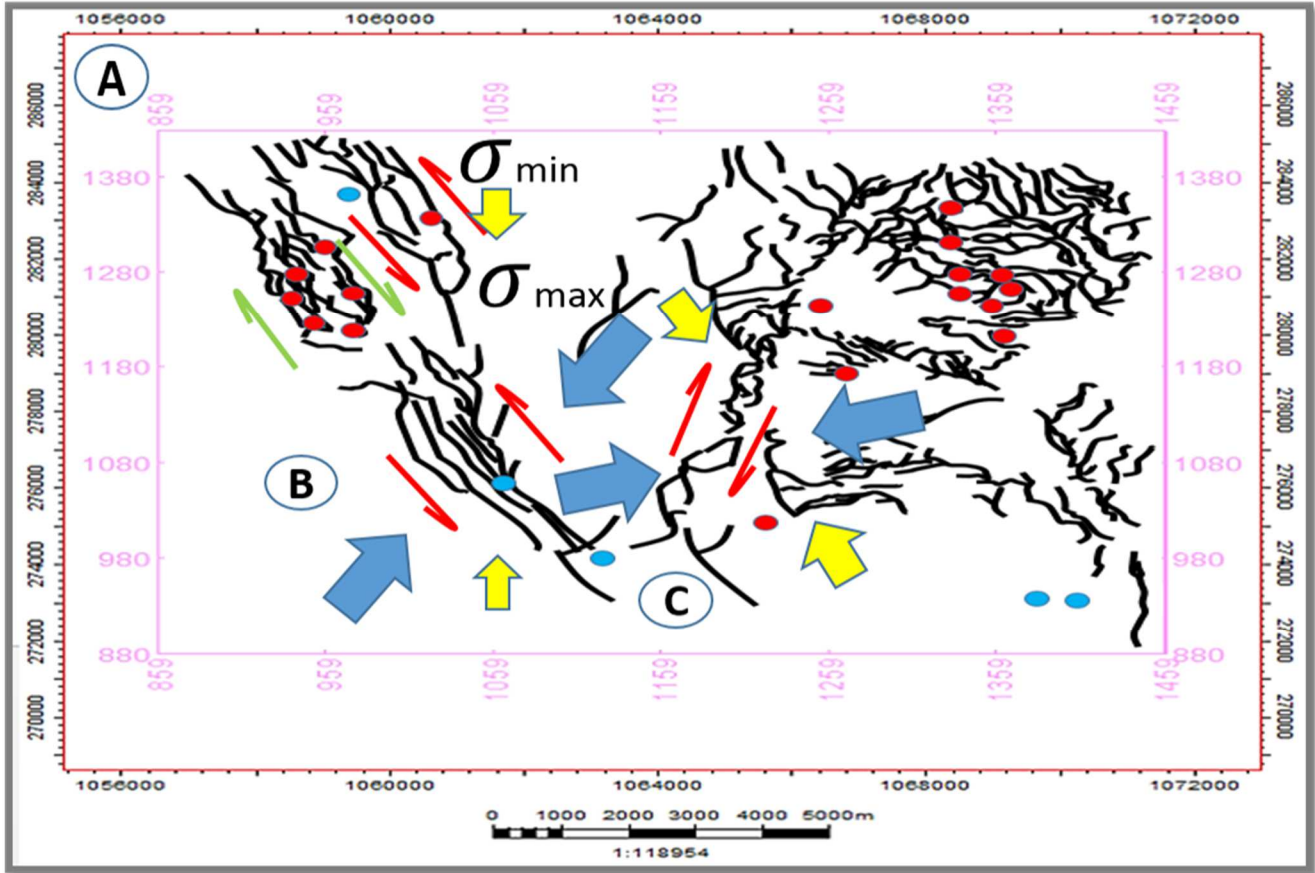


Figure 5.18, (A) interpreted fault polygon represented impact stress in the study area. Proposed stress model illustrating the structural pattern (B) sinistral displacement toward NW direction and (C) dextral displacement towards NE direction.

fault highlighted by the darkest regions and manual fault interpretation displayed by fault polygon (Figure 5.19). Using variance seismic attribute maps on 3D seismic data at different time depths in order to delineate the fault and fold patterns of specific time frames in plan views (Figure 5.19).

The interpreted map (right) and its trace (left) of the Sirt Shale Formation at a time depth of 826 millisecond show the linear geometry of the NW-SE master fault with a left bend releasing bend in the south and propagate to restraining bend along its strike and the distribution of en echelon normal faults in its hanging wall. (As discussed in releasing NW-SE through AA`,BB` and CC` profiles, while restraining through DD` and EE`). The orientation of these en echelon faults is compatible with the main strike of extensional normal faults in the strain ellipse of a left-lateral strike-slip fault system (5.18B).

In the deeper, Tagrift, Etel and Lidam formations at a time depth of 886, 922, 974 millisecond respectively, at this higher structural level in the study area. Figure (5.19) shows geometry of the NW Fault, which subdivided into two closure in the NW of study area. The occurrence of the en echelon normal faults associated with both the NW Fault systems indicates that transtensional deformation continued to affect the Cretaceous deposits. The NE-SW fault system has a major left-bend (restraining bend), where transpressional deformation produced en echelon fold trains oblique to the general orientation of the shear couple. The orientation of these en echelon faults with the main strike of extensional normal faults in the strain ellipse of a Right-lateral strike-slip fault system (Figure 5.18C). This observation is consistent with the transpressional deformation patterns on seismic profiles D-D' and E-E' (Figure 5.12-13). The activity strike-slip indicates that the locally development of transpressional and transtensional deformation domains continued through all the Cretaceous times.

5.7 Orientation analysis of the structural features

Major part of total displacement may take place along just generated Riedel shear, the formation of minor en echelon is possibly to be found in phases within major Riedel shear, where the synthetic shearing cause the minor scale en echelon fracturing. Small-scale releasing bends along this fault are aligned with negative flower structures. These faults seem to be kinematically linked to the active strike-slip fault via a common detachment plane.

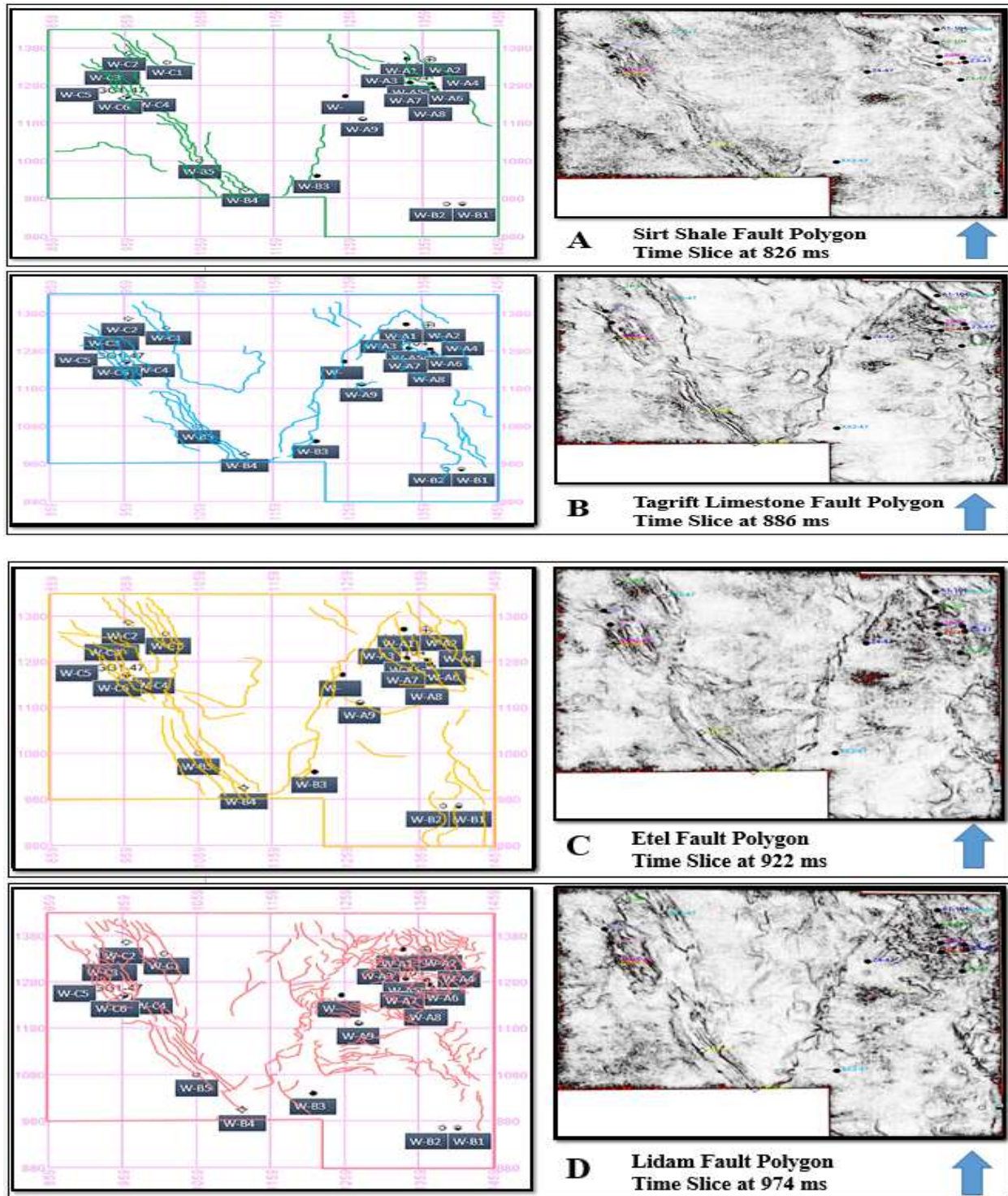


Figure 5.19 Plan view of fault polygons, interpreted from the 3D seismic data for each formation showing the spatial and temporal changes in Upper Cretaceous geometry, which faults that initiated and was re-activated during the Syn- rift phase (A) Sirt Shale, (B) Tagrift Limestone, (C) Etel and (D) Lidam Faults.

In this study, the quantitative analysis have been studied by create points that define the maximum throw and the associated length of each fault within the grid (Figure 5.20 A). The resulting points can be displayed in a function window to produce a classic fault throw vs. length plot (typically a log-log plot) (Figure 5.20 B). This can be useful for checking the consistency and validity of the fault architecture. Understand displacements of the interpreted horizons, play an important role to explain geologic interpretations of the faults based on their nature and types, such as observed fault throws and terminations. The qualitative curve of an example fault can explain the peak of displacement (Figure 5.21A). In order to organize the interpretation all interpreted faults gathered in one folder to interpret precise the length and trend of the faults (Figure 5.21B), which is evaluate the distance along fault and fault displacement in each fault detected (as shown in an example regional fault, Appendix, table 3)

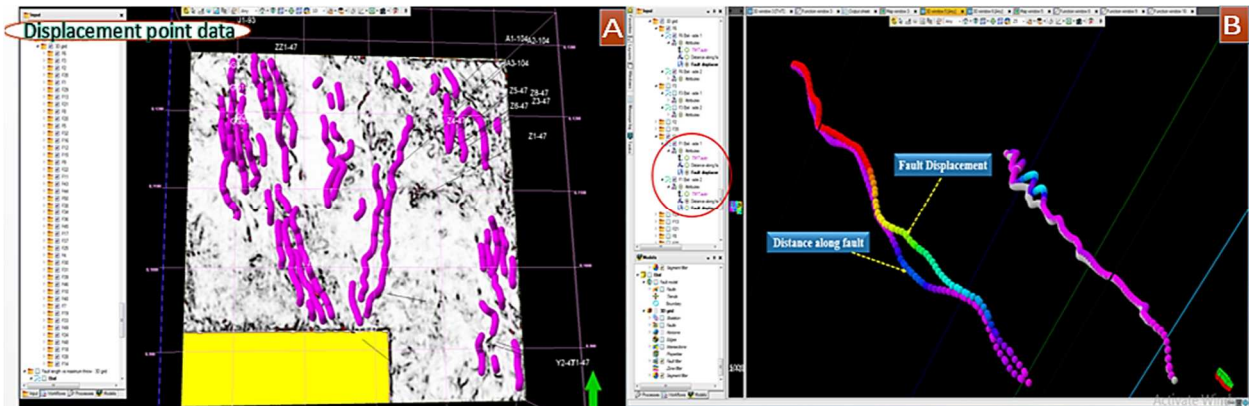


Figure 5.20, (A) displacement point for each fault alone, ensure the accuracy with Variance attribute to trends and lengths. (B) 3D window displayed fault displacement and distance along fault.

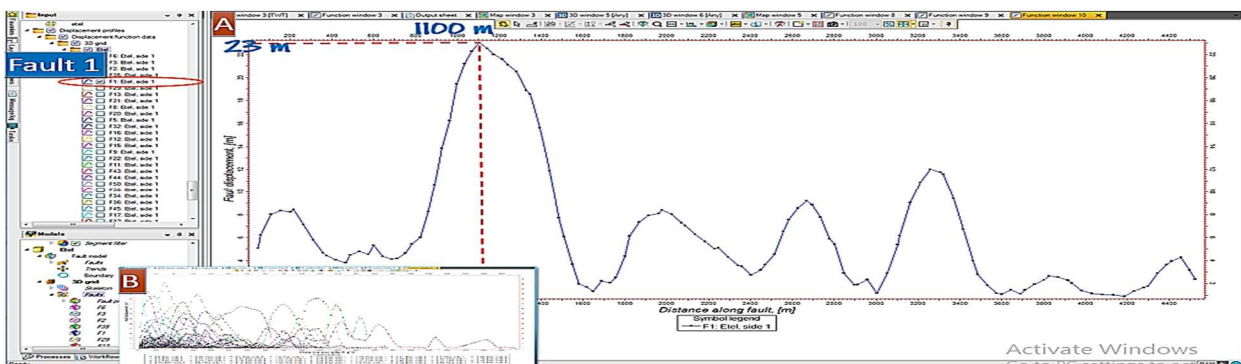


Figure 5.21, (A) function window displayed a quantitative evaluate fault 1, (B) the rest of faults. The important knowing their qualitative and quantitative when the interesting site (prospect) beside the fault.

5.8 Well Log Correlation

One of the best techniques for determining the subsurface structure is the well log correlation technique. In the study area, multiple well logs were available to analyze the Upper Cretaceous Lidam and Etel Formations to identify its lithology between wells. This well correlation was along 18,558 m between W-B3 in the south, W-C2 in the northwest, W-A9 in the east and W-A1 in the northeast. The gamma ray log was mainly used since it was available for correlation purpose across the entire inputted wells. Sonic was used as quality control of the gamma ray interpretation. The gamma ray was interpreted with high values of gamma log interpreted. The interpretation of each formation surface showed that the Lidam reservoir was not purely composed of dolomite with intercalated shales and limestone observed in some of the reservoir surfaces. These interpretations were further delivered to the well correlation panel based on different TVDSS (True Vertical Depth Subsea) of each wells. Well log section cross cutting the major structure trending in NE-SW and NW-SE (Figure 5.22, index map at lower left corner). Lateral changes in Lidam and Etel formations explain structural deformation. Well logs suggest that the Lidam and Etel Formation increases in thickness in the W-C2 dry well, because it was located in the graben structure and other wells are producer due to their locality in the horst. The thickness of Lidam and Etel about 380 ft, 320 ft respectively.

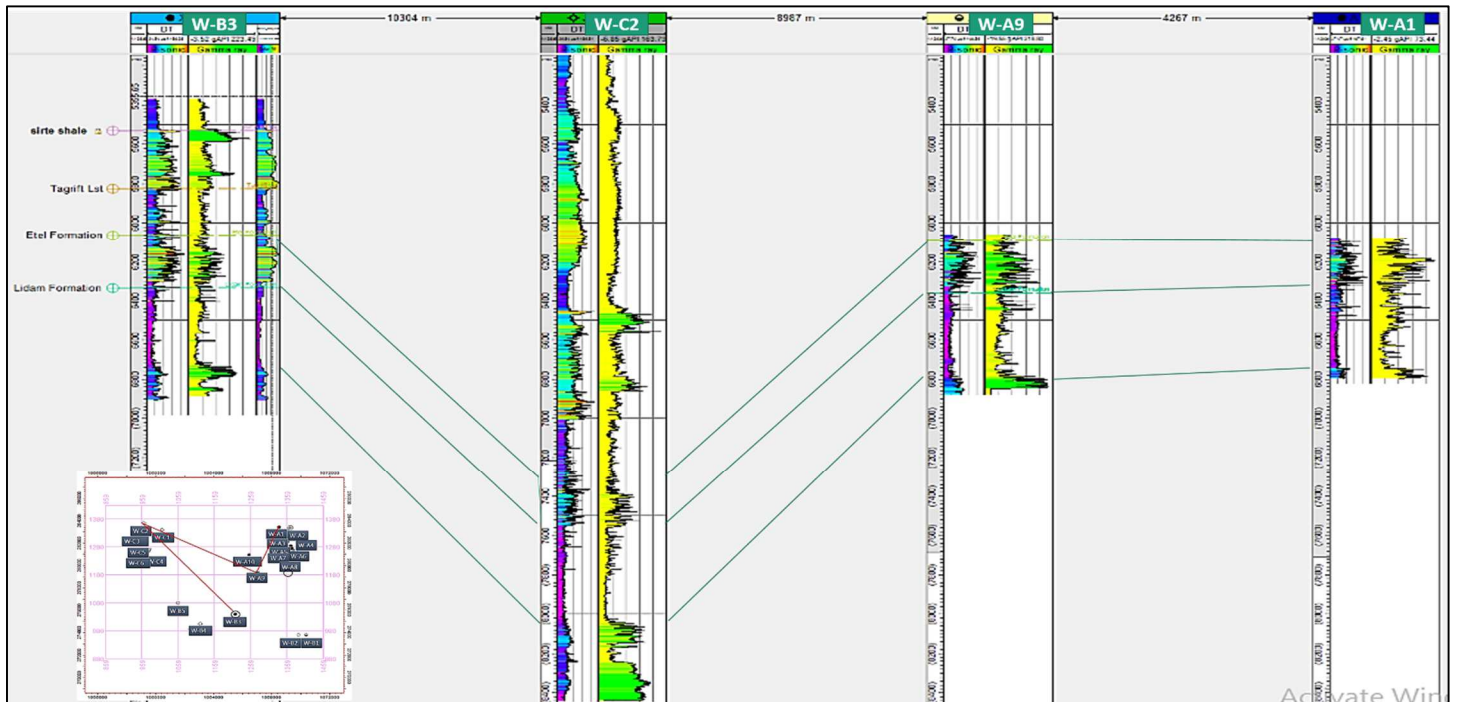


Figure 5.22, well correlation panel for the interpreted horizons, and their lateral changes.

5.9 Horizon Picking, Making and Interpretation

Zone of interest in this study is the Upper Cretaceous sections subdivided into five horizons related to stratigraphic variation, which firstly linked by formation tops then confirmed by well calibration. These horizons were picked with a specific color manually every ten seismic sections spacing, due to great discontinuity in reflectors related to complicated structural regime. The horizons and its corresponding time events on seismic shown in Table. (5.2). Time values of picked horizons were used to generate structural and isochron maps.

Table 5.2 Horizons with their corresponding event on seismic.

Horizon	Corresponding event	Time (ms)
Sirt Shale	Trough	826
Tagreft Limestone	Peak	886
Etel	Peak	922
Lidam	Trough	974
Gergaf	Trough	1066

In this study, Seismic facies analysis used to describe depositional environments out of seismic data, which five horizons were interpreted, Top Sirt Shale, Top Tagrift Limestone, Top Etel, Top Lidam and Top Gergaf. Top (Table, 5.3). Sirt Shale in the seismic section shows a package of high frequency, strong amplitude and good to medium continuity, which is easy identified and regionally traced. Top Tagrift Limestone in the seismic section shows a package of low-moderate frequency, fair-good amplitude and fair continuity. Top Etel shows good frequency, strong amplitude and good continuity. Top Lidam shows low frequency, weak amplitude and acceptable to poor continuity. Top Gergaf shows poor with weaker amplitude and low frequency.

5.9.1 Isochron maps

Isochron maps show spatial variation of thickness of a stratigraphic interval, defined as the time difference between two horizons, these values display the amount of sediment deposition to respect of tectonic activities. Table (5, 4) interpreter the distribution and thickness variation of Sirt Shale, Tagrift, Etel, and Lidam based on their isochron maps (Figure 5.23).

Table (5.3) seismic facies analysis and their interpretation supported by AVO attribute with An Estimated Density Log.

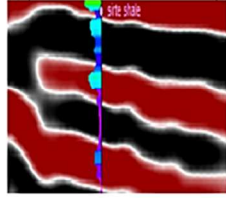
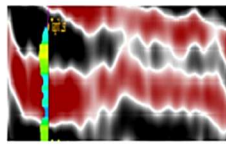
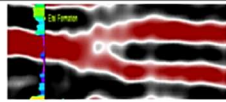
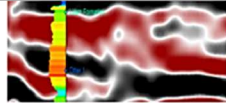
Seismic Facies	Seismic reflection characteristics	AVO Attribute with An Estimated Density Log	Interpretation
Sirt Shale	<p>Sirt Shale contains two seismic facies.</p> <ul style="list-style-type: none"> The first facies is composed of parallel, continuous, and high to moderate-amplitude reflections. It correlates mainly to the argillaceous carbonate deposits. The second facies is composed of short, randomly oriented or domal, discontinuous, variable amplitude reflections. Laterally, the limestone-rich interval changes from seismic facies 1 to 2; but seismic facies 1 is volumetrically dominant. 		<ul style="list-style-type: none"> Marine organic-rich shales Deep marine environment with a homogeneous dominant deposition of shale casing low reflection amplitudes
Tagrift Limestone	<p>contains two seismic facies.</p> <ul style="list-style-type: none"> The first facies is composed of roughly parallel, continuous, and moderate to low amplitude reflections. It correlates mainly to the argillaceous carbonate deposits. The second facies is composed of short, randomly-oriented, domal, high-amplitude reflections and correlates mainly to the limestone. In some areas, the limestone-rich interval changes. laterally from seismic facies 1 to 2; but seismic facies 1 is volumetrically dominant. 		<ul style="list-style-type: none"> Carbonates
Etel	<ul style="list-style-type: none"> The seismic facies has parallel and high-amplitude reflections. 		<ul style="list-style-type: none"> Marine organic-rich shales
Lidam	<ul style="list-style-type: none"> The seismic facies is composed of roughly parallel, continuous, and moderate-to low amplitude reflections. 		<ul style="list-style-type: none"> Shallow marine environment

Table (5.4) interpretation of isochron map of the Upper Cretaceous succession.

Isochron maps	Interpretation
Sirt Shale	<ul style="list-style-type: none"> These are many small grabens and lows which in different places possibly containing local source rocks of Sirt Shale. Laterally, the amount of shale in the upper part of the Sirt Shale interval increase relate to structure agent, toward southwest. That clear when comparing wells W-B3 at south and W-A8 at northeast.
Tagreft Limestone	<ul style="list-style-type: none"> The thickness varies from a few meters to a maximum of about hundred meters. Numerous small, irregular-elongate patches of thins and thicks. The overall thickness pattern is rather uniform; and there is no regional thickening. Some irregular to elongate thicks, are appear, in the middle of the study area.
Etel	<ul style="list-style-type: none"> The thickness increases in low area, whereas limited abundant in the highs, may related to erosion factors.
Lidam	<ul style="list-style-type: none"> Isochron map has two major features. The first is around 90 m thick and has an elongated geometry. The second feature is perpendicular with the first one and around 70 m thick with an elongate shape. The other area is around 50 m thick with irregular geometry.

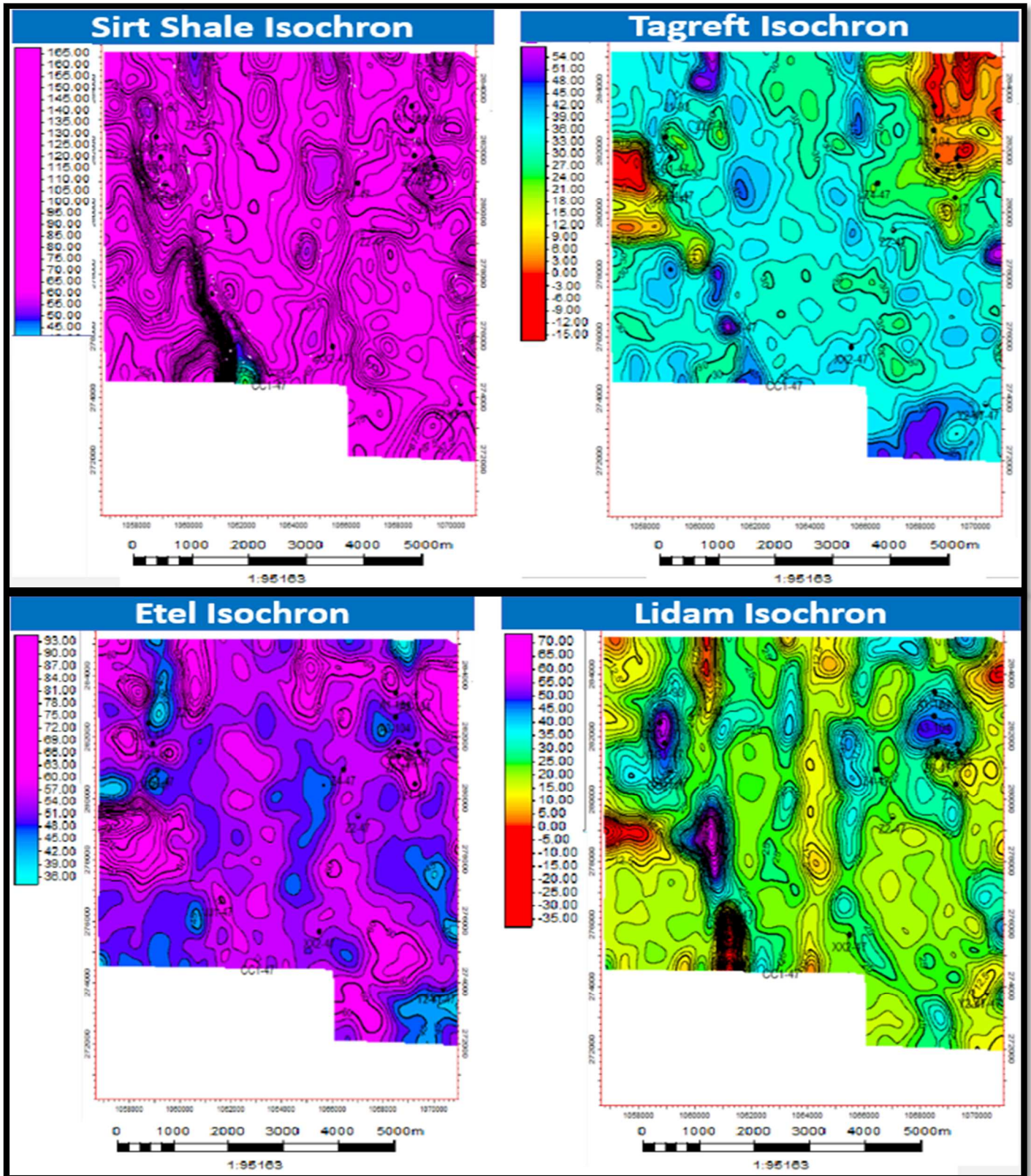


Figure 5.23, Isochron contour map Sirt Shale, Tagrift Limestone, Etel and Lidam

5.9.2 Plan view evolution of Upper Cretaceous history

During the Cenomanian Lidam Formation the first rift-sag cycle was developed, which consists of tectonic subsidence and sag phase. The isochron strongly affected at this period by the tectonic events. Thickness during this phase changed gradually over tens of seconds (about 40 ms) (Figure 5.23, Lidam). Sudden changes can be resulted to the occurrence of faults. The master fault NW-SE (F2) (Figure 5.8, fault sticks) is characterized by strong differences in thicknesses during this phase. The strata display thickening towards the fault in all formation (Figure 5.23). The stratigraphic thickening in the central and southwestern part was produced by movement of F2, F4 and F9 master faults (Figure, 5.8) during the Syn-deposition, which likely occurred in oblique extensional fashion based on the structural setting. NE-SW Major faults in the eastern part during this phase were re-activated during the Upper Cretaceous period.

The second Rift-Sag was developed. The second rift cycle is consists of tectonic subsidence and sag phase. During this phase, many faults were initiated antithetically to the transtensional (oblique) faults (from F11 to F19) (Figure 5.8). These faults are highly controlled by master fault F2, F3, F4 and F5 (Figure 5.8). The isochron strongly affected at this period by the tectonic events. Thickness during this phase changed gradually over tens of seconds (about 45ms) (Figure 5.23 Tagrift); sudden changes can be resulted to the occurrence of faults. The master fault NW-SE (F2) is characterized by differences in thicknesses during this phase. The strata display thickening towards the fault. The stratigraphic thickening in the central and southwestern part was produced by fault movement during the Syn-deposition. Using growth strata as indicators, the faults orientation and location can be determined during the Early Cretaceous rift phase. Certain segments of the master fault (F2) were active during this period (Figure 5.23, Sirt Shale).

5.9.3 Surface Attributes

Surface attribute analysis have been used to extract the different seismic properties to the corresponding to Lidam time surfaces. There are different types of applied surface attributes, whose properties ranges from component parameters of the seismic to the surfaces, it helps to highlight specific properties, which could be stratigraphic or structural, to clarify deteriorates and delineate

prospect within small closure. There were many attributes used to capture common data value, to arrange all the values, then averaging rates of change, measure the reflectivity, etc.

The interpretation of surface attribute as following;

Figure (5.24) gathered Loop Kurtosis to measure loop surrounding Lidam reservoir, to produce amplitude response on the seismic trace. RMS to reduce the background noise, define geological structure and shield light to DHI. Average energy by aiding to map DHI interpreted as hot color. Finally, Window length as indicators for the thickness.

Figure (5.25) displayed Sum amplitude bright of reflection Lidam thickness, by measure reflectivity with amplitude. Stander deviation for separate seismic amplitude degrees. Threshold value detect high amplitude as patches related to structural relief. Average magnitude like RMS but it could isolate geological features.

Most of, to capture highest value within analysis window Median, for arrangement the value to be acceptable to interpret. Harmonic, for define lateral in thickness and lithology (Figure 5.26)

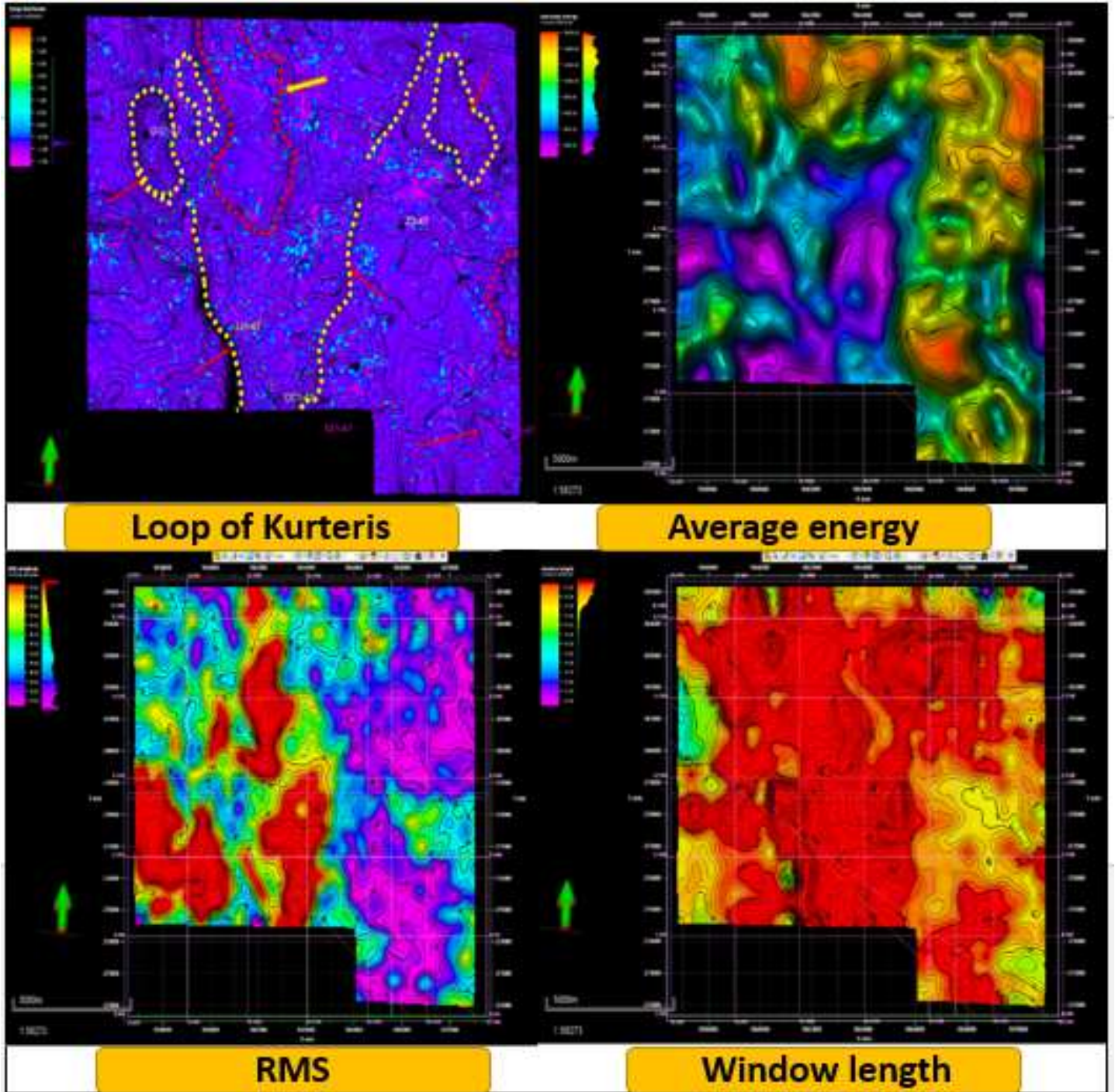


Figure 5.24, Loop Kurtosis surface attribute functions as applied to Top Lidam with the dark color (red arrows) indicating less heterogeneity in the frequency. RMS, average energy and Window length.

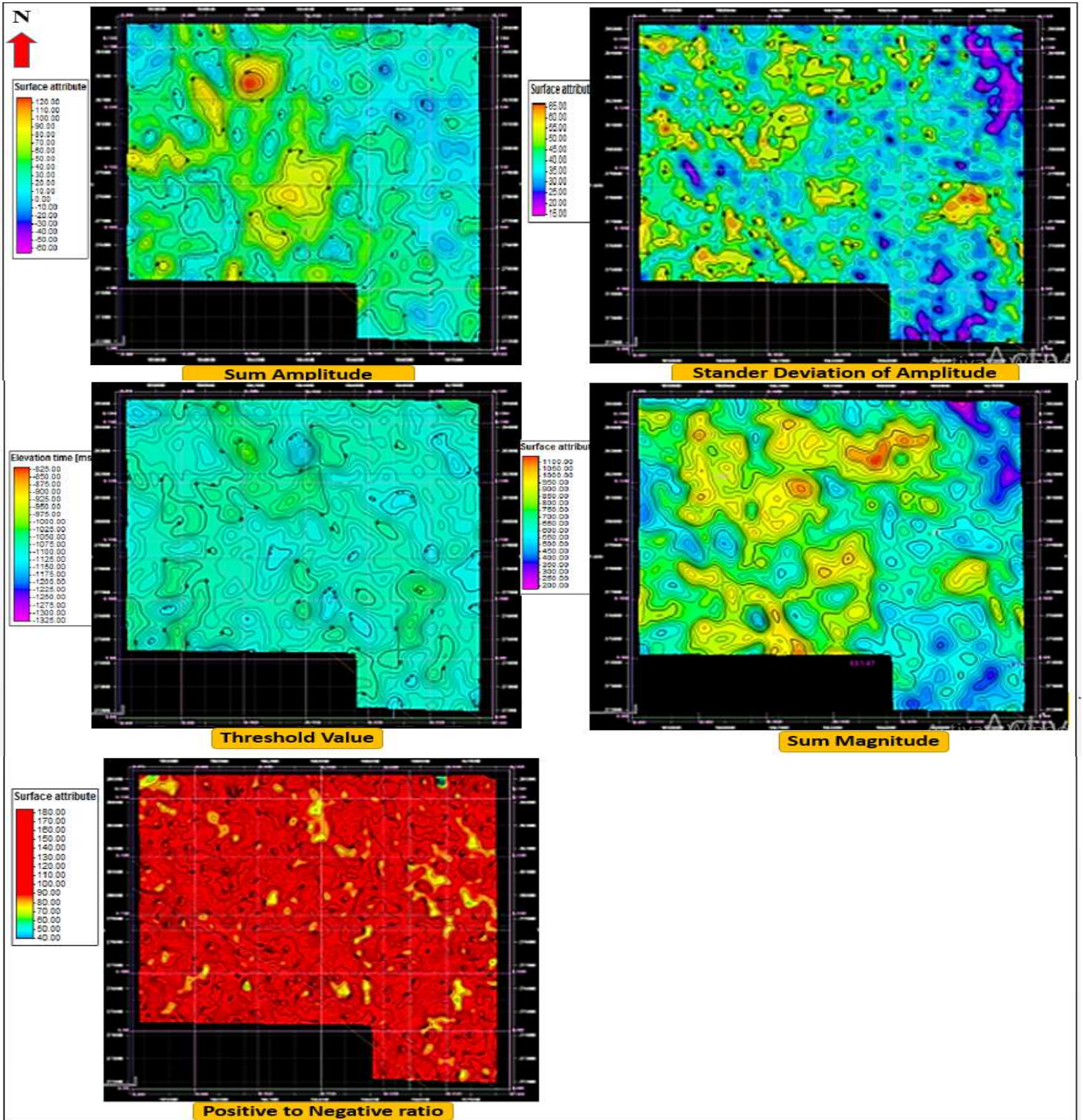


Figure 5.25, Display Statistical Attributes includes Sum amplitudes, sum magnitude, threshold value, positive to negative ratio, and standard deviation of amplitude.

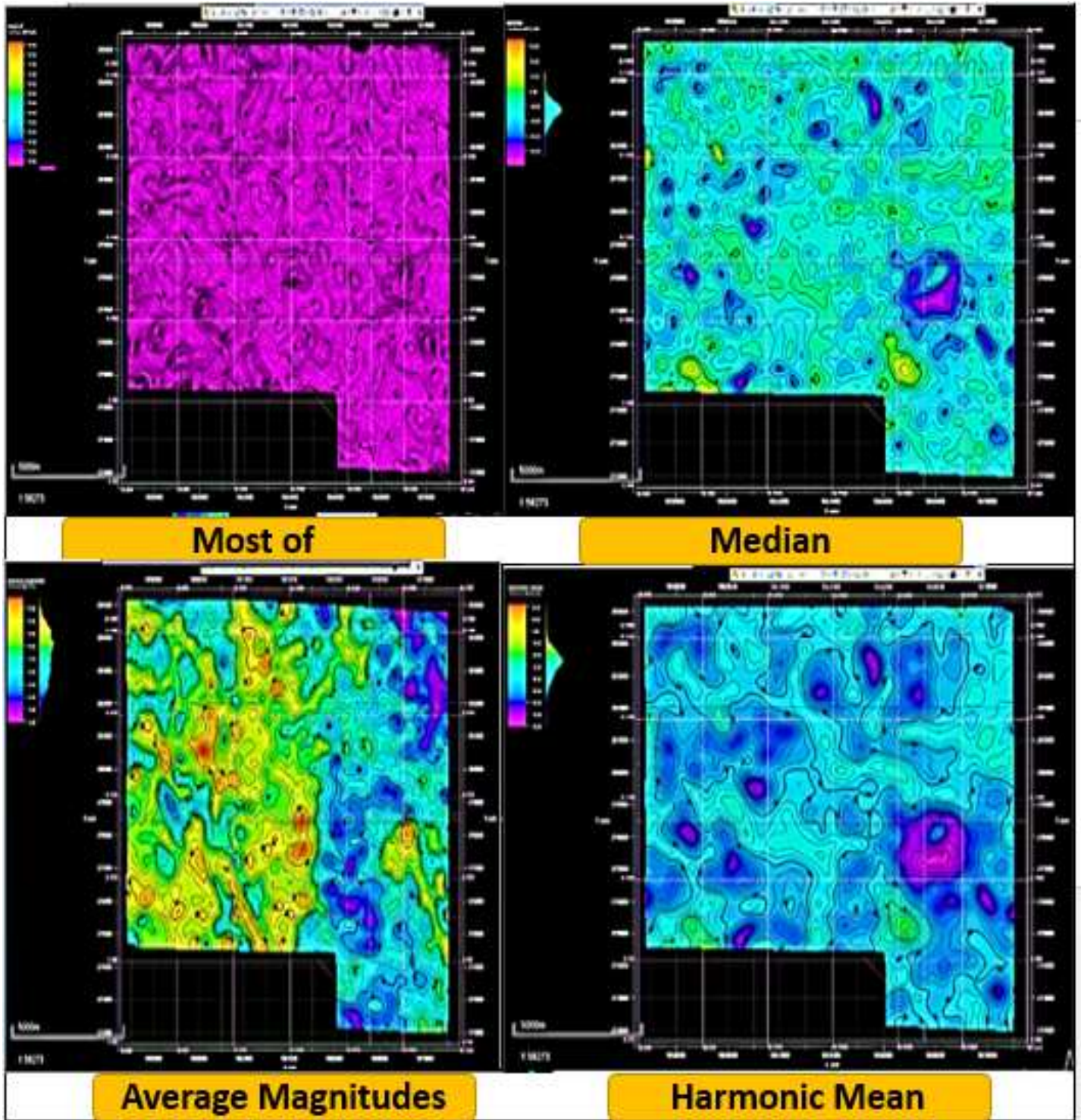


Figure 5.26, Display amplitude surface attribute includes most of, average magnitudes, median and harmonic mean at 974 ms Lidam Formation.

5.9.4 Horizon making

This process is closely linked to the surface attributes and horizon interpretations which provides the needed inputs of surfaces of the respective Upper Cretaceous interpreted surfaces, which involves the creation and inserting these surfaces into the 3D grid. Each horizon modeled based on geologic rules, whether they are erosional such as Gergaf surface, and other formation tops are conformable. Edge control in the 3D frames is defined by the horizons dimension derived from surface boundaries of the seismic interpretation. However, the convergent Gridder method which is used to fill gaps in any undefined area (process pane in Petrel Figure , Appendix).

Make zone process proved relevant in differentiating each of the formation tops into their corresponding formation zones. Zones added (selection horizons) to models by introducing isochrons thickness data. They are also interpreted and fitted into well log intervals to provide detail control to models. The Volume Correction is applied as a measure of the deviation of the isochrons mismatch with the modelled horizons, it was used as a check to quality in the zone process (Figure 5.27).

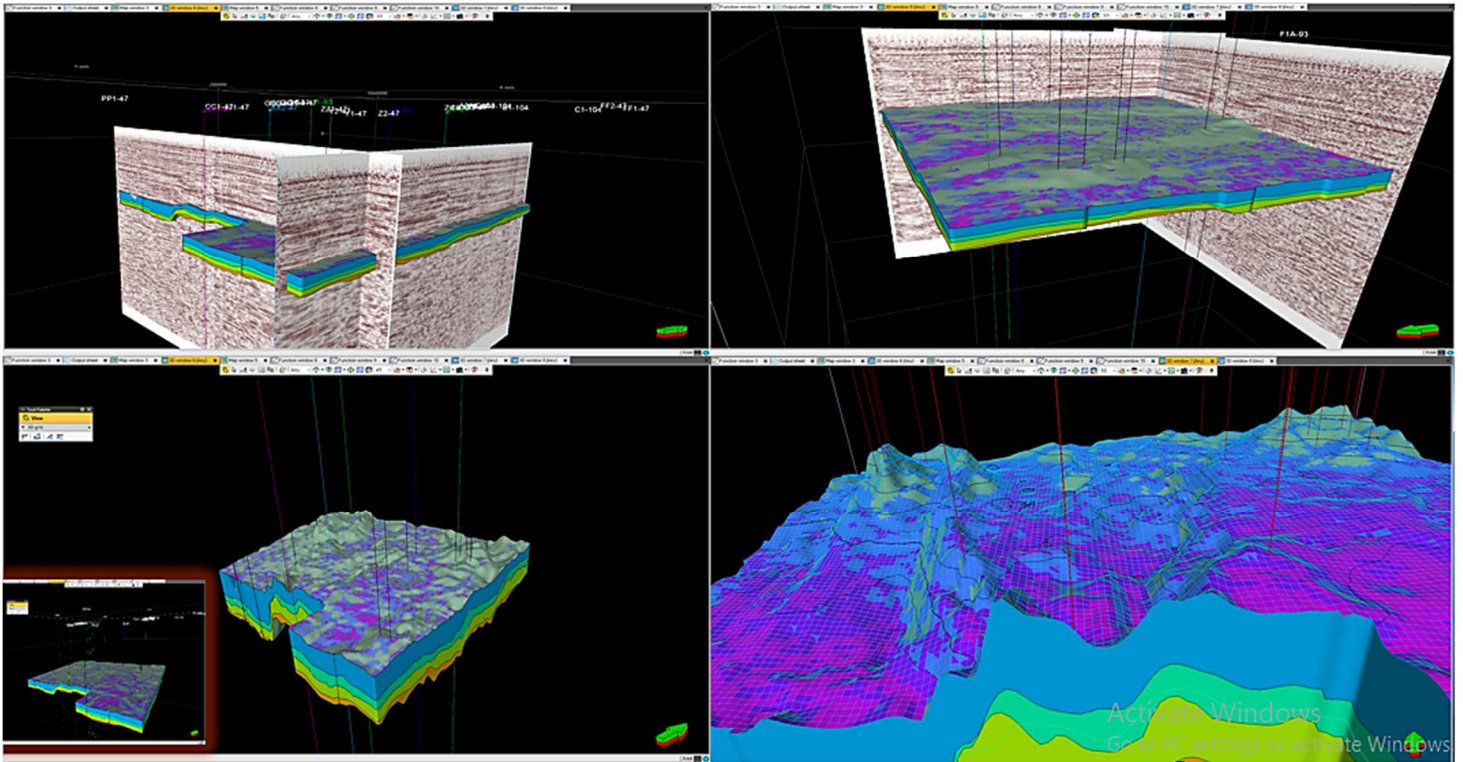


Figure 5.27, 3D structural grid surfaces of the Upper Cretaceous succession, forms the input grids for property modeling (populating the grid surfaces with other properties) which might include facies, saturation models, trend, and petrophysical modeling.

5.9.5 Fault Modeling

The fault modeling process is done by interpreting fault zones of interest manually in the seismic, which are correspondingly used to create fault pillars and patches needed in the model. However, these manual fault pick interpretation, digitization and triangulation, have been tested against automatic fault patches derived from Ant track attribute volumes.

In this study, the interpretation is done by capture the actual geometrical shape dominated by minor and major fault planes to provide actual structural representation, (Figure 5.28 A). Fault digitization helped to maintain the orthogonality of the fault and their geometry across the several interpreted seismic lines (Figure 5.28 B), to avoid cases of faults cross cutting each other when making pillar grids. The faults are triangulated to maintain their orientation across the whole volume, a single fault interpretation folder was used as the only folder for all the interpreted manual faults, which means iterative corrections could be applied to the fault interpretation in a single swoop which makes the pillar grid process of the faults more efficient (Figure 5.28 C).

5.9.6 Pillar Gridding

The process of fault modeling leads to fault gridding which is called pillar gridding, which represents converts the faults with the respective horizon surfaces into pillars in a 3D grid system. However, the consistency of the pillars must be checked against the geologic understanding used in interpreting the faults. The options of the nature of fault planes whether vertical, curve or listric are important inputs needed in maintain the structural interpretations of the fault in the pillar (Figure 5.29 A). The editing pillar options are used to maintain the shape points, make relevant adjustments like cross cutting pillars, truncations, fault connections and other required adjustments (Figure 5.29 B). Pillar gridding is used mainly to develop the skeletal framework of the faults, with the main purpose to guide the gridding framework and orient cells parallel to faults which are further converted into surfaces. The options of using the grids could serve the purpose of Geo-modeling of creating of static models and also in flow simulation grids (Figure 5.29 C) The grid skeleton is a grid consisting of a Top, Mid and Base which are attached to the Top, Mid and Base points of the key pillars consisted in the 3D grid view (Figure 5.29 D). The gridding boundary area was limited to the time surface, automatic rotation angle by faults using the generated fault sticks.

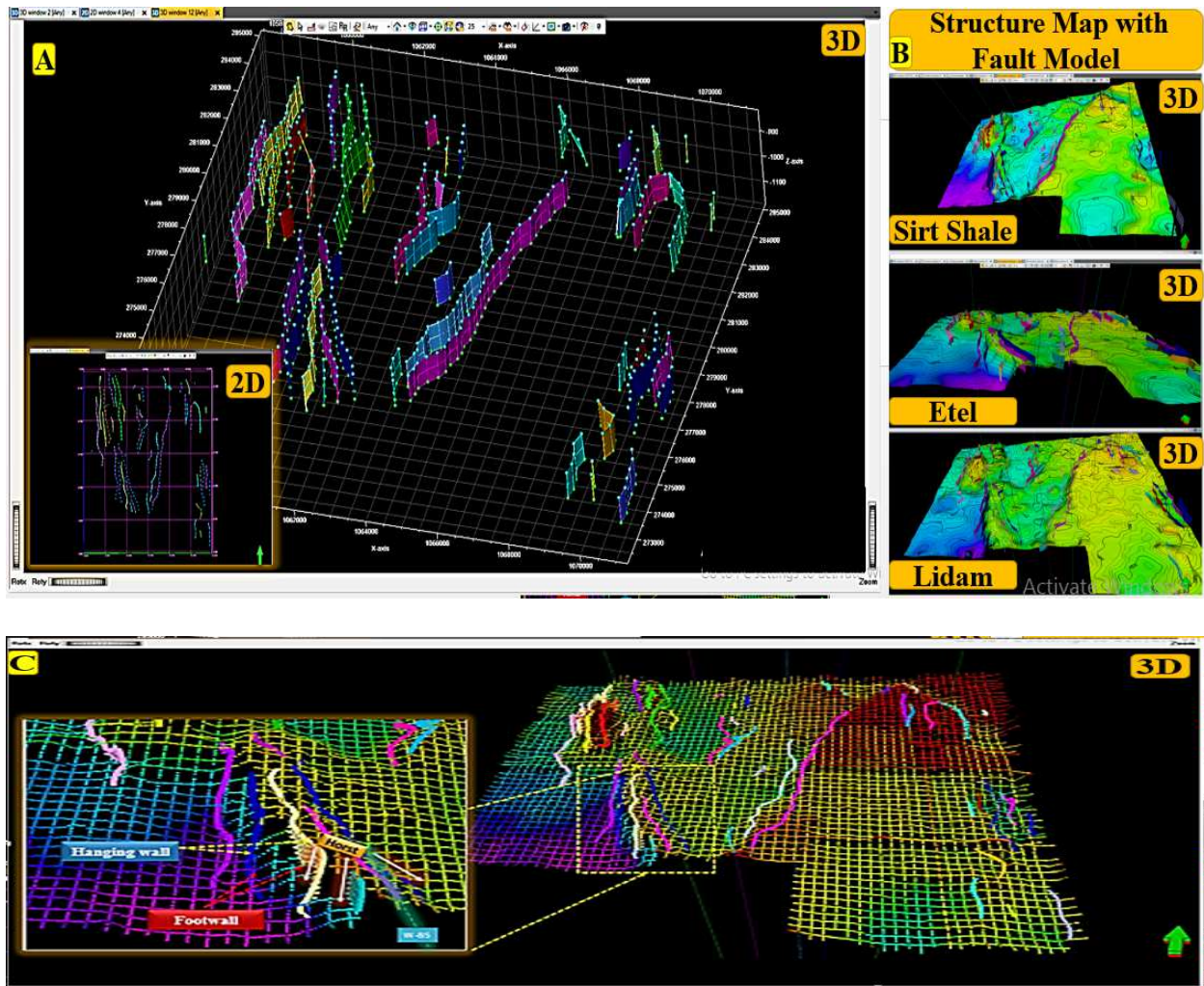


Figure 5.28, (a) the modelled fault in 2D and 3D view interpretation window, showing the different fault segments/compartments. (b) Hanging wall and foot wall displayed in the fault model with the horizon, it is extremely helpful to understand structural and stratigraphic framework. (C) Time structure map of Sirt Shale, Etel, and Lidam are displayed actual structural representation with fault model.

The observed problems of the grids with closely linked faults of shorter distances and also linking faults of different pillar geometry. The deep investigation to control grid increment and the faults quality of the grid skeleton had been done to the Top, Mid and Base skeleton grids the particularly folded grid cells and spikes grid events, To produce an efficient fault pillar grids, so that the modeling process must be effective enough to deliver the accurate fault interpretation from the seismic sections. For the faulted areas, the horizons are deleted in area around the faults and an extrapolation is performed to "stretch" the surface back onto the fault plane. This will ensure

that rollovers or pull-ups near faults are eliminated and a high quality layering of the 3D grid is preserved. The final step in structural modeling is to insert the stratigraphic horizons into the pillar grid.

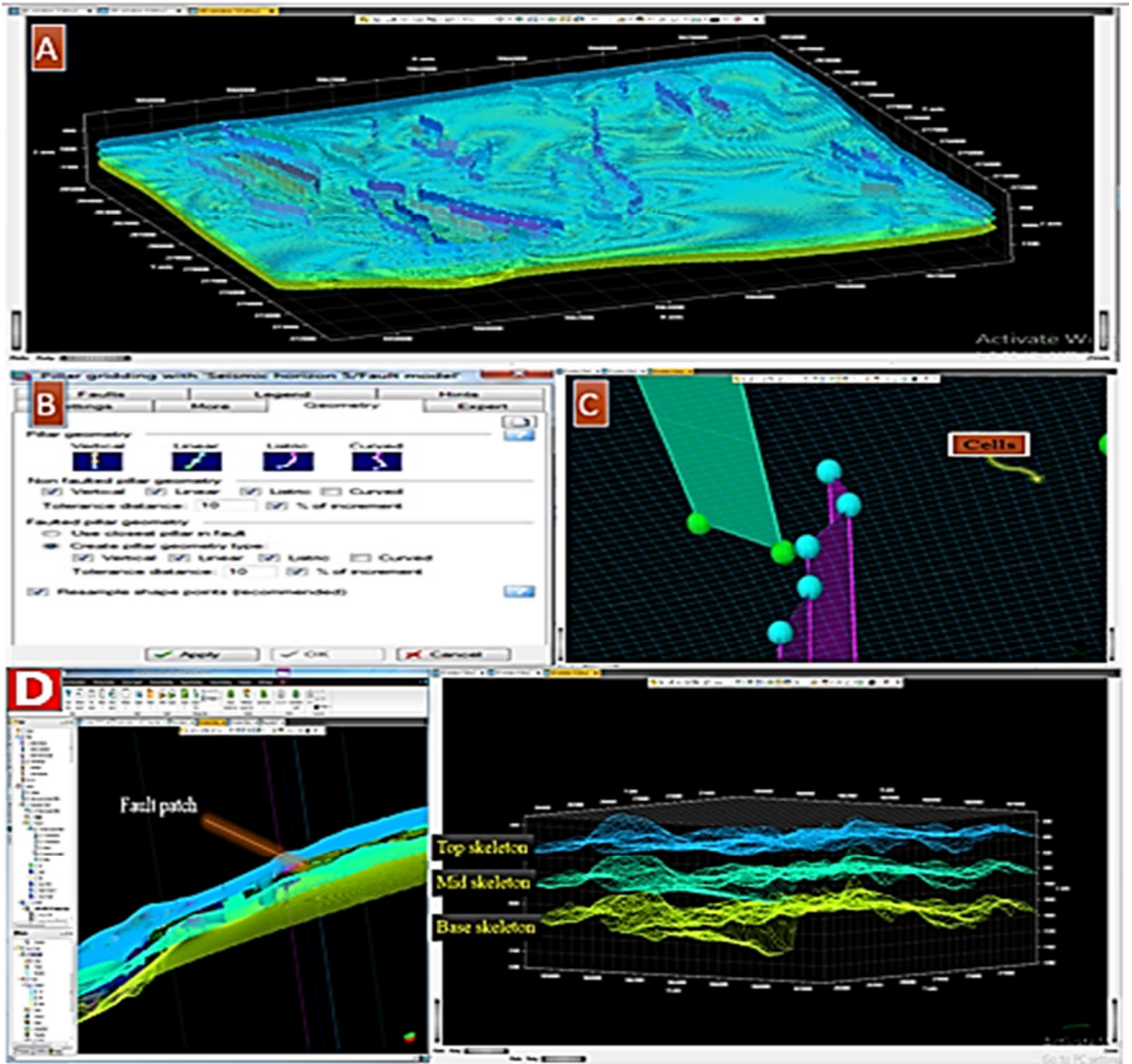


Figure 5.29, Pillar geometry type defined to show the nature of the fault in the 3D frame. (a) Shows the fault geometry and pillar properties (b) The connected pillars of the interpreted manual faults (c). The grid skeleton with the top, base and mid skeleton, showing the fault patch surface.

5.9.7 3D structural grid Surfaces

The final structural modeling is in the creation of 3D structural grid surfaces, which comprise both the fault modeled pillar grids and the horizon surfaces. The skeletal framework of the base, mid and top skeletons inputted with the edges which provides the structure frame as geo-modeling grids. The zones of each models with filters are displayed in the 3D grid except for the Gergaf top skeleton which is an unconformity surface. (Figure 5.30)

3D Visualization was performing as a good way of visual inspection of the 3D structural frame model as a quality control process which gives a better picture of the variability of the grid surfaces across the seismic inline and cross lines. For example inside wall visualization techniques used to establish well positions by seismic to surface tie. This technique is adequate to farming in new drillable locations in exploration area where it could determine the seismic positions to structural reliefs and closures. This provide a clear control on polygons and structure reliefs. It is interesting that the positive horst structural reliefs were characteristically defined as areas within the model which had positive features in the grid and the negative relief captured the graben deposits.

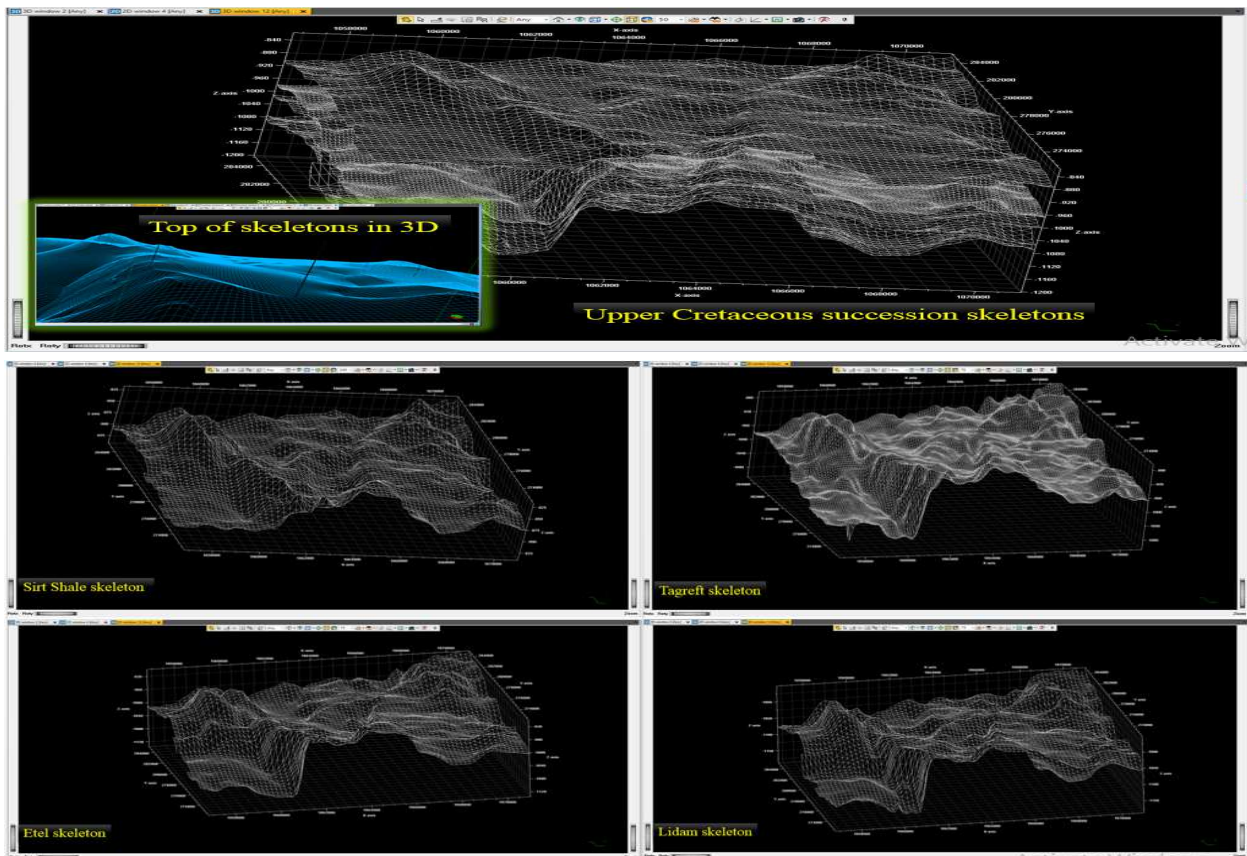


Figure 5.30, Interpreted 3D structural grid skeleton for the Upper Cretaceous surfaces.

5.10 Lithology interpretation by using seismic attributes

5.10.1 Instantaneous frequency

This supported by using instantaneous frequency attribute in many factors. First of all as bed thickness indicator. The next for lithology recognition, which is the low frequency anomaly interpreted as hydrocarbon indicator related to unconsolidated carbonate, while the higher frequencies indicate sharp interfaces such as exhibited by thinly laminated shale. In addition used as edge indicate, it showed that the semblance of frequency events across geologic features of faults, reflectors with distinct red colored patches (Figure 5.31). Stratigraphic characteristics such as lithology recognition, edge indication, and delineate consolidate material.

5.10.2 Sweetness Attribute

Sweetness applied to understand major energy reflectors to identify geological events with a given package (Figure 5.32). Areas of same package with almost same reflection strength are characterized by red color, while areas of main energy reflections have much light patches it shows packages within the interested sections.

5.10.3 Cosine of Phase Attribute

The attribute used to resolve interference of complicated fault structures, which is simplified picking horizons due to capture the continuity of horizons, which is useful in delineating seismic facies and stratigraphy such as chaotic, onlap, downlap (Figure 5.33).

5.10.4 Grey level co-occurrence matrix (GLCM)

In this research, GLCM texture analysis used to correctly predict and characterize the reservoir parameters, by evaluating the response of reservoir to non-reservoir facies with respect to fluid saturation in a development field. The GLCM exhibits high amplitude continuous reflections generally associated with Sirt Shale deposits have relatively low energy, and high contrast and low entropy in general indicative of hydrocarbon accumulation. In contrast the low amplitude discontinuous reflections related to shallow marine deposits have low contrast (Figure 5.34).

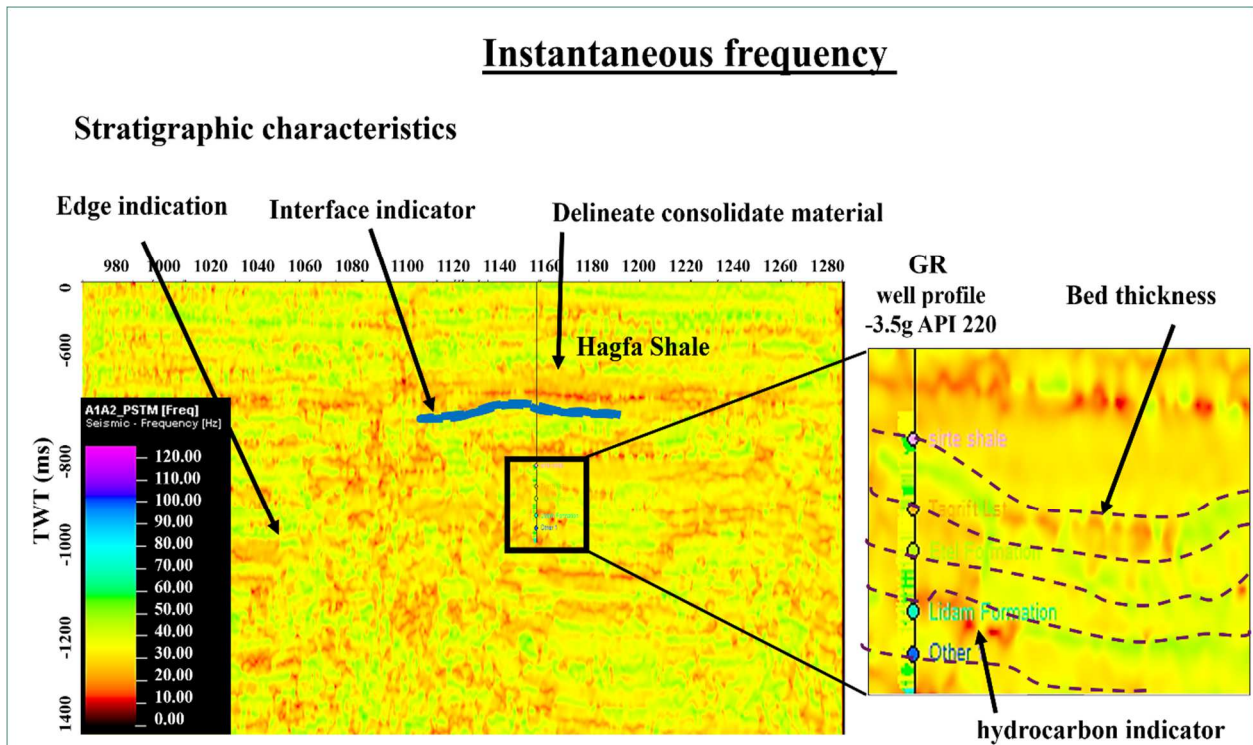


Figure 5.31, inline 1040 (F) Instantaneous frequency attribute (D) reflection intensity attribute section delineate the strong amplitude as a package extend laterally by light color

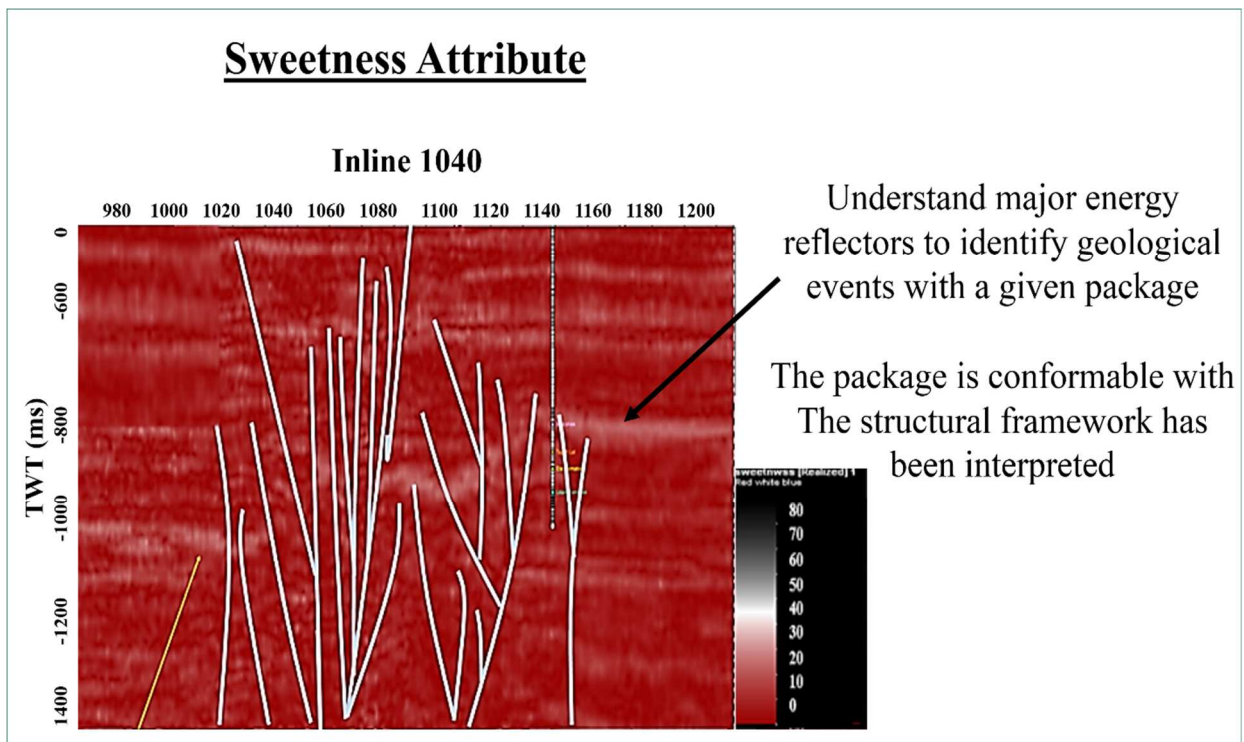


Figure 5.32, inline 1040 shows sweetness attribute.

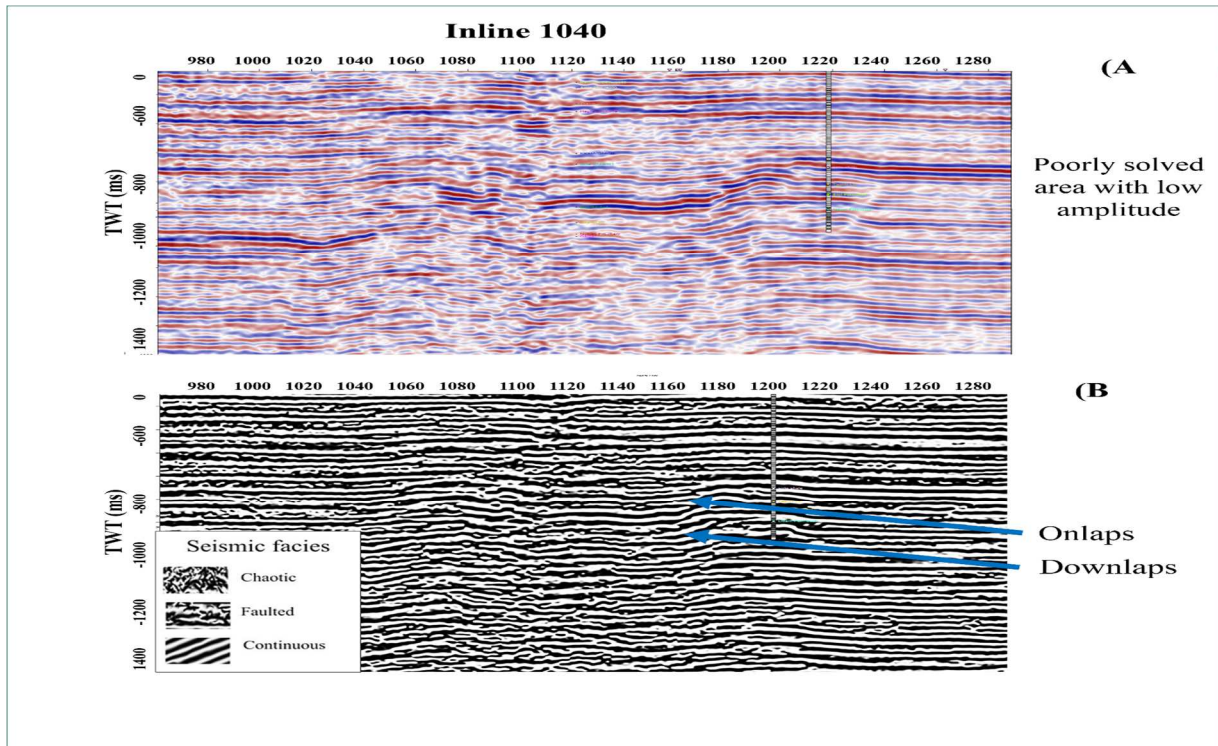


Figure 5.33. (A) The raw data with low amplitude poorly solved seismic events. (B) Cosine of Phase enhances the continuity of the reflectors in those areas and provides a better resolution.

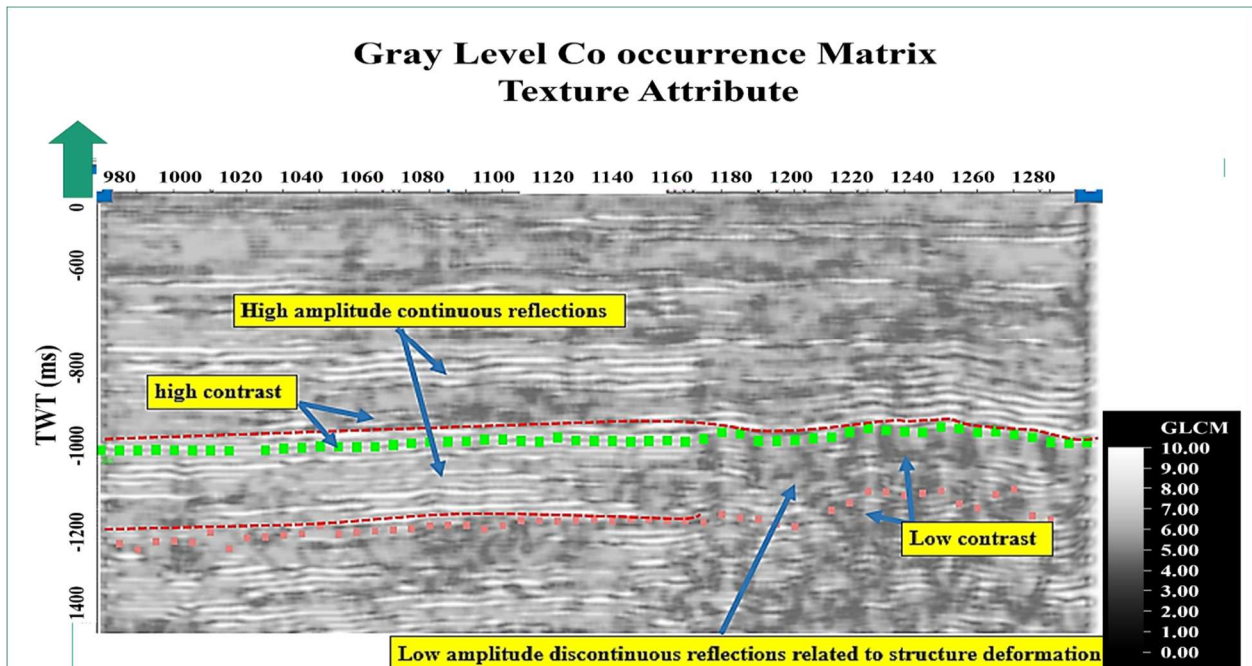
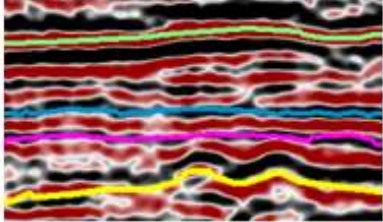
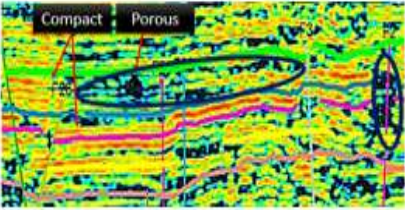
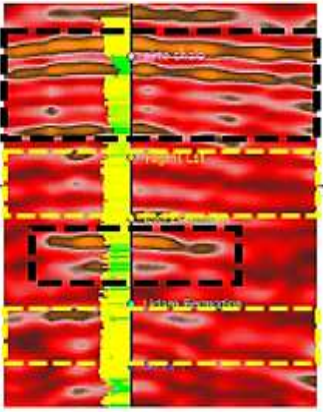


Figure 5.34, The GLCM attribute of crossline 1340 explain analysis properties of seismic textures.

5.10.5 AVO

This study investigated the following polarization attributes: the AVO strength and AVO fluid strength, in order to compare conventional AVO attributes with the polarization attributes. One of the main benefits of this approach is the enhancement of seismic anomalies that either exhibit small anomalies or are embedded in the back ground trend, as shown in the Table (5.5).

Table 5.5, comparison between the conventional AVO attributes with the polarization attributes.

	AVO Attribute	Interpretation
AVO		<ul style="list-style-type: none"> • Identification of reservoir zones enhanced by predicted hydrocarbon from amplitude, with consideration of geological structures with rock physics. • The integration of different derived AVO attribute volumes with other derived seismic attribute volumes can provide geologically meaningful estimates to develop a more comprehensive interpretation
AVO fluid strength		<ul style="list-style-type: none"> • The advantage of this attribute is extremely helpful to define compact and porous lithology. Distinguished the compact Sirt Shale and Etel Formation by orange package
AVO strength		<ul style="list-style-type: none"> • AVO strength used in conjunction with the polarization angle (change in time, and orientation) to characterize the seismic trace events. • Angle of polarization is characterized by weak seismic events with small values of AVO ($L=0$), at reservoir interval of Tagrift and Lidam referred by dashed yellow rectangular, which is the gamma ray log profile aid to calibrated W-B3 with attribute section to delineate the top and base of formations. • The attribute used as lithology and hydrocarbon indicator, which is reflect strong seismic events with large AVO value at Sirt Shale, and Etel interval. GR log support the these results because of shale content in this formation

CHAPTER SIX

DISCUSSION AND PROSPECTIVITY

6.1 Discussion

- Process of modeling requires a high quality control of the input data. The integration of different data inputs posed challenge in the ability to combine and integrate the knowledge and skills. Geologic understanding in combination with window based on visualization and seismic attributes, were used to interpret faults in Upper Cretaceous surfaces. These form the required inputs needed in performing the structural modeling framework.
- Seismic interpretations were done with the Tops of Upper Cretaceous succession used as control surfaces. Faults sticks, with the inputted 20 wells used alongside in creating the structural models and defined in most of the lines by the high structural relief of the Horst.
- The effective implementation of the attributes can be achieved by collecting two or more kind of attribute to make sure the accuracy of interpretation. In such a faulted area, the fault modeling process is done by interpreting fault zones of interest manually in the seismic, which are correspondingly used to create fault pillars and patches needed in the model. These manual fault detections tested by ant track (Automatic fault extraction) precondition process by use chaos and structural smoothing attributes as input data to run the ant attribute separately to see faults clearly. In Figure (6.1) variance time slice at Upper Cretaceous succession invested to detect faults (red line in Figure 6.1A). Cosine of phase well defined in lateral changes and delineate structural features such closures (yellow color), low area (brown color) and uplifted triangle shape so clear (light color) (Figure 6.1B). Conceptual 3D model stratigraphic succession with structural framework (6.1C) shows excellent representation in the paleostructural relief during Upper Cretaceous times.
- Transtensional movement (Oblique extension)

Sirt Basin experienced multi-phase subsidence from the Cretaceous to recent time in response to the change of regional. The widespread distribution of phases were characterized by early-stage of rifting and a late stage of thermal contacted sagging. The combination of strike-slip movement along (shear) and normal extension mechanism (regional stretching) along the study area occurred during this phase. The regional relationship and fault systems

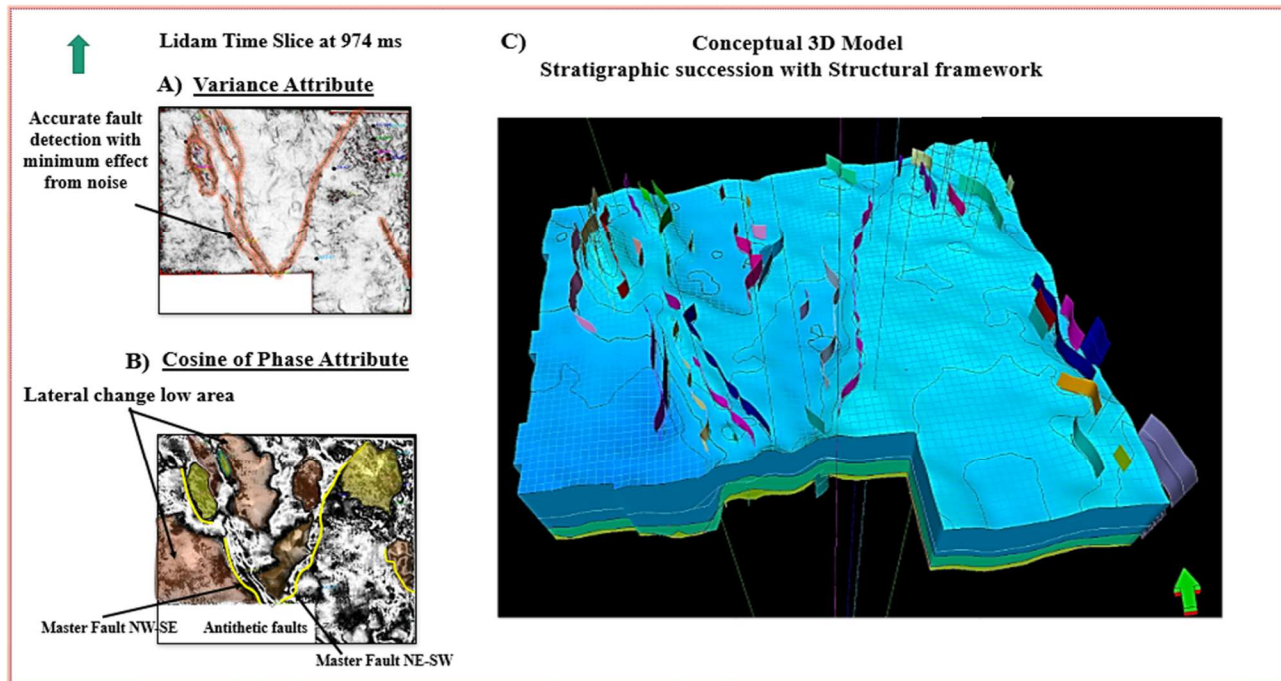


Figure 6.1, (A) Variance time slice at Lidam time, (B) Cosine of phase at at Lidam time and (C) Conceptual 3D model stratigraphic succession with structural framework.

orientation indicated that the possible origin of the study area is a pull-apart that resulted from oblique shear movement. The study area origin is possibly transtensional movement rather than pure strike movement. This suggestion is based on the following observations and characteristics;

- Seismic sections and structural maps confirmed the internal structure interpretation.
- Flower structures (associated with a pull-apart structure) are associated with the strike slip fault (F1 and F2) produce collapse due to contrasting the major faults lateral movement.
- The sense of movement (NW-SE extension) of the F2 during the Early Cretaceous Period first sag phase and the one depocenter controlled by F2 (Figure 5.14), support the interpretation that F2 formed by oblique restricted bend. (Figure 5.18).
- The sense of movement of the F1 fault NE-SW compression, as a result of NW-SE extension during the upper Cretaceous period, the bend in F3 (Figure 5.12 , DD`cross section profile), and the one deocentre controlled by F2, support the interpretation that F2 formed by strike-slip movement (transtension) and it is compatible with the wrenching restraining bend.
- The regional stress regimes were mainly N-S and NE-SW, which reactivated the basement lineaments of the central Sirt Baisn shear zone obliquely.

6.2 Prospectivity of the Bualawn and Dor Mansour Fields

The purpose of the Upper Cretaceous modeling is to evaluate the distribution from seismic volumes with available wells and determine probable prospect locations. Two prospect locations were identified based on time structure map, surface attribute and fault modeled. These prospects are localized within the closures horst structure across the seismic volume (Figure 6.2). Screening the prospects further, using fault surfaces with polygons, several fault segments was observed to segment reservoir surfaces.

Pre drillable well locations would typically be defined based on these structural elements, where targets would be based on the horst highs and fault assisted as the main closure element from seismic section inline and crossline. Elongated anticlinal features bonded by a fault, the bonded faults in the area are providing the oil accumulation migration path to the closures in the area (Figure 6.2).

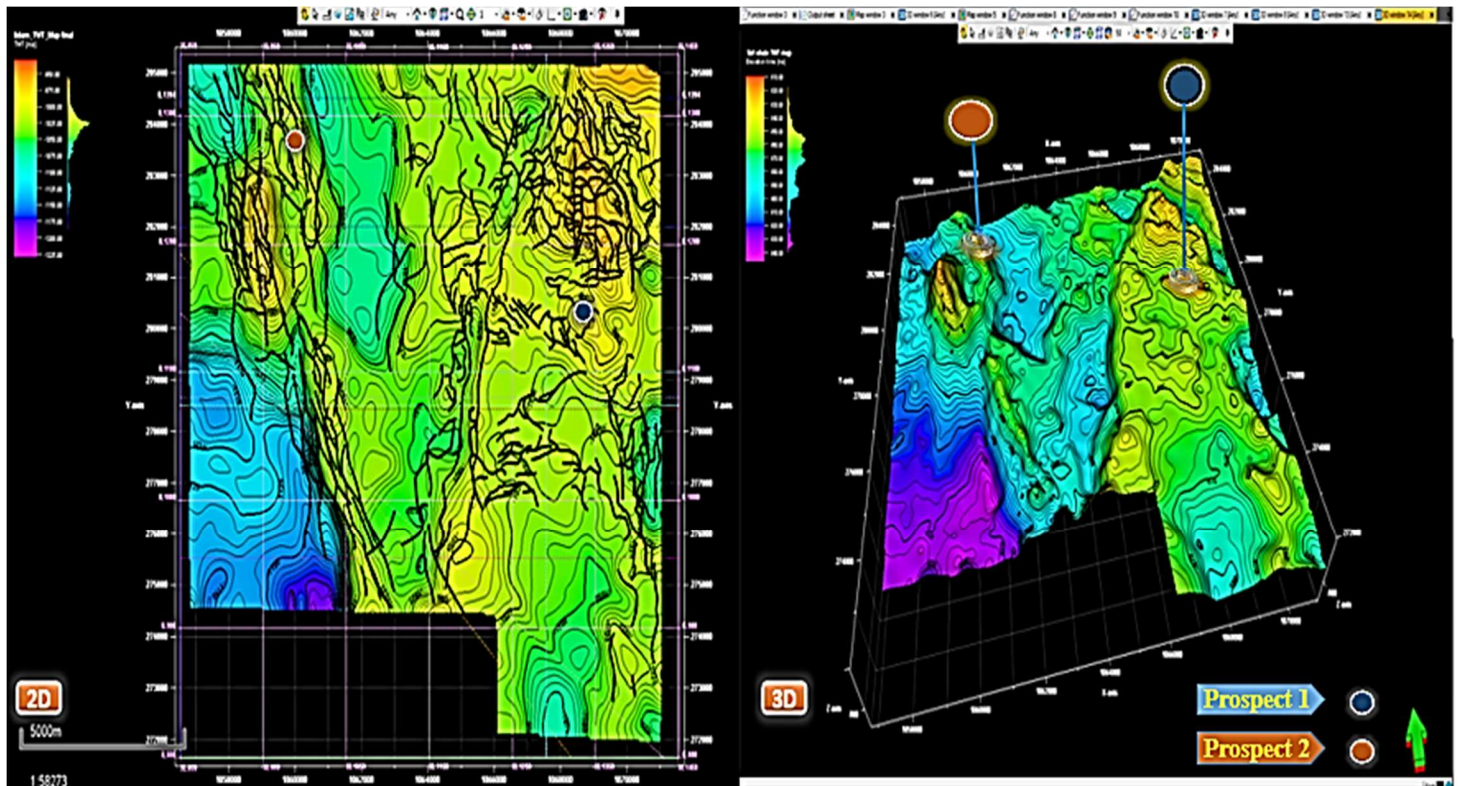


Figure 6.2, Lidam time structure maps prospect well location.

6.2.1 Prospect 1

Prospect oil well located in the eastern part of the study area, roughly in the crossed between Inline 1220 and Crossline 1350. Impact Structure to prospect interpreted through seismic section as NE-SW origin in the Hercynian orogeny, which is reactivate during Upper Cretaceous times to create En echelon related to sinistral movement, strongly influenced by local depression in the central part of study area, related to W-E extension.

Composite seismic line (SE-NW-NE-N) has been used in order to whole understand of structure framework. Seismic section interpreted the prospect as Horst structure bounded by faults as shown in Figure (6.3). Geoseismic section simplified the fault recognition, and clearly define that the strike slip fault is the structure for many wells as pool oil, which the prospect structure has been involved. Lidam structure map shows clearly closure bounded fault, and identified pre-drillable location within the horst crested areas. AVO fluid strength, and AVO strength, support from lithology point of view the prospect. (Figure 6.3). 3D structural grid surfaces gives a better picture of the variability of the grid surfaces across the seismic inline and cross lines.

6.2.2 Prospect 2

Prospect oil well located in the westren part of the study area, roughly in the crossed between Inline 1330 and Crossline 1100. Impact Structure to prospect interpreted through seismic section as NW-SE origin in the Pan African orogeny, which is remained appearance during Upper Cretaceous times to create En echelon related to sinistral movement, strongly influenced by local depression in the central part of study area, related to W-E extension.

Composite seismic crossed well to understand overview of structural framework. Lidam structure map with seismic section, and geoseismic model prove that the prospect within the horst crested areas shows clearly closure bounded fault. AVO fluid strength, support from lithology point of view the prospect. (Figure 6.4). 3D structural grid surfaces gives a better picture of the variability of the grid surfaces across the seismic inline and cross lines. Positive horst structural reliefs were characteristically defined as areas within the model which had positive features in the grid (Figure 6.4).

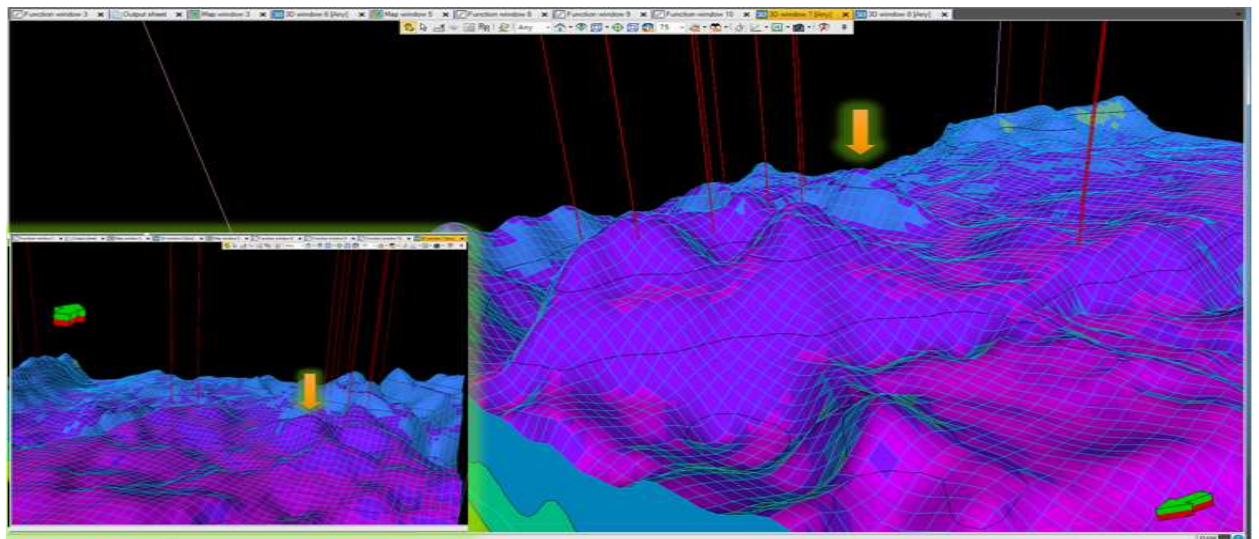
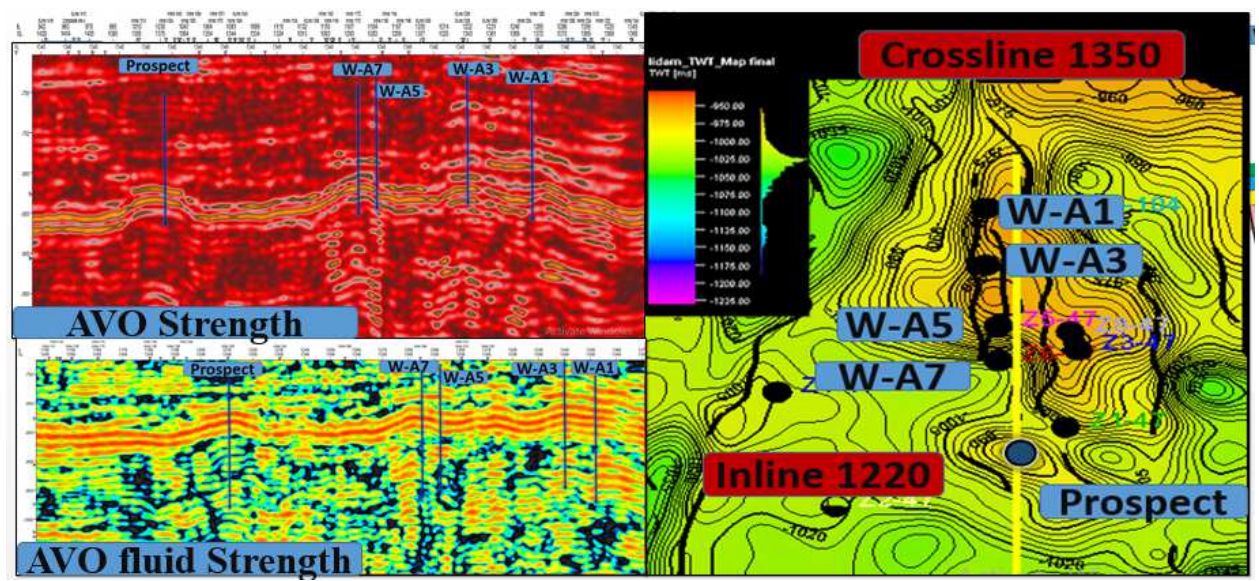
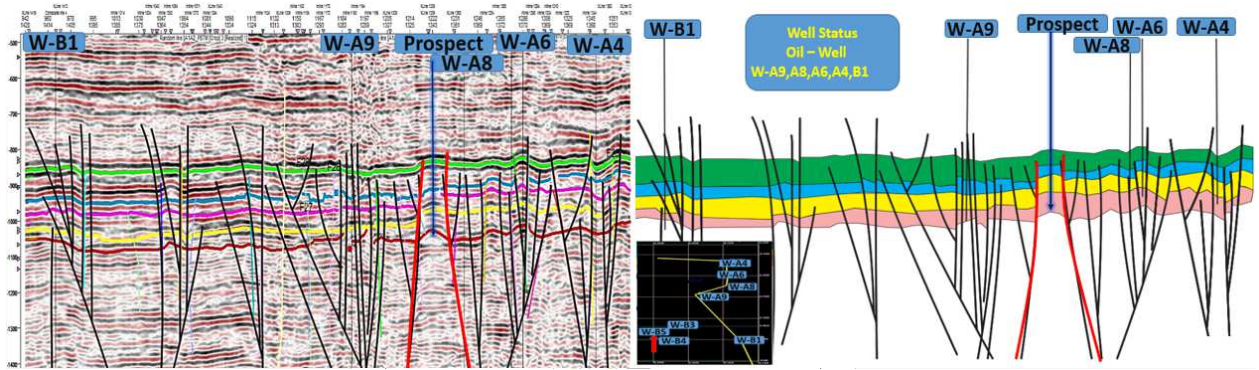


Figure 6.3, Lidam structure map and variance shows clearly closure bounded fault, AVO fluid strength, AVO, and GLCM at corssline 1340 support from lithology point of view.

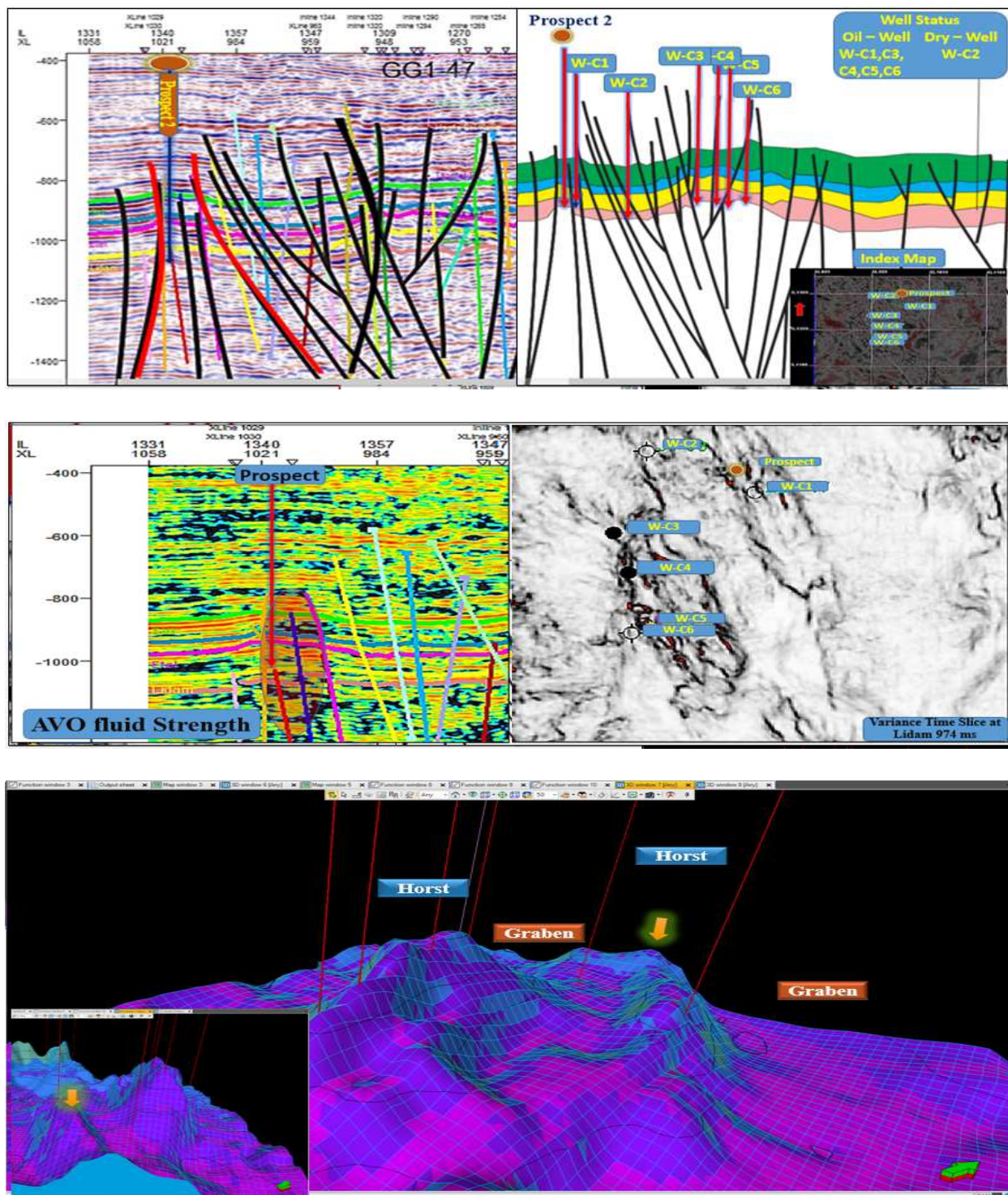


Figure 6.4 Composite seismic cross wells, geoseismic model and 3D structural grid surfaces prove that the prospect within the horst crested areas shows clearly closure bounded fault.

Conclusion

- The combination of wide range procedures and ideas developed from having an understanding in a broader view of the regional geologic framework with integrated seismic attribute for Upper Cretaceous succession to developing the model in its finite dimension in the Petrel workflow.
- The seismic visualization techniques enhanced the seismic interpretations and have provided better display to view the various data types slice in a single window and picture their relationship in 3D space.
- Application of different seismic attributes functions alongside the visualization templates providing structural clarity with smoothing of the seismic reflectors, structural events and horizons. This has really brought a better sense in understanding the response of the seismic volumes to the different seismic derivative functions as to highlighting geologic events by illuminating the seismic volumes.
- The interpreted horizon of the formations and their respective surface maps allows to create the surfaces needed in the structural 3D grid. Surface smoothing application needed to align the surface to the interpreted structural relief. Furthermore, zones were defined in the 3D structural modeling frame based on geologic differentiation of each formation surfaces. These form the necessary skeletons in the 3D structural grid.
- The fault modeling and pillar gridding process was closely monitored to ensure that the geologic based interpretation is preserved in the modeling frame. The automatic fault extraction process were used as quality control/test case to maintain interpretation, provide additional overview of fault segments and compare the value of manual interpretation.
- Ant Tracker attribute is an effective tool suitable to enhanced fault interpretation in 3D seismic data set, the research also shows that for ant tracker attributes to work effectively; one has to apply a fault sensitive attribute such as chaos and structural smoothing attributes before the application of ant tracker attribute and the interpreter has to apply signal enhancing filters to remove residual noise so as to have an optimal result.
- Variance attributes is more suitable to show major faults that are not seen in the amplitude data than the chaos attributes, also within a given area, chaos attributes can show more fractures than the variance attributes.

- Application of texture attributes confirm that these attributes enhance understanding of the reservoir by providing a clearer picture of the distribution, volume and connectivity of the hydrocarbon bearing facies in the reservoir. So that this study suggested that texture analysis can be utilized as an interpretation tool by geoscientists during exploration.
- The faulting style exhibited in the study area is that of normal and strike-slip faulting as a large scale listric faults basement involved with minor sets which were mainly associated with the margins of the horst structures were mostly interpreted. The existing interpretations for their origin range from strike-slip related pull-apart basins to purely extensional sedimentary basins or hybrid basins with combined effects of strike-slip tectonics and tectonic extension.
- The conjugate faults at the time of fault formation is perpendicular to bedding. Normal fault can be interpreted to be related to the extensional stage of basin evolution. However, reactivation of faults as strike-slip or reverse faults during the compressional stages usually precludes interpreting palaeostress orientation corresponding to the extensional stage from striated faults.
- The master faults in NW-SE trend characterized by segmented normal faults associated with horsetail splay faults that may indicate a component of sinistral strike-slip. The NW trends form a series of an elongate fault segments arranged as overlapping normal faults dipping to the SW, where the faults are arranged in a closely spaced en echelon pattern.
- The NE-SW faults are limited in length and not continuous, indicating that the structures were active for considerable amount of time, related to the primary tectonic movement. Based on their characteristics, the NE-SW fault system can be classified as transfer faults.
- Both direction can be interpreted within the same tectonic setting considering the possibility of NW-SE, whose strike-slip or transtensional movement is compatible with the normal movement of the E-W faults.
- The highly prospective areas identified based on this study are the areas of positive flower (plam tree) structure but they are relatively small prospects. Two prospect locations were identified based on time structure map, surface attribute and fault modeled. These prospects are localized within the closures horst structure across the seismic volume.

Furthermore study

3D structural grid surfaces of the Upper Cretaceous forms the input grids for property modeling, such as lithologies, fluid or saturation using well log interpretations. Which might include facies, saturation models, petrophysical modeling etc.

However this modeling could be stretched to include saturation to determine fluid mobility in the Bualawn, Dor Mansour fields due to the long period of production. This modeling provides a good basis for prospect analysis and also for dynamic simulation of the field.

References

- Abadi, A. M. (2002).** “Tectonics of the Sirt Basin”. PhD Dissertation. Vrije Universiteit (Amsterdam), ITC (Enschede): pp187.
- Anketell, J.M. (1996).** “Structural history of the Sirt Basin and its relationship to the Sabratah Basin and Cyrenaican Platform, northern Libya”. First Symposium on the Sedimentary Basins of Libya, Geology of the Sirt Basin, vol. 3. (eds. M.J. Salem, M.T. Busrewil, A.A. Misallati, and M.A. Sola), Elsevier, Amsterdam, p. 57-89.
- Anketell, J.M. and Kumati S. M. (1996).** “structural of Al Hufrah Region, western Sirt Basin”. third Symposium on the Sedimentary Basins of Libya, Geology of the Sirt Basin, vol. 5. (eds. M.J. Salem), Elsevier, Amsterdam, p. 2353-2370.
- Anstey, N., (1973b).** “The significance of color displays in the direct detection of hydrocarbons”: 43rd Annual International Meeting, Society of Exploration Geophysicists.
- Ambrose, Greg. (2000).** “The geology and hydrocarbon habitat of the Sarir Sandstone, Southeast Sirt Basin, Libya”. In: Journal of Petroleum Geology, V. 23, 165-192.
- Arabian Gulf Oil Company, (2009).** Intent To Drill (ITD) of ZZ1-47, (AGOCO Internal Report).
- Baird, D.W., Aburawi, R.M. And Bailey, N.J.L. (1996).** “Geohistory and petroleum in the central Sirt Basin”. First Symposium on the Sedimentary Basins of Libya, Geology of the Sirt Basin, vol. 3. (eds. M.J. Salem, M.T. Busrewil, A.A. Misallati and M.J. Sola), Elsevier, Amsterdam, p. 3-56
- Barr, F T. and Weegar (1972).** “Stratigraphic Nomenclature of the Sirt Basin, Libya”. The Petroleum Exploration Society of Libya (Tripoli, Libya): 179pp.
- Bellini, E., and Massa, D., (1980).** “A stratigraphic contribution to the Palaeozoic of the southern

- basins of Libya”, in Salem, M.J., and Busrewil, M.T., eds., *The geology of Libya*: London, Academic Press, v. 3, p. 3– 57.
- Cosentino, L. (2000).** “Integrated reservoir studies”: Editions Technip.
- Duronio and Colombi, (1983).** “Mesozoic Rocks of Libya”. Unpublished Report, P 15
- El- Bakai, M. T. (1992).** “Environment of Deposition of the Lidam Formation in NW Sirt Basin, Libya”. *Geology of Arab World*, Cairo University .P 343-351.
- El- Shari (2008).** “Stratigraphic Effects and Tectonic Implications at Hinge-Zone Area Between Sirte Basin and Cyrenaica Platform, NE Libya”; Third Symposium on Sedimentary Basins Of Libya- Geology Of East Libya, volume IV, p.269-281.2008.
- Finetti, I. (1982).** “Structure, stratigraphy and evolution of central Mediteixanean”. *Boll. Geofis. Teor. Appl.* vol. 24, p. 247-312.
- Futyan, A., and Jawzi, A.H., (1996).** “The hydrocarbon habitat of the oil and gas fields of North Africa with emphasis on the Sirt Basin”, in Salem, M.J., El-Hawat, A.S., and Sbeta, A.M., eds., *The geology of Sirt Basin*: Amsterdam, Elsevier, v. II, p. 287–308.
- G. de snoo (1961).** “Regional interpretation of gravity data in Libya” June E.P 58.
- Gras, R. (1996).** “Structural style on the southern margin of the Messiah High”. First Symposium on the Sedimentary Basins of Libya, *Geology of the Sirt Basin*, vol. 3. (eds. M.J. Salem, M.T. Busrewil, A.A. Misallati and M.J. Sola), Elsevier, Amsterdam, p. 201-210.
- Gras, R. And Thusu, B. (1998).** “Trap architecture of the early Cretaceous Sarir Sandstone in the eastern Sirt Basin”, Libya. In: *Petroleum Geology of North Africa*. (ed. D.S. Macgregor, R.T.J. Moody, D.D. ClarkLowes), Geol. Soc. Special Publication No. 132, p. 317-334.
- Guiraud, Rene, and Bosworth, William, (1997).** “Senonian basin inversion and rejuvenation of

- Rifting in Africa and Arabia—Synthesis and implication to plate-scale tectonics”: Tectonophysics, v. 282, p. 39– 82.
- Gumati, Y.D. and Kanes, W.H. (1985).** “Early Tertiary subsidence and sedimentary facies, northern Sirte Basin, Libya”. Bull. Amer. Assoc. Pet. Geol. vol. 69, p. 39-52.
- Hallett, D. (2002).** “Petroleum Geology of Libya”. Elsevier, Amsterdam. 503p.
- Hardge, B., (2010).** “Instantaneous seismic attributes calculated by the Hilbert transform”. Search and Discovery article 40563.
- Harding, T.P., (1984).** “Graben hydrocarbon occurrences and structural styles”. American Association of Petroleum Geologists Bulletin, v. 68, p. 333–362.
- Jerzykiewicz, T., Ghummed, M.A., Abugares, M.M. and Tshakreen S.O., (2002).** Evolution of the Western Margin of the Sirt Basin of Libya in Late Cretaceous Time. Abstract, Extended Abstract and Talk at CSPG Convention in Calgary, Compact Disc and Abstract Volume, p. 179.
- Kroner, A., (1993).** “The Pan-African belt of northeastern and eastern Africa, Madagascar, southern India, Sri Lanka and east Antarctica” Terrane amalgamation during formation of the Gondwana Supercontinent, in Thorwiehe, U., and Schandelmeier, H., eds., Geoscientific research in Northeast Africa: Rotterdam, Netherlands, A.A. Balkema, p. 39.
- Liner, Christopher L., (2004).** “Elements of 3D Seismology”. Second Edition. PennWell: Tulsa, Oklahoma.
- Nada, H., and Shralow, J., (1994).** “Evaluating geophysical lithology determination method in The central offshore Nile Delta, Egypt”: 64th Ann .Internat. Mtg.Soc. Expl. Geophys, Expanded Abstracts, 1112–1113.
- Ostrander, W.J., (1984).** “Plane-wave reflection coefficients for gas sands at non normal angles of incidence”: Geophysics, 49, 1637–1648.

Patrice N. M. (2001). “AVO Polarization Attributes and Hodograms”. Ph.D. diss., P 30-38.

Petrel Manual, Version 3.3 by Technoguide Schlumberger., (2015). “Interpreter’s Guide to Seismic Attribute”.

Ramos, A. C. B., (1996). “Three-dimensional AVO analysis and anisotropic modeling applied to Fracture characterization in coal bed methane reservoirs”, Cedar Hill field, San Juan Basin, New Mexico: Ph.D. diss., Colorado School of Mines.

Roohi, M. (1993). “A geological view of source-reservoir relationships in the western Sirt Basin”. First Symposium on the Sedimentary Basins of Libya, Geology of the Sirt Basin, vol. 2. (eds. M.J. Salem, A.S. El-Hawat and A.M. Sbeta), Elsevier, Amsterdam, p. 323-336.

Roohi, M. A. (1996) “A geological view of source-reservoir relationship in the western Sirt Basin”. In: Salem, M. J., El-Hawat, A, S. and Sbeta, A.M (Eds), the geology of Sirt Basin, p 323-336.

Ross, C. P., (2000) “Effective AVO crossplot modeling”. A tutorial: Geophysics, 65, 700–711.

Schlumberger, (2010). “Interpreter’s Guide to Seismic Attribute”.

Schlumberger, (2011). Petrel Geophysics Course.

Sinha, N.R., Mriheel, I.Y., (1996). “Evaluation of subsurface Paleocene sequence and shoal carbonates, south central Sirt Basin”. In: Salem, M.J., Busrewil, M.T., Misallati, A.A., Sola, M.A. (Eds.), The geology of the Sirt Basin, vol. II. Elsevier, Amsterdam, pp. 153–196.

Taner, M.T., (1979). “Complex seismic trace analysis”. Geophysics, v. 44, n. 6. P.1041-1063.

Taner, M.T., (2001). “Seismic attributes”. CSEG Recorder, v. 26, n. 7, p. 49-56.

Appendices

Appendix (1) Check shot dataset for used wells.

well identifier	surface	TVDss feet	TWT ms
W-B4	Gir/gattar	1314	168
W-B4	Kheir/Hofra/Nabiha	3368	488
W-B4	Dahra A/CRA Mbr	4042	581.92
W-B4	Dahra B/3500	4171	598.66
W-B4	Mabrouk/Beda/3900	4850	684
W-B4	Amin Mbr./4000	5000	704
W-B4	Hagfa SH/Kotla	5708	797.46
W-B4	Kalash/Gheriat	6155	868
W-B4	Tagrift/R2	6648	940
W-B4	Lidam/Dor	9470	1448
W-B4	Bahi/Maragh	9817	1497.25
W-B4	Gargaf	9860	1508
W-B4	Basement	9960	1519.11
well identifier	surface	TVDss feet	TWT ms
W-A7	Gir/gattar	810	33.61
W-A7	Facha	2290	275.09
W-A7	Kheir/Hofra/Nabiha	2553	318
W-A7	P Mark/Harash/2900	2846	363.94
W-A7	Zelten Mbr./ C Memb./3200	3020	391.23
W-A7	Khalifa	3306	436.07
W-A7	Dahra B/3500	3435	456.3
W-A7	Mabrouk/Beda/3900	3929	533.76

W-A7	Amin Mbr./4000	4044	551.8
W-A7	Hagfa SH/Kotla	4581	636
W-A7	Kalash/Gheriat	5365	800
W-A7	Sirte Shale/R1	5536	829.42
W-A7	Etel/R4/Anf	6074	922
W-A7	Lidam/Dor	6335	963.58
W-A7	Gargaf	6656	998
well identifier	surface	TVDss feet	TWT ms
W-A2	Gir/gattar	695	27.57
W-A2	Facha	2197	272.64
W-A2	Kheir/Hofra/Nabiha	2467	316.69
W-A2	P Mark/Harash/2900	2744	360.18
W-A2	Zelten Mbr./ C Memb./3200	2930	389.35
W-A2	Khalifa	3216	434.19
W-A2	Mabrouk/Beda/3900	3871	536.9
W-A2	Amin Mbr./4000	3985	554.78
W-A2	Thalith	4342	610.75
W-A2	Hagfa SH/Kotla	4521	639.77
W-A2	Kalash/Gheriat	5349	810.67
W-A2	Sirte Shale/R1	5512	838.72
W-A2	Etel/R4/Anf	6090	938.19
W-A2	Lidam/Dor	6360	974.62
W-A2	Nubian Fm./Sarir	6769	1018.48
W-A2	Gargaf	6874	1029.74
well identifier	surface	TVDss feet	TWT ms
W-B4	Gir/gattar	618	12.48

W-B4	Facha	2183	268.29
W-B4	Kheir/Hofra/Nabiha	2519	320.74
W-B4	P Mark/Harash/2900	2846	367.82
W-B4	Zelten Mbr./ C Memb./3200	3040	395.76
W-B4	Khalifa	3320	436.08
W-B4	Dahra B/3500	3474	458.26
W-B4	Mabrouk/Beda/3900	4024	545.77
W-B4	Amin Mbr./4000	4147	565.43
W-B4	Thalith	4405	606.67
W-B4	Hagfa SH/Kotla	4720	659.42
W-B4	Kalash/Gheriat	5516	807.61
W-B4	Sirte Shale/R1	5606	824.69
W-B4	Etel/R4/Anf	6394	972.94
W-B4	Lidam/Dor	6675	1018.95
W-B4	Gargaf	7116	1065.7
well identifier	surface	TVDss feet	TWT ms
W-C4	Gir/gattar	628	13.17
W-C4	Facha	2270	273.64
W-C4	Kheir/Hofra/Nabiha	2537	316
W-C4	P Mark/Harash/2900	2875	368.28
W-C4	Zelten Mbr./ C Memb./3200	3076	399.36
W-C4	Khalifa	3386	447.31
W-C4	Dahra B/3500	3513	466.95
W-C4	Mabrouk/Beda/3900	4105	558.51
W-C4	Amin Mbr./4000	4231	578
W-C4	Thalith	4603	632.16

W-C4	Hagfa SH/Kotla	4790	659.38
W-C4	Kalash/Gheriat	5474	804
W-C4	Sirte Shale/R1	5676	841.01
W-C4	Etel/R4/Anf	6482	988.7
W-C4	Lidam/Dor	6777	1041.6
W-C4	Nubian Fm./Sarir	7154	1081.76

Appendix (2) list and description of the ant agent parameters (Petrel, 2015).

Name	Min	Max	Passive	Aggressive	Description
Initial Ant Boundary(Voxels)	1	30	7	5	Spacing of the initial ant agents. A larger number results in fewer ants ,and less detail captured
Ant track Deviation(Voxels)	0	3	2	2	Distance to look on either side of the tracking direction. Allows more connections between points
Ant Step Size (voxels)	2	10	3	3	Distance ant advances on a step(search distance to look for discontinuity), increasing allows ant to search farther but lowers resolution
Illegal Steps(voxels)	0	3	1	2	Defines how far beyond its search distance an ant can look if no edge was detected within its search distance. Larger value will connect more discontinuous faults
Legal steps(Voxels)	0	3	3	2	Number of the valid steps that must be taken after an illegal step before another illegal step can be taken
Stop criteria (%)	0	50	5	10	Percent of illegal steps (relative to all steps) that can be taken before an ant is stopped.

Appendix (3) evaluate the distance along fault and fault displacement of selected fault.

	X	Y	Time	Distance along fault	Fault displacement
1	1064526.82	274922.49	-956.76	0.00	
2	1064540.10	274970.10	-955.91	49.43	0.85
3	1064553.38	275017.42	-952.93	98.57	1.40
4	1064557.41	275031.69	-952.03	113.40	0.88
5	1064569.34	275078.64	-947.29	161.84	0.91
6	1064580.85	275126.81	-941.62	211.37	0.61
7	1064589.44	275175.86	-936.94	261.16	0.48
8	1064596.04	275226.20	-934.00	311.93	0.57
9	1064601.15	275275.89	-933.20	361.88	1.13
10	1064606.53	275324.29	-934.34	410.58	1.09
11	1064607.51	275331.08	-934.52	417.45	0.91
12	1064617.22	275381.93	-934.48	469.22	0.91
13	1064631.27	275428.95	-935.89	518.29	1.24
14	1064650.44	275468.77	-936.44	562.48	1.95
15	1064665.58	275493.00	-936.96	591.06	1.20
16	1064689.50	275524.53	-936.97	630.63	0.82
17	1064711.90	275550.98	-937.68	665.29	1.56
18	1064737.27	275576.03	-938.62	700.94	1.08
19	1064759.76	275597.90	-938.98	732.31	1.15
20	1064790.14	275622.22	-939.65	771.23	1.34
21	1064822.40	275647.53	-939.91	812.23	1.85
22	1064845.81	275663.36	-939.61	840.49	2.68
23	1064879.94	275686.47	-939.18	881.71	3.85
24	1064903.35	275702.26	-938.63	909.95	4.89
25	1064937.55	275725.35	-937.84	951.21	5.55
26	1064970.28	275748.63	-937.04	991.38	6.27
27	1064994.14	275765.93	-936.72	1020.85	6.52
28	1065023.31	275789.90	-936.26	1058.61	6.75
29	1065047.88	275811.95	-937.18	1091.62	5.64
30	1065071.28	275835.93	-938.09	1125.12	4.78
31	1065095.60	275864.81	-939.73	1162.88	3.23
32	1065112.17	275886.65	-940.90	1190.29	2.26
33	1065134.51	275922.00	-942.15	1232.12	1.36
34	1065155.38	275960.85	-943.06	1276.21	1.22
35	1065163.99	275979.62	-943.48	1296.86	1.06
36	1065180.30	276020.02	-944.16	1340.43	0.95
37	1065194.01	276065.45	-944.88	1387.88	0.99
38	1065203.24	276113.92	-945.44	1437.23	1.03
39	1065210.39	276163.82	-945.64	1487.64	0.98
40	1065214.62	276213.05	-945.45	1537.05	1.04
41	1065218.84	276262.31	-944.99	1586.48	1.06
42	1065219.18	276266.37	-944.96	1590.56	1.04
43	1065224.58	276316.96	-944.28	1641.44	0.85
44	1065232.40	276365.39	-944.32	1690.50	0.89
45	1065245.07	276412.65	-944.66	1739.43	1.09
46	1065259.15	276456.29	-945.12	1785.28	1.35
47	1065266.51	276473.99	-945.36	1804.45	1.39
48	1065284.13	276516.50	-946.32	1850.46	1.08
49	1065302.61	276558.39	-947.69	1896.25	1.29
50	1065321.06	276600.08	-949.17	1941.84	0.54
51	1065329.23	276618.57	-949.83	1962.05	0.65
52	1065347.63	276660.31	-951.67	2007.67	0.53
53	1065363.15	276705.36	-954.04	2055.32	1.30
54	1065368.45	276720.83	-954.85	2071.67	0.82
55	1065379.70	276765.63	-956.00	2117.86	0.70
56	1065388.10	276812.99	-957.29	2165.96	1.00
57	1065392.68	276862.39	-958.04	2215.58	1.40
58	1065391.88	276912.35	-958.05	2265.55	1.87
59	1065384.15	276960.72	-957.52	2314.52	2.64
60	1065374.61	277007.44	-956.78	2362.21	3.84

Point spreadsheet for 'F6 Etel - side 1'

	X	Y	Time	Distance along fault	Fault displacement
61	1065371.68	277019.10	-956.48	2374.24	4.27
62	1065360.18	277065.30	-955.31	2421.84	5.48
63	1065349.66	277112.89	-954.88	2470.58	6.52
64	1065342.10	277161.19	-955.35	2519.47	7.39
65	1065342.54	277211.02	-956.82	2569.30	7.86
66	1065351.77	277258.61	-958.78	2617.78	7.79
67	1065366.97	277301.21	-959.55	2663.01	6.86
68	1065373.83	277318.35	-959.85	2681.47	5.38
69	1065392.10	277360.89	-958.65	2727.76	3.53
70	1065411.32	277401.81	-957.10	2772.97	1.54
71	1065420.21	277420.67	-956.38	2793.82	1.48
72	1065439.51	277461.65	-955.60	2839.12	0.57
73	1065457.16	277505.47	-955.31	2886.36	0.61
74	1065471.76	277550.70	-955.03	2933.89	1.33
75	1065475.16	277563.43	-954.87	2947.07	1.18
76	1065484.78	277611.37	-954.09	2995.97	1.00
77	1065490.67	277660.02	-955.59	3044.97	1.10
78	1065493.90	277709.89	-957.09	3094.95	1.44
79	1065492.88	277759.98	-958.26	3145.04	1.85
80	1065488.39	277809.29	-958.87	3194.56	2.29
81	1065482.34	277858.42	-958.78	3244.06	2.62
82	1065476.36	277907.35	-957.77	3293.36	2.92
83	1065470.47	277956.77	-958.09	3343.12	2.52
84	1065469.89	277961.97	-957.77	3348.36	2.85
85	1065465.02	278008.73	-954.82	3395.37	3.51
86	1065463.75	278057.88	-951.70	3444.53	3.02
87	1065465.60	278104.50	-949.61	3491.20	1.18
88	1065466.14	278109.67	-949.39	3496.39	1.39
89	1065472.43	278160.52	-949.22	3547.62	1.43
90	1065481.50	278209.49	-952.42	3597.43	2.28
91	1065490.90	278258.52	-956.06	3647.35	3.81
92	1065500.30	278307.31	-958.98	3697.04	4.97
93	1065509.13	278357.38	-960.74	3747.88	5.35
94	1065514.12	278407.01	-961.55	3797.76	4.54
95	1065517.14	278458.19	-961.60	3849.03	3.23
96	1065518.67	278509.00	-961.07	3899.86	1.85
97	1065518.38	278558.74	-960.14	3949.60	0.88
98	1065518.10	278608.44	-958.96	3999.30	0.46
99	1065518.01	278657.56	-957.75	4048.43	0.98
100	1065519.09	278707.02	-955.66	4097.90	2.28
101	1065520.56	278756.17	-952.27	4147.07	5.03
102	1065522.96	278804.40	-945.10	4195.36	10.70
103	1065523.03	278805.44	-944.94	4196.41	10.89
104	1065527.68	278854.78	-937.34	4245.97	19.67
105	1065532.91	278904.31	-932.91	4295.77	26.96
106	1065539.35	278952.93	-930.08	4344.81	33.79
107	1065547.57	279001.98	-928.89	4394.54	39.11
108	1065556.53	279050.26	-929.02	4443.65	42.56
109	1065566.79	279098.46	-931.06	4492.93	43.04
110	1065577.80	279145.64	-934.57	4541.38	40.14
111	1065580.98	279158.50	-935.53	4554.63	38.78
112	1065592.52	279206.53	-940.56	4604.02	32.19
113	1065604.07	279254.64	-945.88	4653.50	25.88
114	1065616.74	279301.59	-950.01	4702.13	19.95
115	1065620.68	279315.84	-951.26	4716.91	18.16
116	1065634.05	279362.36	-953.17	4765.31	14.58
117	1065647.68	279408.68	-954.98	4813.60	15.23
118	1065663.32	279453.25	-955.46	4860.84	15.31
119	1065669.11	279469.45	-955.63	4878.04	14.36
120	1065687.58	279513.04	-953.45	4925.38	14.31

Apply OK Cancel

Point spreadsheet for 'F6 Etel - side 1'

	X	Y	Time	Distance along fault	Fault displacement
121	1065706.12	279553.85	-950.58	4970.20	13.10
122	1065716.25	279573.89	-949.23	4992.66	12.37
123	1065736.96	279612.30	-942.24	5036.29	15.40
124	1065757.50	279651.03	-936.56	5080.13	18.59
125	1065767.87	279670.64	-933.68	5102.31	21.26
126	1065786.21	279708.96	-926.82	5144.80	28.04
127	1065803.78	279752.44	-923.94	5191.70	32.70
128	1065816.66	279801.09	-922.94	5242.02	36.30
129	1065820.69	279853.36	-924.06	5294.44	37.78
130	1065815.74	279906.47	-927.43	5347.78	37.11
131	1065804.75	279955.49	-933.06	5398.03	34.40
132	1065791.53	280004.17	-940.69	5448.46	30.18
133	1065776.25	280055.11	-950.20	5501.65	24.11
134	1065774.00	280064.28	-951.91	5511.09	22.97
135	1065761.36	280114.61	-961.32	5562.98	16.94
136	1065754.90	280164.24	-968.81	5613.03	11.51
137	1065754.47	280214.32	-974.49	5663.11	6.93
138	1065759.76	280264.49	-978.34	5713.57	3.90
139	1065769.76	280310.67	-978.51	5760.82	2.17
140	1065772.62	280322.25	-978.54	5772.74	1.74
141	1065785.93	280369.60	-977.07	5821.93	1.66
142	1065800.61	280415.29	-975.04	5869.92	1.67
143	1065816.17	280460.13	-971.12	5917.38	1.55
144	1065821.17	280474.44	-969.86	5932.54	1.54
145	1065837.99	280519.48	-965.54	5980.62	1.88
146	1065855.20	280562.99	-961.92	6027.41	1.67
147	1065874.75	280602.94	-958.21	6071.88	1.23
148	1065884.46	280622.22	-956.40	6093.48	1.46
149	1065907.66	280659.69	-954.12	6137.54	0.56
150	1065923.21	280682.53	-952.69	6165.17	1.42
151	1065950.03	280714.61	-951.57	6206.99	1.69
152	1065974.96	280741.30	-951.66	6243.51	1.18
153	1065999.13	280765.21	-951.76	6277.51	0.86
154	1066026.60	280789.51	-948.86	6314.19	0.16
155	1066051.95	280811.93	-945.32	6348.02	1.37
156	1066078.11	280836.13	-941.59	6383.66	3.06
157	1066103.89	280859.53	-936.12	6418.48	6.60
158	1066126.43	280883.11	-931.10	6451.10	10.79
159	1066149.71	280912.71	-926.01	6488.76	15.12
160	1066171.64	280953.80	-926.84	6535.33	17.57
161	1066178.00	280970.05	-927.18	6552.78	18.00
162	1066188.86	281014.95	-932.96	6598.97	14.23
163	1066197.02	281064.04	-939.73	6648.74	10.36
164	1066200.27	281115.01	-946.72	6699.82	6.55
165	1066201.95	281166.39	-953.05	6751.22	3.45
166	1066202.48	281217.25	-958.04	6802.09	1.49
167	1066203.53	281267.54	-960.81	6852.39	0.81
168	1066205.99	281316.33	-961.09	6901.24	0.41
169	1066211.09	281364.81	-958.68	6949.99	1.35
170	1066220.32	281409.04	-952.45	6995.17	1.30
171	1066222.56	281418.20	-951.16	7004.60	1.16
172	1066236.05	281464.10	-942.55	7052.44	2.58
173	1066253.71	281505.87	-936.29	7097.79	3.16
174	1066272.66	281541.72	-931.51	7138.34	3.61
175	1066285.64	281562.88	-928.54	7163.17	4.92
176	1066307.02	281597.40	-925.82	7203.77	4.78
177	1066323.28	281620.72	-923.95	7232.20	5.96
178	1066345.63	281653.54	-922.29	7271.90	6.63
179	1066367.29	281687.76	-922.39	7312.40	7.51
180	1066381.87	281710.84	-922.45	7339.70	8.25

Apply OK Cancel

Point spreadsheet for 'F6 Etel - side 1'

	X	Y	Time	Distance along fault	Fault displacement
181	1066401.48	281747.90	-923.14	7381.63	8.86
182	1066409.25	281766.27	-923.34	7401.57	9.43
183	1066422.26	281807.50	-924.48	7444.81	10.05
184	1066431.66	281853.21	-925.57	7491.48	11.27
185	1066437.39	281901.11	-926.82	7539.72	12.32
186	1066442.67	281949.29	-928.19	7588.19	13.16
187	1066448.70	281997.43	-929.88	7636.71	13.58
188	1066457.76	282042.57	-932.10	7682.75	13.27
189	1066461.99	282055.98	-932.79	7696.81	12.98
190	1066480.19	282098.21	-936.08	7742.79	10.90
191	1066501.05	282131.42	-938.31	7782.01	9.01
192	1066519.90	282155.63	-939.95	7812.69	6.79
193	1066543.70	282182.26	-941.39	7848.41	4.69
194	1066565.99	282207.03	-942.74	7881.73	2.64
195	1066589.95	282233.20	-942.86	7917.21	1.77
196	1066612.84	282258.06	-942.98	7951.00	0.98
197	1066635.96	282286.28	-942.10	7987.49	1.13
198	1066651.12	282308.06	-941.52	8014.03	1.61
199	1066670.12	282344.12	-941.26	8054.78	1.71
200	1066684.26	282388.58	-942.20	8101.44	1.55
201	1066691.66	282437.85	-943.47	8151.26	1.34
202	1066691.76	282490.28	-945.07	8203.69	1.05
203	1066688.10	282539.68	-946.87	8253.23	0.66
204	1066682.26	282589.63	-948.81	8303.52	0.07
205	1066675.18	282639.04	-949.87	8353.43	

Apply OK Cancel

الخلاصة

الاستكشاف بواسطة تقنية الإنعكاسات السيزمية يعتبر من الأهمية بمكان في دقة تفسير التراكيب الجيولوجية تحت سطح الأرض، وذلك لأن الخصائص السيزمية تتميز بتأثيرها الفعال بالشكل البنائي للطبقات، وفي بعض الأحيان يكون تفسير المقاطع السيزمية صعب نتيجة للتداخلات المعقدة. الهدف الرئيسي لهذه الرسالة هو تقديم مجموعة من السمات السيزمية كأداة فعّالة لتفسير التداخلات سواء كانت تركيبية أو فيزيائية، وذلك من خلال استخدام مجموعة من السمات يكمل بعضها البعض، وتساهم في فهم النشأة التركيبية وما ترتب عليها من تأثير في الترسيبات الطبقيّة المهمة اقتصادياً في حقلي بلعون و دور منصور النفطيين.

الدراسة تضمّنت تحليلاً كمياً ووصفياً لفهم التغيرات الجيولوجية ابتداءً من تحسين جودة الخصائص الجيولوجية الظاهرة في الأبعاد الثلاثة وربطها بالسمات السيزمية. وبناءً على استخدام كلا الطريقتين اليدوية والأتمتكية لتحليل وتفسير نمط الصدوع و لربط السمات ببعضها لإنشاء مجسم يحاكي أبرز الصدوع ومجسم شبكي ثلاثي الأبعاد يظهر تتابع الطبقات المستهدفة. أختيرت في هذه الدراسة لفيغ من السمات التركيبية لتحديد الصدوع ومقدار إزاحتها، فساهمت في رفع كفاءة ودقّة التفسير.

الدراسة أظهرت شبكة صدوع وانشقاقات معقدة لحدّ ما في الزمن الطباشيري لما لها من تفرعات تبعاً للحركات التكتونية العامة، تلك الحركات صاحبها تمدد نتج عنه انهيار طبقي بشكل عمودي اعقبه حركة أفقية أدت لتكوين نظام تدرجي معقد En echelon يسمى حسب مصطلح الإجهاد Riedel اتجاه الإجهاد ضد عقارب الساعة في الشمال الغربي، إلا أنها تكونت بانزلاق يساري في وضعية بحيث أن الإجهاد الإنضغاطي الأعلى لمجال الإجهاد الأصلي كان يعمل بزواوية عظمي في نطاق الصدوع العام. التحليلات السيزمية المقطعية بيّنت مجموعة من الصدوع مقوّسه listric fault رافقتها صدوع في اتجاهها أو مائلا عليه synthetic or antithetic وكونت بشكل عام ما يعرف structure positive or negative flower الخرائط التركيبية معظم الصدوع تأخذ أحد إتجاهين إما في إتجاه الشمال الغربي حيث يظهر كصدوع خطية تعكس الحركة الأفقية Sinistral مرتبطة بالحدث المسمّى Pan-African، والاتجاه الثان للصدع هو الشمال الشرقي محدود في ظهوره مرتبط ب Hercynian structures orogeny .

الخصائص الداخلية للطبقات تأثرت بالبيئة الجيولوجية في وقت الترسيب وتعتبر السعة الموجية (Amplitude) كمقياس فيزيائي لتلك التغيرات من حيث القوة أو الضعف، وقد استخدمت عدّة سمات سيزمية فيزيائية لتحسين جودة التفسيرات.

وبالتالي من أبرز المشاهدات في المنطقة البحثية أن للصدوع اتجاهين متضادين مرتبطن بأحداث جيولوجية عامة , هذه الصدوع تتباعد في الجزء الشمالي للمنطقة مما أدى إلي هبوط المنطقة الواقعة بينها بينما ترتفع في كلا جانبي الصدعين لتكوّن مصائد ممتازة تجمّع البترول وتتميز بارتفاعها ، أمّا في الجزء الجنوبي فتقترب جدًا لتكون منطقة مرتفعة في الجانبي الشرقي وأخري منخفضة في الجانِب الغربي ، وبطبيعة الحال بيّنت دراسة ربط الأبار أن الترسيبات الطبقيّة عكست هذه التأثيرات بزيادة السُمك في منطقة الاتساع او التمدد والانخفاض خلافا لما هو عليه في الأكثر ارتفاعاً.



تحليلات السمات السيزمية لتحسين تفسير البيانات ثلاثية
الأبعاد لتتابع الزمن الطباشيري العلوي , في حقلي بلعون و
دور منصور , غرب حوض سرت , بليبيا

قدمت من قبل :

محمد نجيب فرج الفارسي

تحت إشراف

د. سعد مصباح الشاعري

قدّمت هذه الرسالة استكمالاً لمتطلبات الحصول علي درجة الماجستير في علوم الأرض

جامعة بنغازي

كلية العلوم

فبراير 2018